

GC  
7.1  
H88  
1976

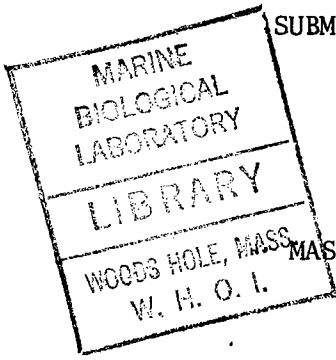
THE HYDROTHERMAL ALTERATION OF OCEANIC  
BASALTS BY SEAWATER

by

SUSAN ELIZABETH HUMPHRIS

B.A., University of Lancaster, Great Britain  
(1972)

SUBMITTED IN PARTIAL FULFILLMENT OF THE  
REQUIREMENTS FOR THE DEGREE OF  
DOCTOR OF PHILOSOPHY



at the

MASSACHUSETTS INSTITUTE OF TECHNOLOGY

and the

WOODS HOLE OCEANOGRAPHIC INSTITUTION

October, 1976

Signature of Author ..... *Susan E. Humphris* .....  
Joint Program in Oceanography, Massachusetts Institute  
of Technology - Woods Hole Oceanographic Institution,  
and Department of Earth and Planetary Sciences, and  
Department of Meteorology, Massachusetts Institute of  
Technology, June 1971

Certified by ..... *Geoffrey Thompson* .....  
Thesis Supervisor

Accepted by ..... *J. M. Gluskap* .....  
Chairman, Joint Oceanography Committee in the Earth  
Sciences, Massachusetts Institute of Technology -  
Woods Hole Oceanographic Institution

THE HYDROTHERMAL ALTERATION OF OCEANIC BASALTS BY  
SEAWATER

by

Susan Elizabeth Humphris

Submitted to the Massachusetts Institute of Technology- Woods Hole Oceanographic Institution Joint Program in Oceanography on October 14, 1976, in partial fulfillment of the requirements for the degree of Doctor of Philosophy.

ABSTRACT.

Considerable geological and geophysical evidence now exists to support the hypothesis that seawater circulates through freshly intruded basalt at the mid-ocean ridges. As a consequence of this process, reactions between basalt and seawater take place at elevated temperatures.

The mineralogy and chemistry of hydrothermally altered pillow basalts dredged from the Mid-Atlantic Ridge, and belonging to the greenschist facies, have been studied in order to determine the mineralogical changes that result from hydrothermal alteration, and to assess the chemical fluxes that result from these reactions in terms of their possible significance in elemental geochemical budgets as potential sources and sinks for elements in seawater. Where possible, pillow basalts were studied that showed various degrees of alteration within a single rock. Such samples provide the best evidence that they have been affected by hydrothermal alteration, rather than regional burial metamorphism, and provide the most useful information for elemental flux calculations.

During hydrothermal alteration, plagioclase is generally albitised, sometimes with the formation of epidote, and albite may be subsequently altered to chlorite. Plagioclase, in association with skeletal clinopyroxene, alters to chlorite and epidote. Olivine is pseudomorphed by chlorite, and clinopyroxene alters to actinolite. The glassy matrix alters to an intergrowth of actinolite and chlorite. Vein minerals include chlorite, actinolite, epidote, quartz, and sulphides. On the basis of their mineralogy, the samples may be subdivided into chlorite-rich (>15% chlorite and <15% epidote) and epidote-rich (>15% epidote and <15% chlorite) assemblages. The chlorite-rich assemblages lose CaO and gain MgO, while the epidote-rich samples show very little change in composition compared with their basalt precursor. The epidote-rich samples are more oxidised than their precursors, while the chlorite-rich rocks can be further subdivided into those that maintain the same proportions of ferrous and ferric iron, and those that show an increase in ferrous iron due to the precipitation of pyrite.

The major chemical changes that occur during hydrothermal alteration of pillow basalts are uptake of MgO and H<sub>2</sub>O, and loss of

1978-WHOI

SiO<sub>2</sub> and CaO. The concentrations of Na<sub>2</sub>O and K<sub>2</sub>O are apparently not greatly changed, although they do show some variations in the core-to-rim analyses. Consideration of the elemental fluxes in terms of steady-state geochemical mass balances indicates that hydrothermal alteration provides a sink for Mg, which is extremely important in solving the problem of apparent excess magnesium input to the oceans. The amount of calcium that is leached from the rock may be of significance in the geochemical budget of calcium. The concentration of silica in the circulating fluid is probably controlled by the solubility of quartz, and considerable redistribution of silica takes place within the basaltic pile. The changes in the redox conditions during hydrothermal alteration do not affect the present-day oxidation states of the atmosphere and hydrosphere.

Trace element analyses indicate that copper and strontium are leached out of the rock and migrate in the circulating fluid, with local precipitation of Cu as sulphides in veins. Li, B, Mn, Ba, Ni and Co show sufficient variation in concentration and location within the altered basalts to indicate that some leaching does take place, and hence hydrothermal alteration of basalts could produce a metal-enriched solution, which may be important in the formation of metalliferous sediments at active mid-ocean ridges.

Thesis Supervisor: Dr. Geoffrey Thompson  
Title: Associate Scientist

ACKNOWLEDGEMENTS.

I should like to thank my adviser, Geoffrey Thompson, for his invaluable guidance and support throughout the course of this work.

Thanks are also due to the other members of my thesis committee for many helpful discussions during the preparation of this thesis: Bill Bryan, Fred Frey, Dick Holland and Bill Jenkins.

Interactions with many other members of the staff and students at the Woods Hole Oceanographic Institution have proved stimulating, and have made my work in Woods Hole particularly rewarding.

I also wish to thank my family, who have provided much encouragement and support, not only during the last four years, but throughout my life.

Most of this work was supported by the National Science Foundation Grants OCE-74-22971 and DES-75-16596. I was supported by Woods Hole Oceanographic Institution, and by the National Fellowship for the American Association of University Women.

TABLE OF CONTENTS.

	<u>Page</u>
ABSTRACT	2
ACKNOWLEDGEMENTS	4
LIST OF FIGURES	9
LIST OF TABLES	12
1. General Introduction and Experimental Design	14
1.1 Introduction	14
1.2 Evidence for Hydrothermal Circulation at the Mid-Ocean Ridges	16
A. Heat flow	16
B. Metalliferous sediments	16
C. Metamorphosed igneous rocks	19
D. Ophiolites	20
1.3 Hydrothermal Circulation and Inferred Effects	22
A. Circulation model	22
B. Inferred effects	23
1.4 Experimental Design.	27
A. Selection of sample type	27
B. Selection of specific samples	28
2. Mineralogy and Petrology of Hydrothermally Altered Basalts	36
2.1 A. Previous studies	36
B. Present study	42
2.2 Mineralogy of Greenschist Facies Meta- basalts	42

	<u>Page</u>
A. Fresh rocks	43
B. Feldspars	43
C. Chlorite	44
D. Actinolite	45
E. Epidote	48
F. Quartz	48
G. Pyrite	48
2.3 Bulk Chemical Composition	52
2.4 Mineral Conversions	65
A. Plagioclase	65
B. Olivine and pyroxene	68
C. Alteration of the glass matrix	70
2.5 Conclusions	70
3. Elemental Fluxes During Hydrothermal Alteration of Basalts	72
3.1 Introduction	72
3.2 Major Elemental Analyses	74
A. Silica	74
B. Calcium	78
C. Magnesium	78
D. Iron	87
E. Sodium and other major elements	90
3.3 Mass Balances During Alteration	95
3.4 Magnitudes of Fluxes and Significance in Mass Balances	107
3.5 Water-to-Reacted Rock Ratio	110
3.6 Geochemical Budgets	110

	<u>Page</u>
A. Magnesium	112
B. Calcium	118
C. Silica	124
D. Sulphate	128
E. Water	130
F. Oxygen	134
3.7 Conclusions	134
4. Trace Element Disribution in Hydrothermally Altered Basalts	137
4.1 Introduction	137
4.2 Results and Discussion	140
A. Boron	140
B. Lithium	143
C. Strontium	146
D. Barium	152
E. Nickel and cobalt	158
F. Vanadium	166
G. Chromium	166
H. Copper	169
I. Manganese	169
J. Yttrium and zirconium	174
4.3 A. Water-to-reacted rock ratio	182
B. Elemental fluxes	182
4.4 Hydrothermal Alteration and Implications for Metalliferous Sediments and Ore Deposit Formation	185

	<u>Page</u>
4.5 Conclusions	187
REFERENCES	189
APPENDIX I - Results of mineralogical and chemical analyses	203
APPENDIX II - Analytical Procedures	231
VITA	247



LIST OF FIGURES

	<u>Page</u>
1-1. Ocean ridge heat flow vs. age	18
1-2. Velocity structure and possible composition of the oceanic crust	29
1-3. Hydrothermally altered pillow fragment (AII-60 2-142) showing two alteration zones surrounding the relatively fresh interior	32
1-4. Dredge locations and slope profiles	35
2-1. Compositions of actinolites and chlorites plotted on an AFM diagram	47
2-2. Scanning electron micrographs for Fe, S, Cu and Zn in a sulphide vein (AII-60 2-141)	50
2-3. ACF diagram of greenschist facies metabasalts	54
2-4. Correlation between wt.% $H_2O^+$ and modal chlorite for analysed metabasalts	57
2-5. Magnesium vs. calcium contents for fresh and altered basalts	60
2-6. Ferric iron contents vs. water contents showing separation of different mineral assemblages	62
2-7. Ferrous iron contents vs. water contents showing separation of different mineral assemblages	64

	<u>Page</u>
3-1. SiO <sub>2</sub> concentrations vs. water content	76
3-2. SiO <sub>2</sub> concentrations- previously published data	77
3-3. CaO concentrations vs. water content	80
3-4. CaO concentrations- previously published data	82
3-5. MgO concentrations vs. water content	84
3-6. CaO vs. MgO contents for fresh and hydrothermally altered basalts	86
3-7 Fe <sub>2</sub> O <sub>3</sub> concentrations- previously published data	88
3-8. FeO concentrations- previously published data	89
3-9. Al <sub>2</sub> O <sub>3</sub> concentrations vs. water content	92
3-10. TiO <sub>2</sub> concentrations vs. water content	94
3-11. TiO <sub>2</sub> concentrations- previously published data	94
3-12. Examples of mass fluxes- chlorite-rich, pyrite containing assemblages	102
3-13. Examples of mass fluxes- chlorite-rich assemblages with no pyrite	103
3-14. Examples of mass fluxes- epidote-rich assemblages	104
3-15. Dependence of Mg <sup>2+</sup> uptake by basalt on the vol. rock altered annually	117
3-16. % available crust to be altered to account for the excess Mg vs. depth of penetration	120
3-17. Dependence of Ca <sup>2+</sup> concentration leached from basalt on the vol. rock altered annually	123

	<u>Page</u>
4-2. Lithium concentrations vs. water contents	145
4-3. Strontium concentrations vs. water contents	148
4-4. Sr concentrations- previously published data	151
4-5. Correlation between Sr and CaO contents in fresh and hydrothermally altered basalts	154
4-6. Barium concentrations vs. water contents	156
4-7. Barium concentrations- previously published data	159
4-8. Nickel concentrations vs. water content	161
4-9. Cobalt concentrations vs. water content	163
4-10. Ni concentrations- previously published data	165
4-11. Co concentrations- previously published data	165
4-12. V concentrations vs. water content	168
4-13. V concentration- previously published data	168
4-14. Cu concentrations vs. water content	171
4-15. Cu concentrations- previously published data	171
4-16. Mn concentrations vs. water content	173
4-17. Mn concentrations- previously published data	173
4-18. Y and Zr concentrations vs. water contents	176
4-19. Relation between Ti and Zr concentrations for basalts from different tectonic settings	179
4-20. Relation between Zr and Y contents for basalts from different tectonic settings.	181

LIST OF TABLES

	<u>Page</u>
1-1. Compositions of fluids from Reykjanes geothermal system and from experimental basalt-seawater reactions	24
1-2. Locations of dredge hauls from which samples were selected	33
2-1. Some reported occurrences of metabasalts and metagabbros from the ocean floor.	37
2-2. Reactions during hydrothermal alteration of plagioclase	66
2-3. Reactions during hydrothermal alteration of olivine and pyroxene	69
3-1. Gains and losses during hydrothermal alteration of basalts	97
3-2. Comparison of estimates of major element fluxes during hydrothermal alteration of basalts	106
3-3. Calculation of water-to-reacted rock ratios in the hydrothermal system	111
3-4. General parameters for mass balances calculations	113
3-5. The magnesium budget	114
3-6. Silica flux calculations	127
3-7. Water flux during hydrothermal alteration	131
3-8. Oxygen consumption during hydrothermal alteration	133
4-1. Trace element analyses of metalliferous sediments	138
4-2. Trace element concentrations in Reykjanes geothermal brines, Iceland	183

	<u>Page</u>
AI-1. Feldspar analyses- fresh basalts and interiors	205
AI-2. Olivine analyses- fresh basalts	207
AI-3. Feldspar analyses- altered basalts	209
AI-4. Epidote analyses- altered basalts	213
AI-5. Chlorite-analyses- altered basalts	215
AI-6. Amphibole analyses- altered basalts	219
AI-7. Major element analyses of fresh and altered basalts	221
AI-8. Modal analyses of fresh and altered basalts	226
AI-9. Trace element analyses of fresh and altered basalts	229
AI-10. Mn analyses of fresh and altered basalts	230
AII-1. Microprobe standards used for mineral analyses	233
AII-2. Analyses of JB-1 during electron microprobe analyses	234
AII-3. Determination of FeO content of BCR-1 and CRPG-BR.	238
AII-4. Analyses of standard rocks determined during trace element analyses by direct-reading emission spectroscopy.	240
AII-5. Ignition loss of reference rocks	242
AII-6. Determination of $H_2O^+$ on standard reference rocks	242
AII-7. Synthetic basalt matrix.	244
AII-8. Reference rock analyses during Mn determinations	245
AII-9. Density of aluminium powder measured during density determinations for samples.	247

## 1. GENERAL INTRODUCTION AND EXPERIMENTAL DESIGN.

### 1.1. INTRODUCTION.

One of the principal objectives in marine geochemistry is to gain an understanding of the physical and chemical controls on the composition of seawater. This requires definitive information concerning the cycling of elements through the biosphere, atmosphere, hydrosphere and lithosphere. In addition to quantitatively evaluating the elemental fluxes in the system, it is necessary to identify the sources and sinks for each element, and to understand the interactions in which it is involved. Geochemical mass balances (e.g. Goldschmidt, 1954; Horn and Adams, 1966; Li, 1972) have generally been based upon a concept of chemical uniformitarianism for the weathering of continents and the deposition of sedimentary rocks, and have assumed that all the geochemical reservoirs included in the sedimentary cycle (i.e. biosphere, atmosphere, hydrosphere and the upper crust) constitute a closed system. Except for the addition of 'excess volatiles', the mantle does not play an active role in these models.

Modern theories of sea-floor spreading and plate tectonics assume that the mid-ocean ridges are regions of plate divergence where new oceanic lithosphere is generated by injection and extrusion of molten material. Geological and geophysical data suggest that massive hydrothermal circulation occurs beneath the mid-ocean ridges. Such a process would result in interaction between the fresh crust and the circulating seawater, and could give rise to large-scale chemical fluxes between the oceanic crust and seawater. Since the basalt is

initially derived from the upper mantle, such interaction could be significant in introducing new material from the upper mantle into the hydrosphere, and removing material from it. Thus, the geochemical mass balances, and consideration of the chemical controls on seawater composition, should include such interactions. However, the elemental fluxes involved in such a mechanism, and their significance for geochemical mass balance calculations, are unknown.

This thesis represents an attempt to test the following hypothesis: 'Reactions between seawater and oceanic igneous crust lead to significant chemical exchange between the hydrosphere, lithosphere and upper mantle. These reactions and fluxes are significant in geochemical mass balance calculations, and are important sources and sinks for elemental cycles in the oceans'.

The experiment designed to test this hypothesis was to study carefully selected oceanic igneous rocks that show textural and mineralogical evidence of having undergone hydrothermal alteration by seawater. The aims of this study are:

- a) to identify and determine the compositions of the alteration products by petrographic study and microprobe analyses;
- b) to describe the reactions between seawater and igneous rock during hydrothermal alteration;
- c) from the petrographic observations and chemical analyses and measurements, to identify the sources and sinks in the rock for individual elements;
- d) to assess the fluxes of elements in terms of their significance for elemental geochemical mass balances.

## 1.2. EVIDENCE FOR HYDROTHERMAL CIRCULATION AT THE MID-OCEAN RIDGES.

### A. HEAT FLOW.

Hydrothermal circulation beneath the mid-ocean ridges was originally postulated in order to account for the discrepancy between the theoretical heat flow and the lower, observed values close to the ridge axis (Anderson, 1972; Hyndman and Rankin, 1972; Langseth and Von Herzen, 1971; Sclater and Klitgord, 1973; Talwani et al, 1971). This anomaly is illustrated in Fig. 1-1 for both fast-spreading (3 - 6 cm/yr) and slow-spreading (1 - 2 cm/yr) ridges, and these are compared with the theoretical curve for a conductively cooling, spreading plate. Many investigators invoked large-scale circulation of seawater through the oceanic crust as a means of removing excess heat by convective transport (e.g. Elder, 1965; Le Pichon and Langseth, 1969; Palmason, 1967; Bodvarsson and Lowell, 1972; Deffeyes, 1970; Lister, 1972; Sleep, 1969; Wolery and Sleep, 1976). In fact, Williams and Von Herzen (1974) have suggested that seawater circulation may be the dominant heat loss mechanism of young (less than 2 myr.) oceanic crust, and account for about 20% of the total heat loss of the Earth's interior. Thermal anomalies in the seawater on the Galapagos Rise (Williams et al, 1974) and in the TAG hydrothermal field at 26°N. on the Mid-Atlantic Ridge (Rona et al, 1974) have been interpreted as indications of local hydrothermal activity.

### B. METALLIFEROUS SEDIMENTS.

The occurrence of heavy-metal enriched sediments along active spreading centres in all three major ocean basins has also been

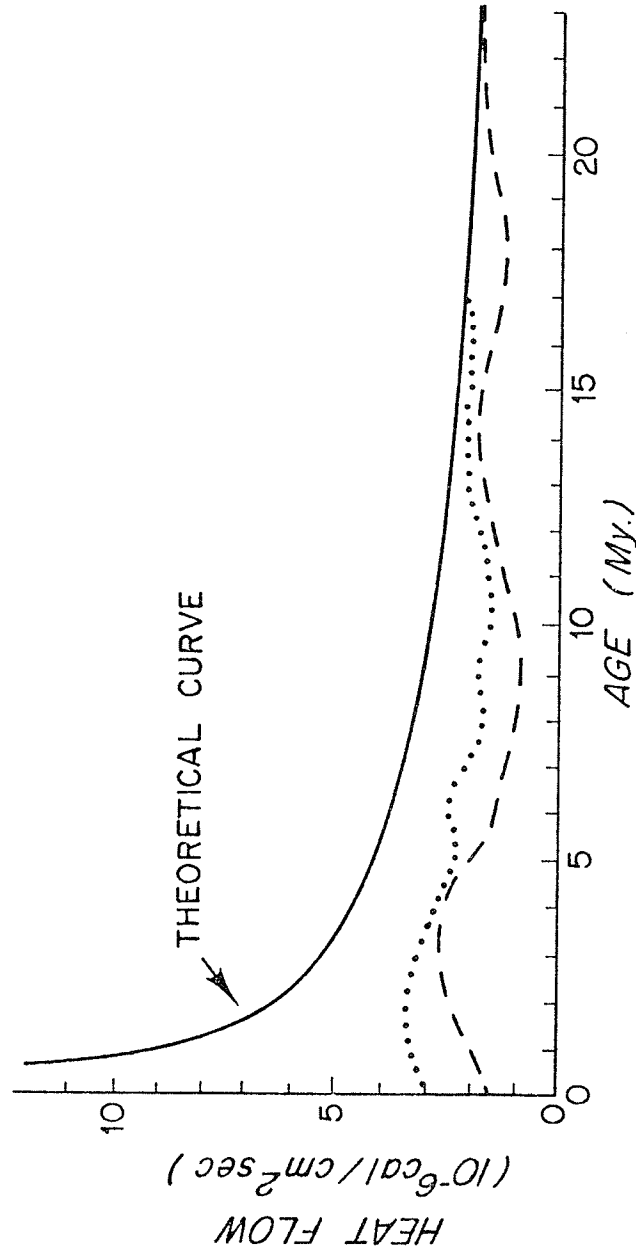


FIGURE 1-1.

Theoretical (—) vs. average observed heat flow profiles as a function of age for fast spreading (.....) and slow spreading (-----) ridges.

(Redrawn from Wolery and Sleep, 1976).

FIGURE 1-1.



attributed to hydrothermal circulation (Arrhenius and Bonatti, 1965; Bonatti and Joensuu, 1966; Bostrom and Peterson, 1966; Bostrom and Fisher, 1971; Dmitriev, Barsukov and Udintsev, 1970; Skornyakova, 1964). These sediments show highly variable iron-to-manganese ratios, and enrichment in Ni, Zn, Cu, Co, Pb, Hg, Ba, and U relative to pelagic sediments. The accumulation rates of manganese on the East Pacific Rise are two orders of magnitude faster than the average pelagic accumulation rates (Bender et al, 1971). In addition, the lead isotope ratios in these heavy-metal enriched sediments resemble those of the mid-ocean ridge basalts suggesting that this component is of basement origin (Bender et al, 1971; Dasch et al, 1971; Dymond et al, 1973). The Deep Sea Drilling Project has encountered similar metalliferous sediments overlying the basaltic basement at sites away from the present active spreading centres (e.g. von der Borch and Rex, 1970; von der Borch et al, 1971; Cook, 1971; Cronan et al 1972; Cronan, 1973, 1974; Horowitz and Cronan, 1976). These represent ancient hydrothermal deposits that were precipitated at the ridge crest and have moved to their present positions as a result of sea-floor spreading, suggesting that hydrothermal circulation at the mid-ocean ridges has been a geologically continuous process.

#### C. METAMORPHOSED OCEANIC IGNEOUS ROCKS.

Some of the most convincing evidence of hydrothermal circulation comes from the rocks dredged from the mid-ocean ridges and fracture zones. Metamorphic rocks, ranging from zeolite to amphibolite facies, have been dredged from the median valleys and fracture zones (e.g. Cann and Funnell, 1967; Cann, 1971; Melson et al, 1966 a, b; Miyashiro et al, 1971), and serpentinites have been dredged from fracture zones

(e.g. Aumento and Loubat, 1973; Udintsev and Dmitriev, 1970).

Greenschist facies metabasalts are the most frequently recovered metamorphosed rocks, and consist of assemblages of primarily albite, chlorite and epidote. All the rocks are hydrated and therefore required an extraneous fluid for metamorphism. Oxygen isotope fractionations between coexisting mineral phases in greenstones suggest alteration temperatures of up to 300°C. (Muehlenbachs and Clayton, 1972), and whole rock oxygen isotope data for greenstones and serpentinites (Wenner and Taylor, 1971) indicate that the fluid involved in metamorphism was seawater.

Metal sulphide mineralisations have recently been discovered within basalts from the Mid-Atlantic Ridge (Bonatti et al, 1976), in the Indian Ocean (Dmitriev et al, 1970), and during the DSDP on the Nazca Plate (Hart et al, 1974; Swanson and Scott, 1974). These have also been attributed to chemical interactions between circulating seawater and the crust during hydrothermal activity.

#### D. OPHIOLITES.

Metal sulphide mineralisations and metal-enriched sediments are also associated with ophiolite complexes, which are generally considered to be vertical sections through the oceanic crust and upper mantle that have been obducted on to the continent along convergent plate margins. The ophiolites consist of an assemblage of peridotite and gabbro that grade upwards into pillow basalts, various units of which have been metamorphosed before tectonic emplacement. Oxygen isotope data from the metabasic rocks indicate that they were produced during interaction of the rocks with seawater (Spooner et al,

1974). Basaltic lava flows may be interbedded with metal-enriched sediments, as in the Troodos Massif in Cyprus (Corliss et al, 1972), or overlain by metalliferous deposits in association with chert, as in the northern Apennine ophiolites (Bonatti et al, 1976). The upper unit of the ophiolites consists of marine sedimentary sequences, including limestones and chert. The composition of the ophiolitic metalliferous sediments is very similar to that of the deposits on the active spreading centres, and they probably formed through the same process of hydrothermal precipitation that has been inferred to be occurring at the ridges.

Metal sulphide deposits often occur within the basaltic unit of the ophiolites, both as massive ore bodies and as disseminated mineralisations. Pyrite and chalcopyrite are usually the most prevalent minerals (Bonatti et al, 1976) and these deposits are thought to have been formed at the ridges by a hydrothermal deposition mechanism (Elderfield et al, 1972; Sillitoe, 1973; Constantinou and Govett, 1973).

In summary, a considerable amount of geological, geochemical and geophysical evidence exists to support the hypothesis that hydrothermal circulation occurs at the active spreading centres. However, much of the geological and geochemical evidence depends on the occurrence of anomalous deposits that are thought to be produced by elemental exchange reactions between seawater and the oceanic crust. It is therefore essential to determine the basalt-seawater reactions and the related elemental exchanges in order to substantiate or refute these ideas, and to determine the significance of the chemical fluxes for geochemical mass balances.

### 1.3. HYDROTHERMAL CIRCULATION AND INFERRED EFFECTS.

#### A. CIRCULATION MODEL.

A number of workers have suggested models for the circulation process (e.g. Corliss, 1971; Lister, 1972; Williams et al, 1974). In general, these models suggest the following sequence of events. Magma is injected along a narrow zone at the ridge crest. The surface is cooled rapidly, and cracks propagate through the hot rock. This permits the overlying seawater to penetrate into the rock and to remove heat from the cooling crust. Chemical reactions between the rock and the circulating seawater at high temperatures may occur, changing the composition of the circulating fluid and altering the rock to various metamorphic grades. As the water is heated, density gradients will be set up, and the hot fluid will rise to be debouched on to the sea floor, where some of the trace elements leached from the rock will be precipitated, and thus form the metalliferous sediments.

There are two requirements for a hydrothermal circulation system to be set up. Firstly, there must be sufficient permeability for the seawater to circulate. Deffeyes (1970) estimated the fracture permeability by considering the flow between parallel plates, and calculated that fractures 0.035 cm. wide would allow circulation at geologically reasonable rates. Adequate permeability could therefore be provided by thermal contraction, normal faulting, and irregular contacts on the large scale, and by small cracks, veins and vesicles on the small scale. Lateral variations in permeability will also influence the position of the convective cells. As these fractures get blocked with sediment, and the veins become filled with secondary

minerals, the system will become sealed and prevent further hydrothermal circulation.

The second requirement is that there be a heat source of sufficient strength to create and maintain a convection system. This will obviously influence the position of the convection cells, and will also mean that the circulation tends to be sporadic in occurrence. As the circulating fluid removes heat from the rock by convection, the thermal gradients will decrease, and the circulation will eventually stop.

#### B. INFERRED EFFECTS.

The observations regarding heat flow, metalliferous sediments, ophiolites and metamorphic rocks discussed in the previous section provide evidence that circulation occurs. Information concerning the directions of elemental fluxes during interaction between seawater and the circulating fluid, and inferences on the composition of the solutions, can be obtained from geothermal systems in volcanic regions or from direct experimental observations.

The Reykjanes geothermal system in Iceland represents a subaerial analogue to the hydrothermal systems envisaged beneath the mid-ocean ridges (Tomasson and Kristmannsdóttir, 1972; Björnsson et al, 1972). In this area, the circulating fluid, which is originally seawater, reacts with basalt at temperatures ranging from 10- 280°C. Chemical analyses of water from the drillholes (Table 1-1) indicate that the concentrations of  $Mg^{2+}$  and  $SO_4^{2-}$  decrease considerably, while  $Ca^{2+}$ ,  $K^+$ , and  $SiO_2$  increase substantially. In addition, Fe, Mn and the trace elements Ba, Mo, Ga, and V also become enriched in the drillhole water.

TABLE 1-1. Compositions of Fluids from Reykjanes Geothermal System and from Experimental Basalt-Seawater Reactions.

(Concentrations in ppm)

Land Geothermal System	Water to Rock Ratio	Temp. (°C)	SiO <sub>2</sub>	Na	K	Ca	Mg	SO <sub>4</sub> <sup>2-</sup>	B	Fe	Mn
Reykjanes Spring <sup>1</sup>	--	99	544	14325	1670	2260	123	206	12.0	0.2	--
Reykjanes <sup>1</sup> - Drill Hole 2	--	221	374	10440	1382	1812	8	72	11.6	0.5	--
Reykjanes <sup>1</sup> - Drill Hole 8	--	277	636	9610	1348	1530	16	30.8	7 <sup>2</sup>	0.5 <sup>2</sup>	2.0 <sup>2</sup>
<u>Experimental</u>											
<sup>3</sup> Seawater reacted with basalt for 4752 hrs.; 500 bars	10:1	200	800	--	530	900	30	60	--	5	5
<sup>4</sup> Seawater reacted with basalt for 336 hrs.; 500 bars	5:1	200	574	11350	365	1400	3.6	--	--	0.4	0.26
<sup>5</sup> Seawater reacted with basalt for 14,448 hrs.; 500 bars	1:1	200	633	11235	628	917	200	290	4.1	12	16
<sup>5</sup> Seawater reacted with basalt for 6432 hrs.; 1000 bars	1:1	500	1832	11322	1107	425	14.6	131	9.9	653	116
Seawater	--	25	3	10520	416	386	1282	2640	~5	<0.01	<0.01

<sup>1</sup>Bjornsson et al. (1972); <sup>2</sup>Mottl et al. (1975); <sup>3</sup>Bischoff and Dickson (1975); <sup>4</sup>Hajash (1975); <sup>5</sup>Mottl (1976).



However, there are some problems associated with direct application of these data to subsea floor hydrothermal systems. The major difference is that boiling of water probably will not occur in the ocean ridge systems (Spooner and Fyfe, 1973), and so chemical effects caused by boiling, seen in some regions of the Reykjanes area, will not be observed. In addition, the volcanic rock in the Reykjanes area is composed of considerable amounts of tuffaceous material, which may react with seawater differently from the massive pillows and flows of the oceanic crust. Furthermore, the mineral assemblages described in the Reykjanes system are different from those observed in dredged, metamorphosed oceanic rocks. In particular, anhydrite, K-feldspar and calcite are found in abundance in the Reykjanes area, but actinolite and talc are absent.

Experimental studies, carried out under various conditions of temperature and pressure (Bischoff and Dickson, 1975; Hajash, 1975; Mottl, 1974, 1976) have also shown the same directions of elemental fluxes as seen in Iceland (Table 1-1), but again the mineral assemblages produced show marked differences from the typical greenschist assemblages. Neither chlorite nor epidote have been identified in the experiments, and actinolite does not form until temperatures of 400°C are reached - an observation that is in conflict with the isotopically-deduced temperatures for the alteration of oceanic rocks. In addition, ground rock powders are used in these experiments which means that the 'wall rock' effects, seen in the dredged samples, are not reproduced. The water-to-rock ratios that have been used have been quite low (less than 10:1), whereas in the subsea

floor system, they may be higher and very variable. The other factor that must be considered is that these experiments deal with rock-seawater interactions in a closed system, so elemental changes will approach equilibrium between the solid and liquid phase - a situation that is probably not the case in the subsea floor systems.

However, with these reservations, the experimental data and the Reykjanes drillhole data do corroborate the hypothesis that interactions between seawater and basalt at elevated temperatures can occur, and provide a mechanism for elemental exchange between the lithosphere and hydrosphere. The results from the studies of these systems need to be compared with the observations and measurements made in the natural system; this will be one of the aims of this thesis.

1.4. EXPERIMENTAL DESIGN.

A. SELECTION OF SAMPLE TYPE.

In order to evaluate the importance of hydrothermal alteration for elemental geochemical budgets, it is necessary to determine, and study, the most abundant rock types that constitute that portion of the oceanic crust which is subject to hydrothermal circulation.

Dredging introduces a bias into the sampling, as it is always carried out on tectonic escarpments, and so it is not completely certain whether the recovered rocks are representative of the oceanic crust, or are associated exclusively with tectonic features. However, sufficient dredge hauls of tholeiitic basalt have now been recovered to indicate that this rock type is a major component of the upper crust, and drilling into the oceanic basement near ridges and in the basins has confirmed that this is true for at least the upper few hundred metres.

Additional evidence, and further constraints on the other feasible rock types, are provided by geophysical data. The magnetic properties (natural remanent intensity and susceptibility) of various rock types have been compared with transoceanic profiles to determine which rocks are compatible with the anomaly patterns (Fox and Opdyke, 1973). Only two oceanic rock types, basalt and serpentinised peridotite, have intensities strong enough to produce the observed anomalies. The magnetic layer comprises the upper few hundred metres of Layer 2 (Vine, 1968), and since this is known to be composed of basaltic flows and pillows from bottom photographs and DSDP cores, serpentinised peridotite can be excluded as a major component of this layer; also its intensities are too high to be an important component

in any other region of the oceanic crust. The intensities of metabasalts, gabbros, metagabbros and actinolite-rich rocks suggest that they could be components of the lower part of Layer 2, and Layer 3.

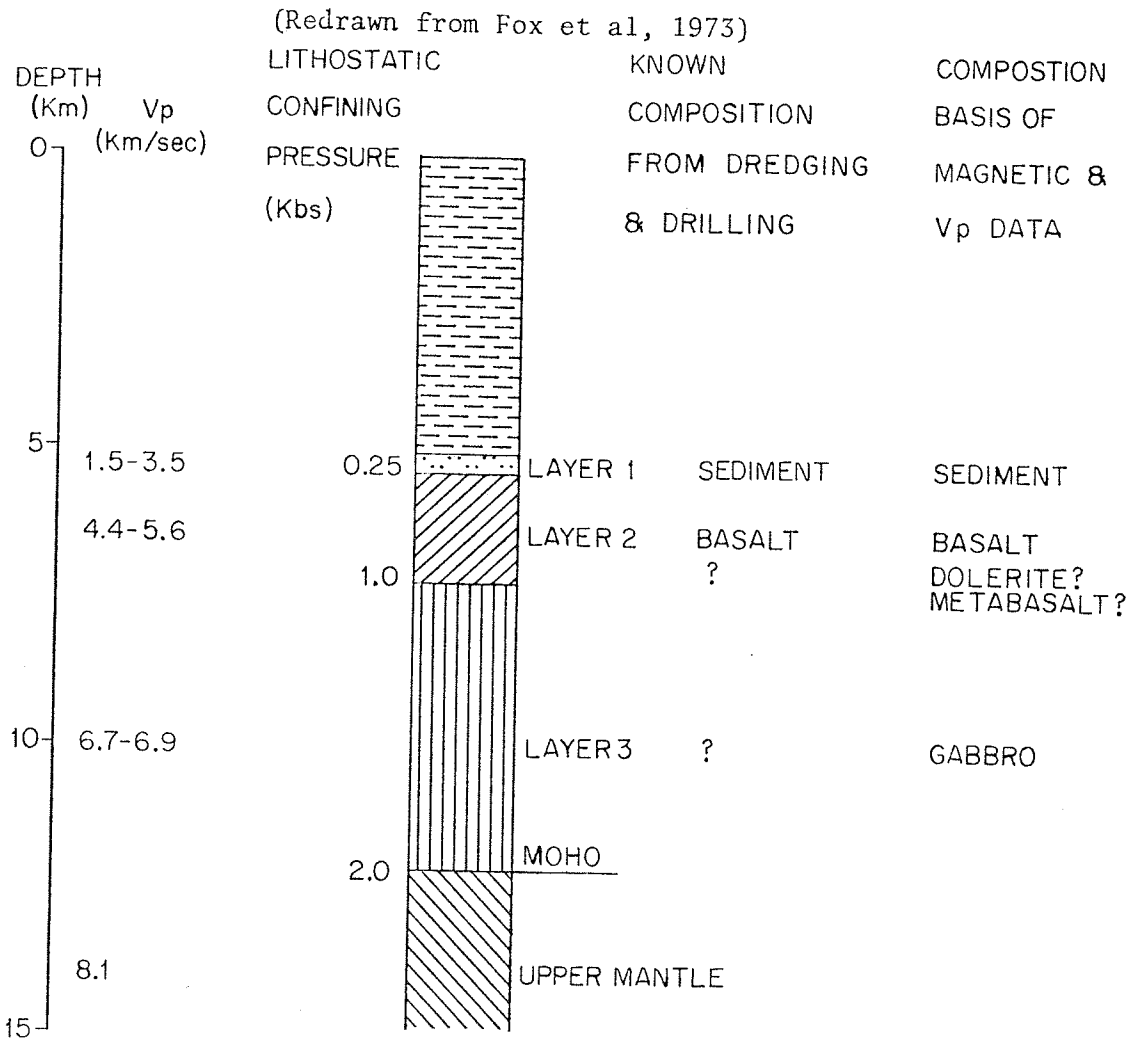
Compressional wave velocity measurements on the same variety of rocks at in situ pressures have been compared with seismic refraction results from the oceans (Fox et al, 1973). The measured velocities of metagabbro ( $V_p = 5.8 - 6.4$  km/sec) and serpentinised peridotite ( $V_p = 3.4 - 4.2$  km/sec) are not compatible with the velocity structure of the ocean basins. Layer 2, with compressional wave velocities falling mainly in the range 4.4 - 5.6 km/sec, may be composed of basalt ( $V_p = 5.0 - 5.8$  km/sec), dolerite ( $V_p = 4.6 - 5.8$  km/sec) or metabasalt ( $V_p = 4.3 - 5.4$  km/sec). Layer 3 is probably composed of gabbro ( $V_p = 6.7 - 6.9$  km/sec). A generalised oceanic crustal structure, based on all this information, is shown in Fig. 1-2. It is generally accepted that the most abundant rock type that is exposed to seawater circulation is tholeiitic basalt, and hence a study of the basalt-seawater interactions will be the most meaningful for geochemical mass balances.

#### B. SELECTION OF SPECIFIC SAMPLES.

Two criteria were used for the selection of the samples. Oceanic basalts vary in major and trace element composition mostly in response to fractional crystallisation processes (e.g. Thompson et al, 1972b; Thompson, 1973b). Thus, the quantification of the elemental exchanges during hydrothermal alteration is more meaningful when the precursor of the altered rock is known, and is required for careful mass balances between original and altered rock. Therefore, where possible, samples were selected that showed various degrees of alteration within a

FIGURE 1-2.

Velocity structure and possible composition of the oceanic crust.



single rock (an example is shown in Fig. 1-3). Such basalts were available from two areas on the Mid-Atlantic Ridge; 4°S latitude (cruise AII-42) and 22°S latitude (cruise AII-60). Samples that show a fresh core but an altered outer rim provide the best evidence that they have been affected by hydrothermal alteration. In addition, analyses of the two zones provide the most useful information as to the directions and magnitudes of elemental fluxes for use in geochemical mass balance calculations.

These were supplemented by additional hydrothermally altered and fresh basalts from the same and other oceanic regions. The criteria used for the selection of these samples were that they should come from areas that had been intensively studied, and the composition of the fresh basalts had been characterized, or could be determined, by analyses of fresh basalts from the same dredge hauls that recovered the metamorphic rocks. Additional samples from 4°S and 22°S were selected, and also a set of samples from 22°N (cruise Ch-44). Dredge locations are reported in Table 1-2, and Fig. 1-4 shows their positions. On the one hand, limiting the samples to specific areas and, in many cases, to the same dredge haul, will minimize the variation in composition of the initial basalts. On the other hand, these areas are sufficiently widespread that the effects can be generally applied to the Mid-Atlantic Ridge region, and probably to the Mid-Indian Ocean Ridge system, from which metabasalts have been recovered (Cann, 1969; Chernyseva, 1971), and which has a similar spreading rate and topography to the Mid-Atlantic Ridge. In this manner, the effects of hydrothermal alteration on global mass balances can be quantitatively assessed.

FIGURE 1-3.

Hydrothermally altered pillow fragment (AII-60 2-142) showing two alteration zones surrounding the relatively fresh interior.

FIGURE 1-3.

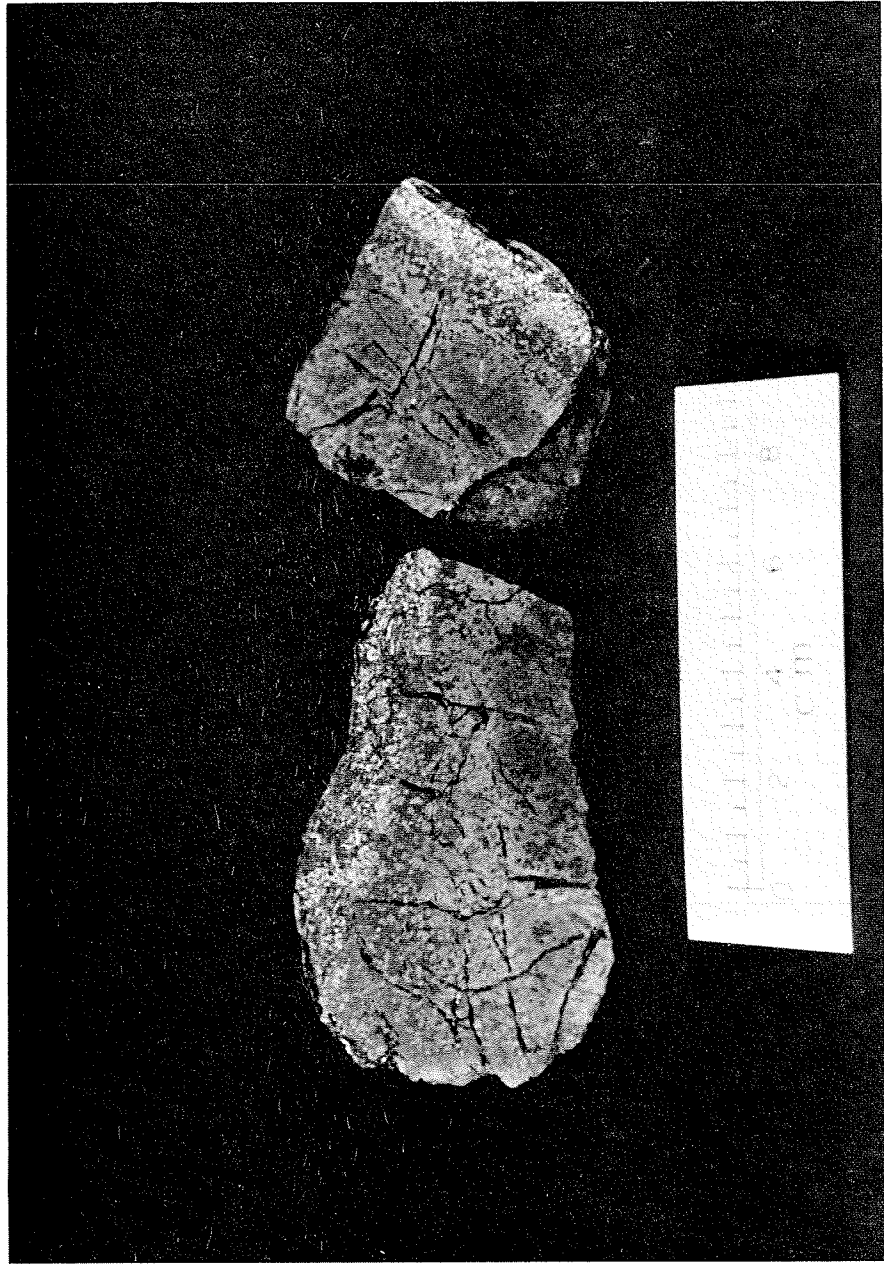




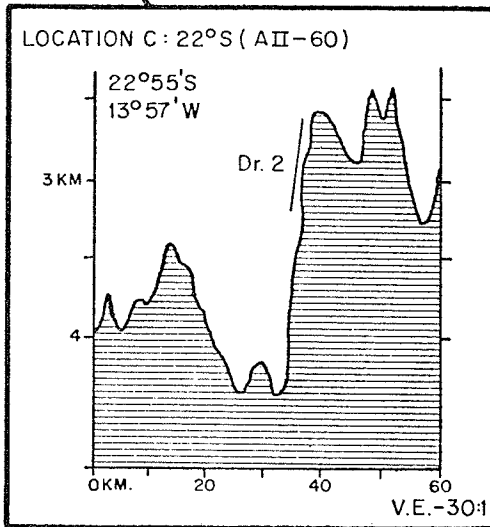
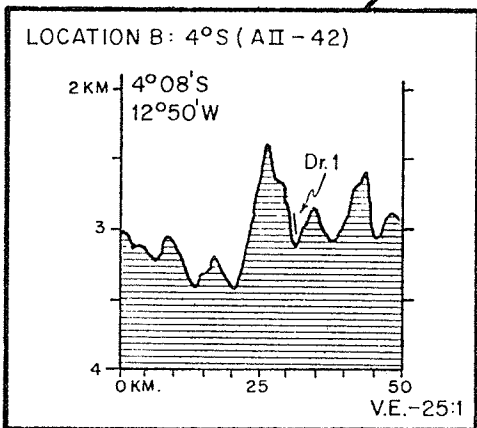
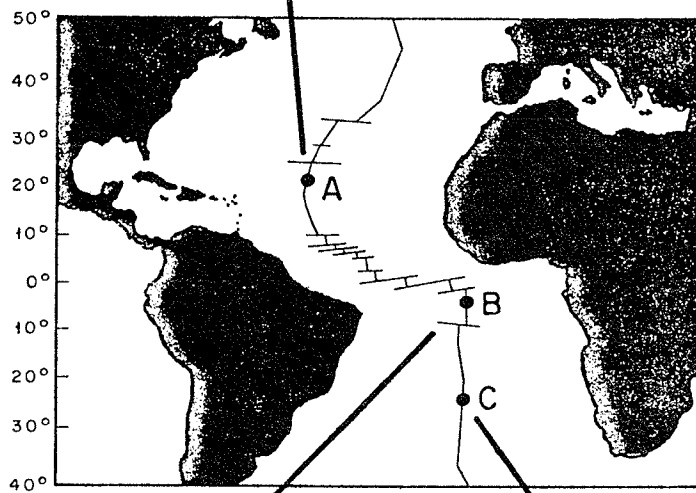
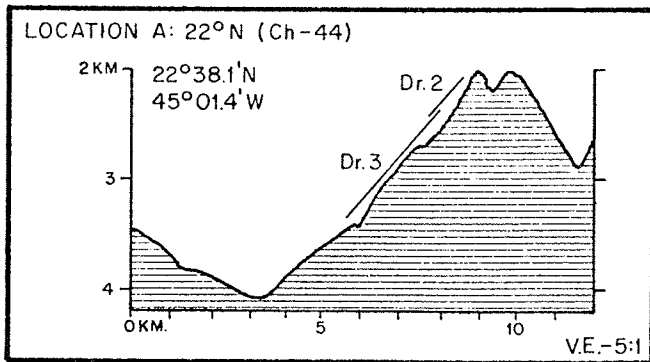
TABLE 1-2.  
Locations of Dredge Hauls from which Samples were  
Selected.

Dredge #.	Latitude	Longitude	*Region
Ch-44-2	22° 38' N.	44° 58' W.	Eastern slope- median valley
Ch-44-3	22° 38' N.	45° 00' W.	Eastern slope- median valley
AII-42-1	4° 08' to 4° 06' S.	12° 07' to 12° 09' W.	Eastern slope- median valley
AII-60-2	22° 55' to 22° 57' S.	13° 30' to 13° 32' W.	Eastern slope- median valley

\* - all from the Mid-Atlantic Ridge

FIGURE 1-4.  
Dredge locations and slope profiles.

FIGURE 1-4.



## 2. MINERALOGY AND PETROLOGY OF HYDROTHERMALLY ALTERED BASALTS FROM THE MID-ATLANTIC RIDGE

### 2.1

#### A. PREVIOUS STUDIES

The most commonly dredged rocks from the ocean floor are fresh or weathered tholeiitic basalts and gabbros. However, a wide variety of metamorphic rocks have been recovered from areas along the mid-ocean ridges in all three major ocean basins. Massive hydrothermal circulation beneath the mid-ocean ridges has been suggested as a mechanism for the alteration of these rocks. All the metamorphic rocks are hydrated, and oxygen isotope data for greenstones (Muehlenbachs and Clayton, 1972) suggest that the fluid involved in the alteration was probably seawater.

Table 2-1 shows some reported occurrences of metabasalts and metagabbros recovered from the ocean floor, together with their mineralogy, and the chemical changes due to alteration. Metabasalts and metagabbros occur in the zeolite, greenschist and amphibolite facies (Melson et al., 1966a, b; Cann and Funnell, 1967; Miyashiro et al., 1971), although greenschist facies metamorphism is probably the most abundant in the oceanic crust (Cann, 1969, 1971; Melson et al., 1968). Previous studies (Cann and Vine, 1966; Melson and Van Andel, 1966; Miyashiro et al., 1971) demonstrated that considerable mineralogical changes accompany hydrothermal alteration. During greenschist metamorphism, the mafic minerals are generally destroyed, calcic plagioclase becomes albitised and is partially replaced by chlorite, and a new mineral

TABLE 2-1. Some Reported Occurrences of Metabasalts and Metagabbros from the Ocean Floor.

Location	Facies	Mineralogy	Chemical Changes		Reference
			Gained by Rock	Lost from Rock	
Mid-Atlantic Ridge 53°N	Prehnite - pumpellyite?	Chlorite, epidote, prehnite, calcite, zeolites, Ca-plag., clinopyroxene	No Major Chemical Changes		Hekinian and Aumento (1973)
Bald Mountain 45°N, 29°W	Greenschist	Albite, tremolite, actinolite, chlorite, epidote, quartz, sphene, hornblende	H <sub>2</sub> O	CaO	Aumento and Loncarevic (1969)
-----					
	Zeolite	Analcite, stilbite, heulandite, zeolites in series natrolite-mesolite-scolectite	SiO <sub>2</sub> H <sub>2</sub> O	CaO Al <sub>2</sub> O <sub>3</sub>	
Crest Mountain, Mid-Atlantic Ridge 45°N	Greenschist	Albite, actinolite, chlorite, epidote, tremolite, quartz, talc, titanian maghemite	Na <sub>2</sub> O/K <sub>2</sub> O Increases		
	Amphibolite	1) Qtz., plag., biotite, hornblende, epidote, sericitized orthoclase, magnetite, sphene 2) Hornblende, diopside, plag., sericitized orthoclase, biotite		Very Little Overall Chemical Migration	Aumento et al. (1971)
-----					
Palmer Ridge 43°N	Amphibolite	Hornblende, plagioclase	No Major Chemical Changes		Cann and Funnell (1967) and Cann (1971)
-----					
Mid-Atlantic Ridge 30°N	Greenschist	Quartz, epidote, magnetite	No Chemical Analyses Reported		Quon and Ehlers (1963)

Cont....

Table 2-1 (Continued)

Location	Facies	Mineralogy	Chemical Changes		Reference
			Gained by Rock	Lost from Rock	
Mid-Atlantic Ridge 24°N and 30°N	Zeolite	Natrolite, thomsonite, analcime, chabazite, laumontite, stilbite, mixed layer chlorite - smectite and vermicu- lite	Na <sub>2</sub> O H <sub>2</sub> O	--	Miyashiro et al. (1971)
	Greenschist	Group I: Ca-plag., chlorite, actinolite, qtz. Group II: Chlorite and qtz. dominant, albite, actinolite, epidote	H <sub>2</sub> O H <sub>2</sub> O	CaO Fe <sub>2</sub> O <sub>3</sub> Variable SiO <sub>2</sub>	
	Amphibolite	Hornblende, plag., chlorite		No Major Chemical Changes	
Mid-Atlantic Ridge 22°N	Greenschist	Albite, chlorite, actinolite, epidote, nontronite, sphene.	SiO <sub>2</sub> H <sub>2</sub> O Fe <sub>2</sub> O <sub>3</sub> Na <sub>2</sub> O MgO	K <sub>2</sub> O CaO	Melson and Van Andel (1966) and Melson et al. (1968)
	Greenschist	Chlorite, albite, actinolite, sphene		No Chemical Analyses Reported	Melson and Thompson (1971)
Mid-Atlantic Ridge 10°N to 3°S	Greenschist	Albite, actinolite, chlorite, epidote		No Chemical Analyses Reported	Bonatti et al. (1971) and Bonatti et al. (1975)
	Amphibolised gabbro	Calcic palg., hornblende			

Cont...

Chemical Changes

Location	Facies	Mineralogy	Gained by Rock	Lost from Rock	Reference
Mid-Atlantic Ridge 50°N	Greenschist	Apatite, haematite, ilmenite, albite, muscovite, epidote, chlorite, calcite, qtz.	SiO <sub>2</sub> Na <sub>2</sub> O H <sub>2</sub> O	CaO	Ozima et al. (1976)
Mid-Atlantic Ridge 1°S	Amphibolite	Hornblende, plag., actinolite, leucoxene	No Chemical Analyses Reported		Bogdanov and Ploshko (1967)
Mid-Atlantic Ridge 4°S	Greenschist	Chlorite, albite, actinolite	H <sub>2</sub> O Na <sub>2</sub> O	CaO	Thompson and Melson (1972)
Carlsberg Ridge, Indian Ocean 5°N	Greenschist	Albite, chlorite, augite, sphene, actinolite, epidote (in glass - chlorite dominant)	1) Alteration of Glass FeO* MgO H <sub>2</sub> O 2) Alteration of Pillow Interior SiO <sub>2</sub> Al <sub>2</sub> O <sub>3</sub> Na <sub>2</sub> O H <sub>2</sub> O	SiO <sub>2</sub> CaO Na <sub>2</sub> O CaO	Cann (1969)
Carlsberg Ridge 5°N	Greenschist transitional to amphibolite?	Hornblende, plag., clinzoisite, chlorite, sphene	No Chemical Analyses Reported		Cann and Vine (1966)
Carlsberg Ridge 2°N	Greenschist	Albite, chlorite, epidote	No Chemical Analyses Reported		Hekinian (1968)
Arabian-Indian Ridge 5°N	Greenschist	Amphibole, albite, chlorite, epidote, qtz.	Na <sub>2</sub> O H <sub>2</sub> O	CaO	Chernysheva (1971)

Cont...

Table 2-1 (Continued)

Location	Facies	Mineralogy	Chemical Changes			References
			Gained by Rock	Lost from Rock		
Arabian-Indian Ridge 50S	Amphibolite	Hornblende, qtz. actinolite, chlorite, sphene rutile, apatite	No Chemical Analyses Reported			Rozanova and Baturin (1971)
Mid-Atlantic Ridge 24° to 30°N	Zeolite	Smectite, mixed-layer clay minerals, analcime, natrolite, thomsonite	Na <sub>2</sub> O K <sub>2</sub> O H <sub>2</sub> O* FeO	CaO		Shido et al. (1974)
	Greenschist	Chlorite, plag., actinolite, smectite	MgO FeO*	CaO		



assemblage is formed, consisting of varying proportions of albite, actinolite, chlorite and epidote. Subordinate minerals that have been reported include sphene, pyrite, nontronite, talc and quartz.

Basalt-seawater interactions in both the Reykjanes geothermal system and in experimental studies result in rather different alteration mineralogies from those observed in dredged metabasalts. The mineralogy of the Reykjanes geothermal system has been described by Tomasson and Kristmannsdottir (1972). The transition from zeolite to greenschist facies occurs between 200° and 300°C., with chlorite appearing at about 320°C., and epidote becoming a major phase at about 260°C. However, in contrast with the dredged metabasalts, actinolite is absent, while anhydrite, K-feldspar and calcite are present. In the experimental systems (Bischoff and Dickson, 1975; Hajash, 1975; Mottl, 1976), neither chlorite nor epidote have been identified in the altered assemblage, and actinolite did not occur until the experiments were performed at 400°C. Other minerals that were found include pyrite, smectite, zeolites, albite, talc, anhydrite and quartz.

Hydrothermal alteration generally results in significant increases in  $H_2O^+$  and, to a lesser extent, in MgO and  $Na_2O$  contents, and a decrease in CaO and  $K_2O$  contents of the rock. However, mass balances and fluxes have not been calculated with respect to compositional variations between the fresh basalt and the altered outer rims of the pillows. Such calculations would be more meaningful in assessing the significance of hydrothermal alteration in elemental budgets, since the precursor of the altered rock is known.

## B. PRESENT STUDY.

In this chapter, I describe the petrography, mineral genesis, mineral and bulk analyses of selected hydrothermally altered basalts and their precursors. All the mineralogical and chemical analyses are listed in Appendix I. From these observations and analyses, the reactions between various minerals and seawater are delineated, and the mineralogical changes are assessed in terms of the bulk chemistry of the rocks.

The suite of samples used for this study was described in the previous chapter. A few of the metamorphic rocks have been reported previously by Melson and Van Andel (1966) and Melson et al (1968); additional greenstones from those same dredge hauls are described in this study. Samples from 4°S. (AII-42) are particularly amenable for this work because several of them show zones of progressive alteration which facilitate a study of the sequence of mineralogical transformations. A considerable amount of information is already available concerning the chemical composition and petrogenesis of unaltered rocks from 22°S. (AII-60) (Carroll, unpublished thesis, M.I.T.), which aids in the interpretation of metamorphic rocks from the same dredge hauls.

### 2.2. MINERALOGY OF GREENSCHIST FACIES METABASALTS.

All the samples are altered basaltic flows, and consist chiefly of the minerals albite, actinolite, chlorite, and epidote, which characterise greenschist facies metabasalts. Mineralogical differences between samples consist largely of differences in the proportions of these secondary

minerals, and in the degree to which the original mineral assemblage is still present. This latter feature of the rocks is helpful in elucidating the stages in the transformation of the source rock to a greenstone.

#### A. FRESH ROCKS

The fresh basalts found in the same dredge hauls, and the interiors of the pillows from which these altered samples are derived, are composed of glass containing microlites of plagioclase ( $An_{60-70}$ ) (Table AI-1), olivine (Table AI-2), and occasionally skeletal clinopyroxene, which is too small to be analyzed by microprobe. The larger microlites of plagioclase show the 'belt-buckle' structures typical of plagioclase in ocean floor basalts; the very fine microlites have a feathery texture. Occasional phenocrysts of plagioclase (up to  $An_{86}$ ), some of which are resorbed, and olivine ( $Fo_{80-85}$ ) occur. Clinopyroxene was not identified in the 4°S (AII-42) samples, which were more glassy and contained fewer phenocrysts than the 22°N (Ch-44) samples. However, the clinopyroxene in the samples from 22°N (Ch-44) and 22°S (AII-60) generally occurs in small aggregates associated with plagioclase laths. The vesicles in most of the fresh interiors are filled with chlorite, suggesting that they may have been subject to some slight alteration. Iron-titanium oxides are extremely fine-grained and are scattered throughout the rock.

#### B. FELDSPARS

The plagioclase in the altered samples has, in most cases, been albitised, although in some phenocrysts the original cores are preserved, and a few relict microlites and phenocrysts persist, suggesting that the

reaction was not completed. Twinning is still discernible in the unaltered cores of the phenocrysts, but it is destroyed by alteration. In some of the greenstones, both plagioclase and albite have been further altered to chlorite. Two other types of plagioclase alteration are observed. Calcic plagioclase phenocrysts are replaced by albite + epidote; the feldspar has a composition between An<sub>10</sub> and An<sub>15</sub>, and the epidote contains about 11.5% FeO\* (Tables AI-3 and AI-4). In the 22<sup>0</sup>N (Ch-44) samples, aggregates of pyroxene and plagioclase are commonly observed in the fresh samples. During alteration, these plagioclase-pyroxene aggregates are replaced by epidote and chlorite.

The microprobe analyses of several of the feldspars (Table AI-3) show that, although the fresh plagioclase contains varying amounts of FeO\* (0.1-0.9%) and MgO (0.1-0.3%), the altered phenocrysts lose both elements during albitisation, the MgO decreasing to below detection limits at about An<sub>15</sub>, and the FeO\* decreasing to below detection limits at a lower anorthite content.

### C. CHLORITE

The olivine phenocrysts are generally replaced by chlorite and, in many cases, by euhedral pyrite. This is particularly evident in the 4<sup>0</sup>S (AII-42) samples, but in the 22<sup>0</sup>N (Ch-44) samples, olivine is more frequently replaced only by chlorite. The chlorite is extremely fine-grained, appears green to brown in thin section, and gives anomalous blue interference colors. Microprobe analyses using a defocussed beam indicate that it is ripidolitic in composition (Table AI-5) with MgO/FeO\*

of about one, and there are no detectable compositional variations between the chlorite in different mineralogical settings. Chlorite comprises the principal vesicle filling, although, in the more highly altered samples, the quartz also occurs in the vesicles. Chlorite is abundant in veins, where it may be associated with epidote, quartz, actinolite, and occasionally pyrite. Chlorite and actinolite are intergrown as the replacement minerals of the glassy matrix. However, in the more strongly altered samples, these are often accompanied by albite and quartz.

#### D. ACTINOLITE

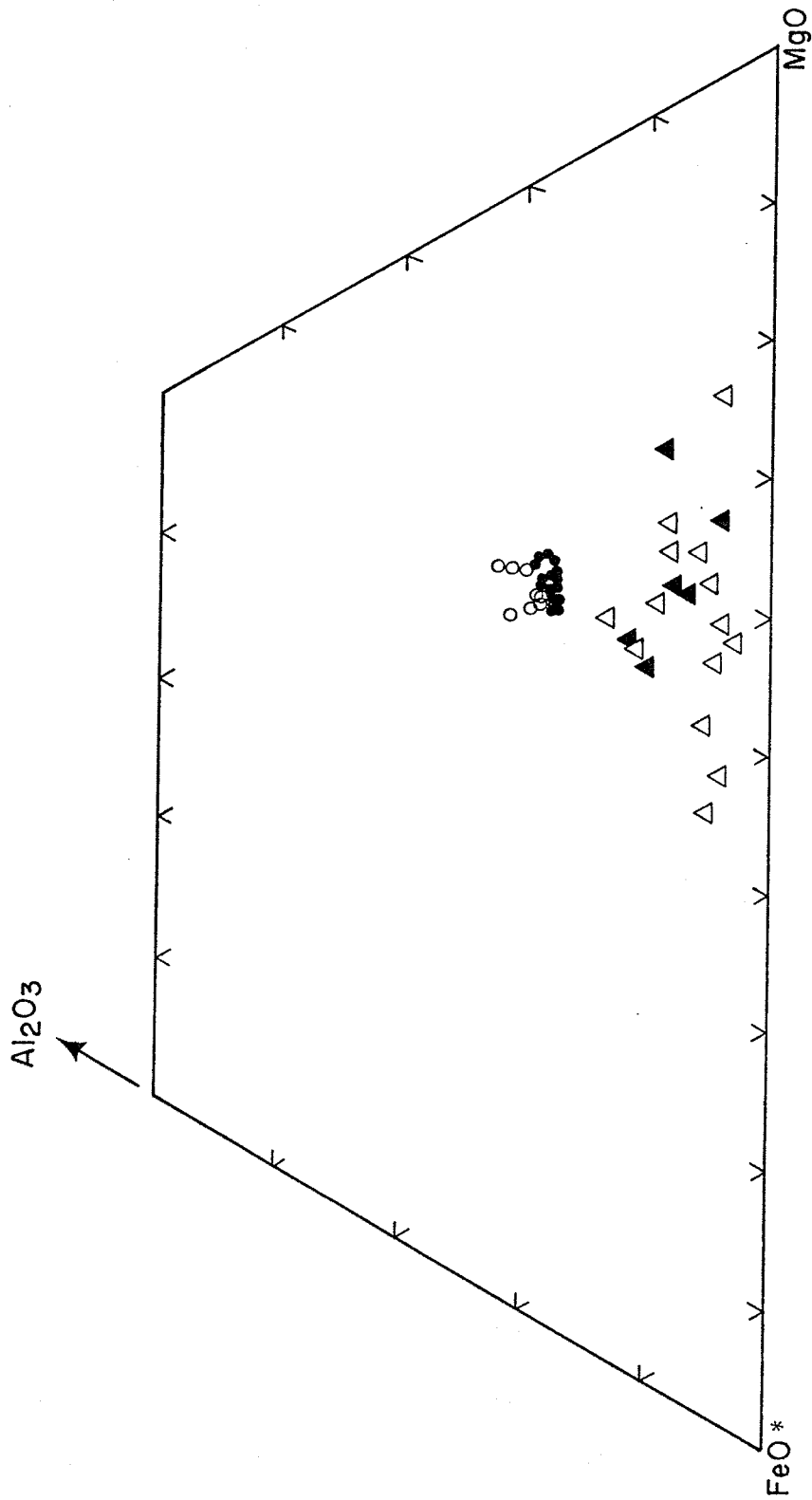
The actinolite is very variable in composition (Table AI-6) and in optical properties. It is colorless to pale green in thin section and generally occurs in fibrous aggregates or small needle-like crystals. The actinolites range in composition from 3-7%  $Al_2O_3$  and contain up to 17% total iron. Figure 2-1 shows the compositions of the actinolites and chlorites plotted on an  $Al_2O_3$ -FeO<sup>\*</sup>-MgO diagram. Although the chlorites show very little variation, the actinolites show a wide range in composition even in a single rock; this is an indication that equilibrium was not attained in the formation of actinolite. The actinolite replaces the groundmass, and also occurs in veins, usually associated with quartz and chlorite. In sample Ch-44 3-12, actinolite also replaces pyroxene microphenocrysts. However, no systematic differences between the compositions of actinolite in these various mineralogic settings are evident.

FIGURE 2-1.

Compositions of actinolites (triangles) and chlorites (circles) plotted on an  $\text{Al}_2\text{O}_3$  -  $\text{FeO}^*$  -  $\text{MgO}$  diagram.

Data listed in Tables AI-5 and AI-6.  
Analyses for Ch-44 3-3 and 3-6 (open circles and triangles) from Fig. 4 of Melson and Van Andel (1966)

FIGURE 2-1.



#### E. EPIDOTE

Epidote occurs in concentrations ranging from zero to 25% by volume. In most of these samples, large, euhedral crystals fill veins and are usually associated with quartz and chlorite. However, in some samples it is also present as a replacement of plagioclase and in aggregates in the groundmass, as previously discussed.

#### F. QUARTZ

Quartz is present in veins, in the matrix, and in vesicle fillings. It is present only in minor amounts in the 22<sup>0</sup>N (Ch-44) samples, but is more abundant (up to 20% by volume) in some of the altered margins of the 4<sup>0</sup>S (AII-42) rocks. These margins are frequently brecciated, and the chlorite of the groundmass is often associated with albite and quartz.

#### G. PYRITE

Pyrite occurs as small euhedral crystals associated with chlorite pseudomorphs after olivine, in veins, and also in small patches within the matrix. In many cases, it has been partially oxidized to haematite, probably during later exposure to seawater at ambient bottom water temperatures. It is more abundant in the 4<sup>0</sup>S (AII-42) and 22<sup>0</sup>S (AII-60) samples than in the 22<sup>0</sup>N (Ch-44) samples, and in AII-60 2-143 forms a large pod at the termination of a vein. Use of the scanning facility on the electron microprobe indicates that pure pyrite is present in the patches within the matrix and the crystals associated with the chlorite pseudomorphs. However, in the veins, copper and zinc sulphides are also present, as shown in Figure 2-2.



FIGURE 2-2.

Scanning electron micrographs of iron (a), sulphur (b),  
copper (c), and zinc (d) for a sulphide vein in sample  
AII-60 2-141.

(Magnification: x300)

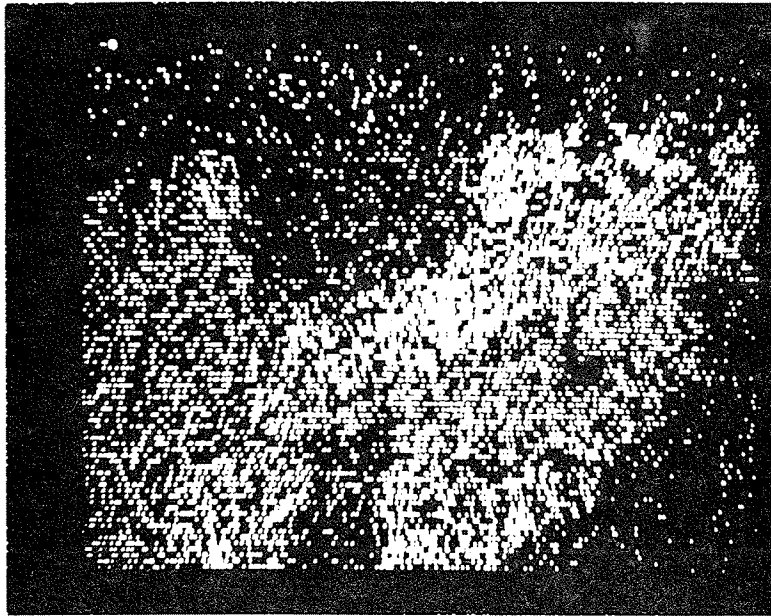


FIGURE 2-2 a) IRON

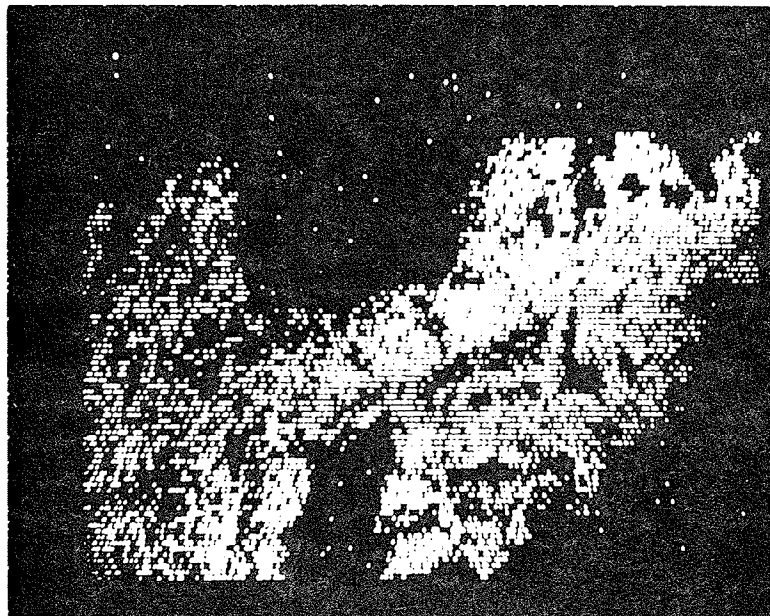


FIGURE 2-2 b) SULPHUR

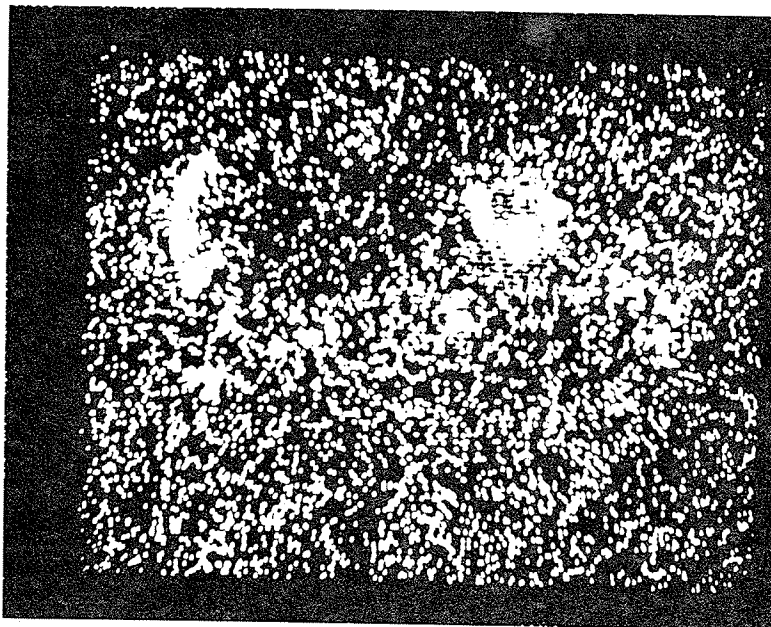


FIGURE 2-2 c) COPPER

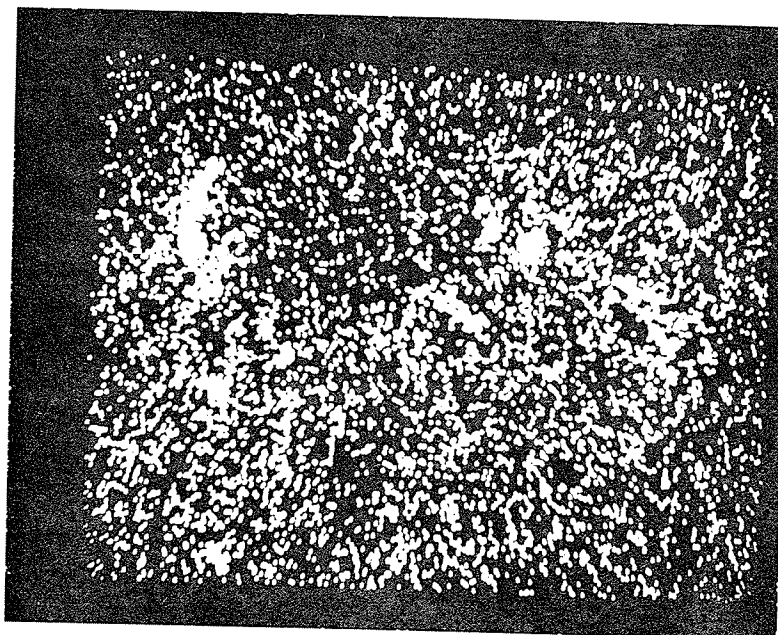


FIGURE 2-2 d) ZINC

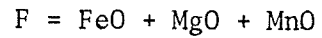
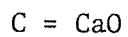
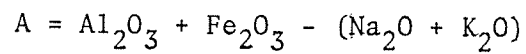
### 2.3 BULK CHEMICAL COMPOSITION

The chemical compositions of the samples are reported in Table AI-7. Major element analyses were determined by electron microprobe analyses of fluxed glasses. Ferrous iron was analyzed by titration, and  $H_2O^+$  was determined using a C-H-N analyzer. Full details of all methods, and their precision and accuracy, are reported in Appendix II. These analyses are plotted on an ACF diagram (where  $A = Al_2O_3 + Fe_2O_3 - (Na_2O + K_2O)$ ,  $C = CaO$ , and  $F = FeO + MgO + MnO$ ) in Figure 2-3 for comparison with the modal analyses (Table AI-8). The epidote, chlorite and actinolite fields are based on the microprobe analyses (Tables AI-4 to AI-6), with all the iron assumed to be ferrous iron in actinolite and chlorite, and ferric iron in the epidote.

As previously indicated by Melson and Van Andel (1966), a separation between rock types according to their mineralogies, is observed. The epidote-rich rocks are Ca-rich compared with the fresh samples, while the chlorite-rich assemblages plot closer to the A-F join. The modal analyses suggest that a division between these two types can be made so that the chlorite-rich rocks contain more than 15% chlorite and less than 15% epidote. The chlorite-rich assemblage type includes all the altered samples from AII-42 ( $4^0S$ ) and AII-60 ( $22^0S$ ), and samples 2-5, 3-3, 3-6, 3-17, and 3-126 from Ch-44 ( $22^0N$ ). Sample Ch-44 3-8 is also included as although about 40% of the groundmass is unaltered, it shows the stages

FIGURE 2-3.

ACF diagram of greenschist facies metabasalts.



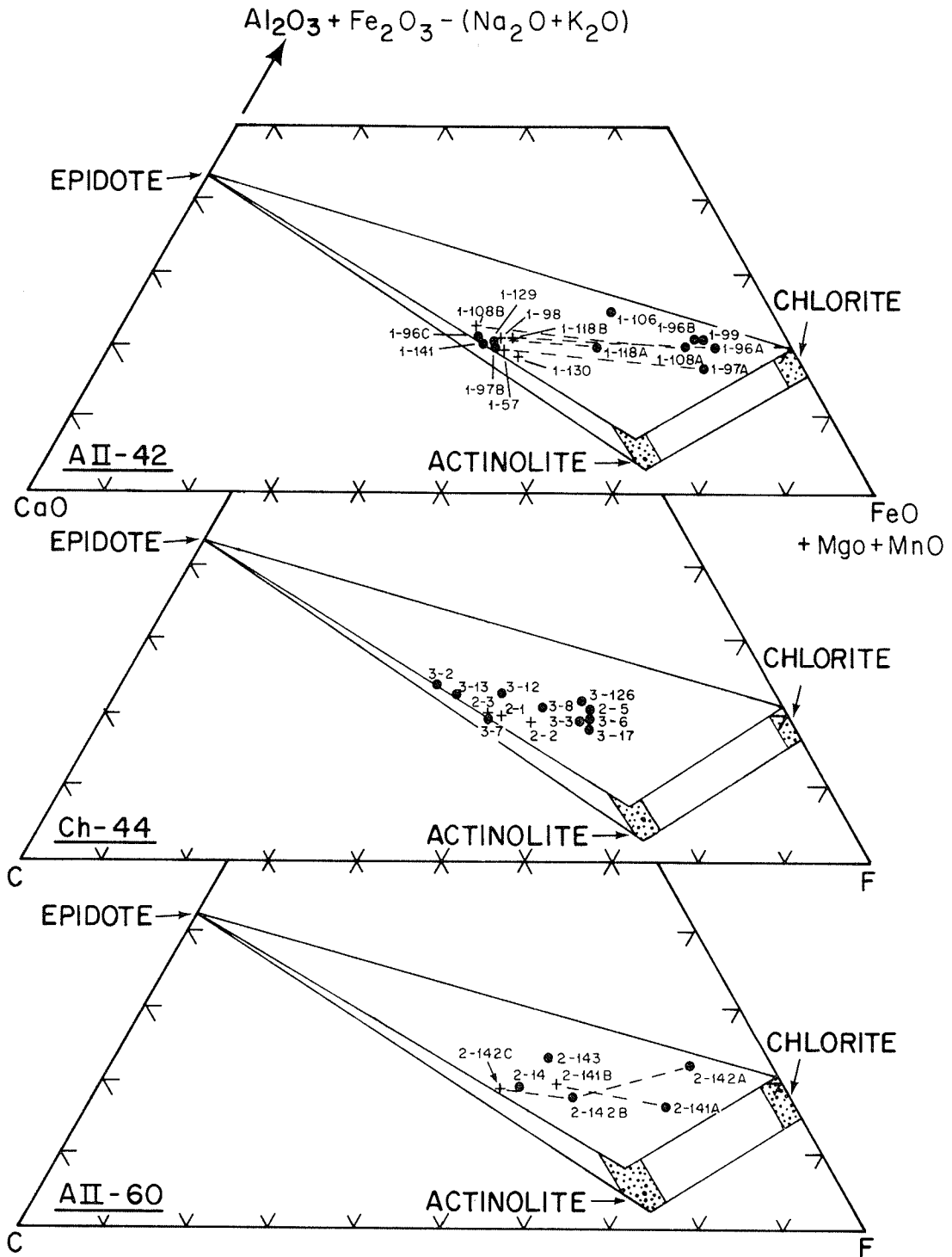
Mineral composition fields from microprobe analyses in Tables  
AI-4 to AI-6.

+ - fresh basalts and interiors of pillows

• - altered samples

(tie lines join cores and rims of individual pillows).

FIGURE 2-3



in the transformation of a pyroxene-olivine-plagioclase assemblage to an albite-chlorite-actinolite assemblage, with little evidence of epidote as a major alteration product.

The agreement between the plotted chemical compositions of the samples and their modal analyses is reasonably good. For example, samples AII-60 2-142A and AII-42 1-99, which contain only small amounts of actinolite, plot close to the epidote-chlorite join, whereas the chlorite-rich samples of AII-42 and AII-60 plot closer to the chlorite corner. However, samples Ch-44 3-6, 2-5, and 3-17, and AII-42 1-118A do not contain as much epidote as would be predicted from the diagram. This lends further support to the idea that the reactions with seawater may not have gone to completion, as suggested by the mineralogical observations.

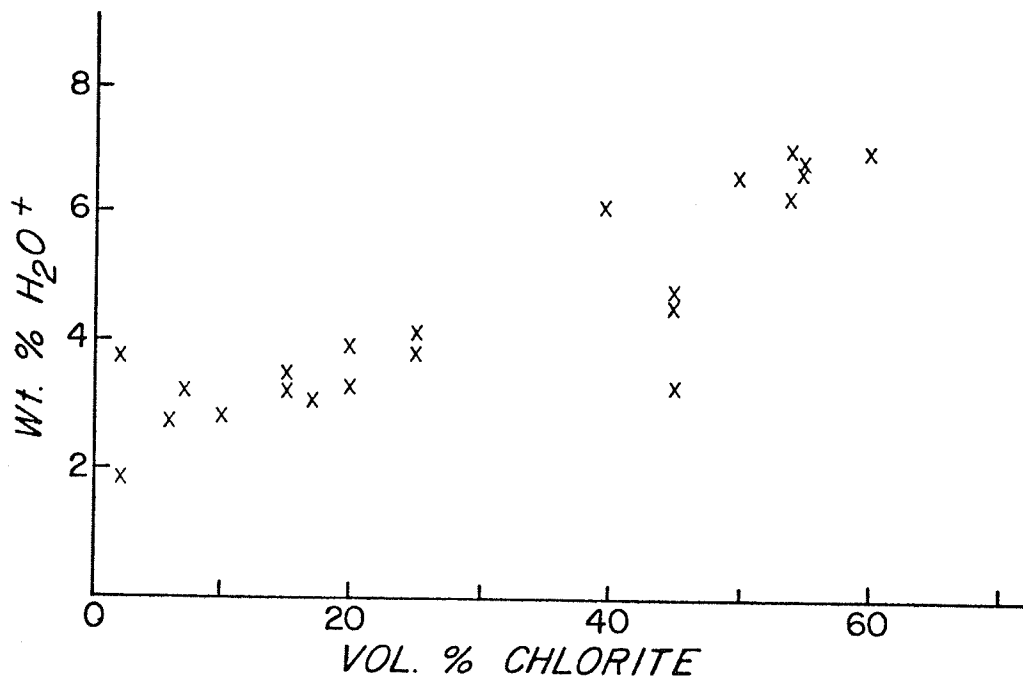
The subdivision of the samples into epidote-rich and chlorite-rich assemblages is also reflected in other aspects of their chemistry. In all the samples, there is a correlation between the amount of chlorite and the  $H_2O^+$  content (Figure 2-4). This relationship is to be expected because, of all the alteration products formed, chlorite is the most hydrated, and so plays the major role in the uptake of water during alteration. The changes in the MgO and CaO contents of the rocks during hydrothermal alteration are different for the two mineral assemblages. The epidote-rich assemblages have slightly lower MgO contents while the CaO stays constant or increases slightly relative to the fresh

FIGURE 2-4.

Correlation between wt.%  $H_2O^+$  and modal chlorite for all analysed greenschist facies metabasalts.



FIGURE 2-4.



samples (Figure 2-5). The chlorite-rich assemblages lose CaO and gain significant quantities of MgO due to the production of chlorite; these trends are particularly evident in the core-to-rim analyses.

The fluxes of iron and changes in oxidation state during hydrothermal alteration can also be correlated with the mineralogy (Figures 2-6 and 2-7). The epidote-rich assemblage appears to become more oxidized (i.e. lose FeO and gain  $Fe_2O_3$ ) relative to the fresh basalts. The epidote in these samples shows very little compositional variation, and it has been shown by numerous investigators that it is very insensitive to metamorphic grade (e.g. Cooper, 1972). However, its composition is dependent on the iron content of the rock, the oxidation state maintained during metamorphism, and temperature. Since the iron content of the source rocks does not vary greatly, the important factors may be the temperature and the oxidation state.

In the chlorite-rich assemblage, a further subdivision is necessary. The Ch-44 ( $22^{\circ}N$ ) samples show very little change in the FeO and  $Fe_2O_3$  contents during alteration suggesting that the same proportions of iron that were in the precursors have been taken up in the chlorites and actinolites. However, a small group of the AII-42 ( $4^{\circ}S$ ) samples and the AII-60

FIGURE 2-5.  
Magnesium vs. calcium contents for fresh and altered  
basalts.

(2-1, 2-2, and 2-3: fresh basalts from Ch-44)

(1-96A and B, and 1-118A and B: examples of rim (A)  
to core (B) trends in chlorite-rich assemblages)

• - 22°N. samples (Ch-44)

x - 4°S. samples (AII-42)

FIGURE 2-5.

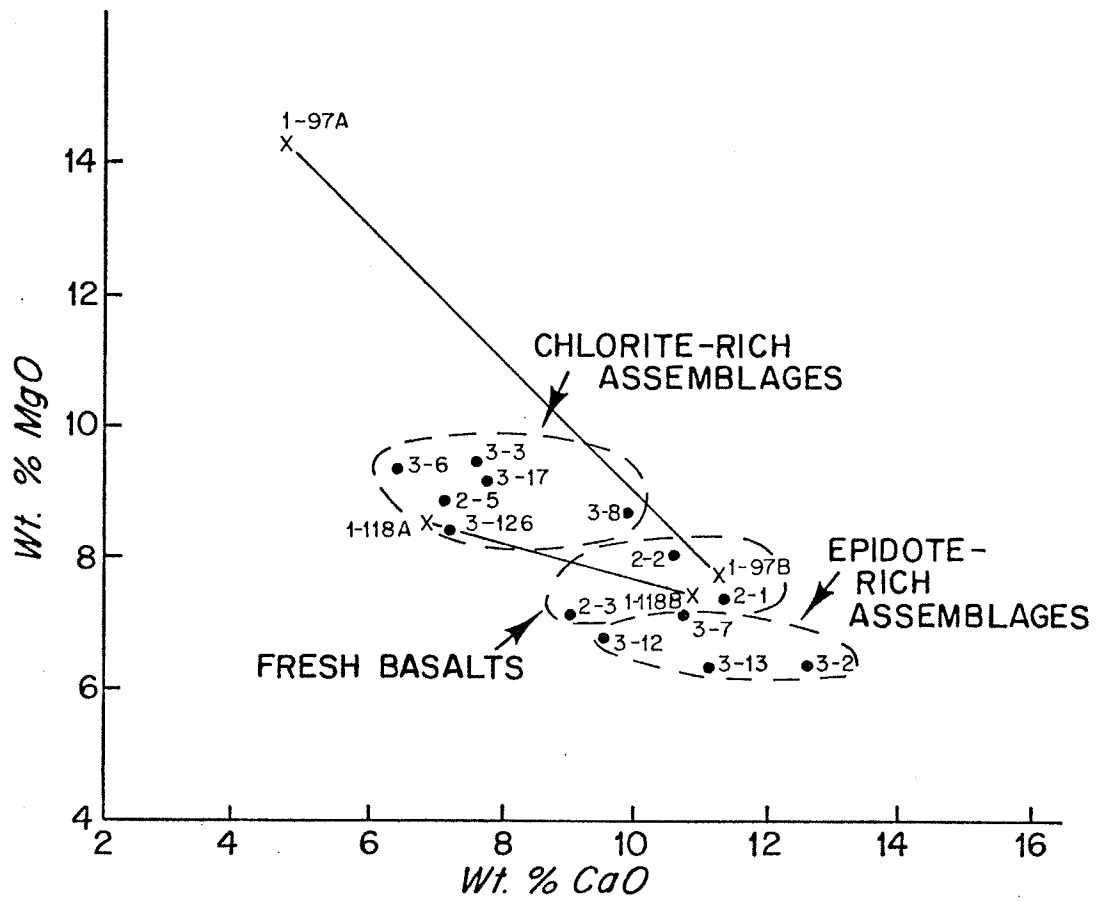


FIGURE 2-6.

Ferric iron trends vs. water content for hydrothermally altered basalts showing separation of different mineral assemblages.

(Symbols as for previous Figure).

-----DILUTION: apparent change in concentration  
of  $\text{Fe}_2\text{O}_3$  due to the uptake of water.

FIGURE 2-6.

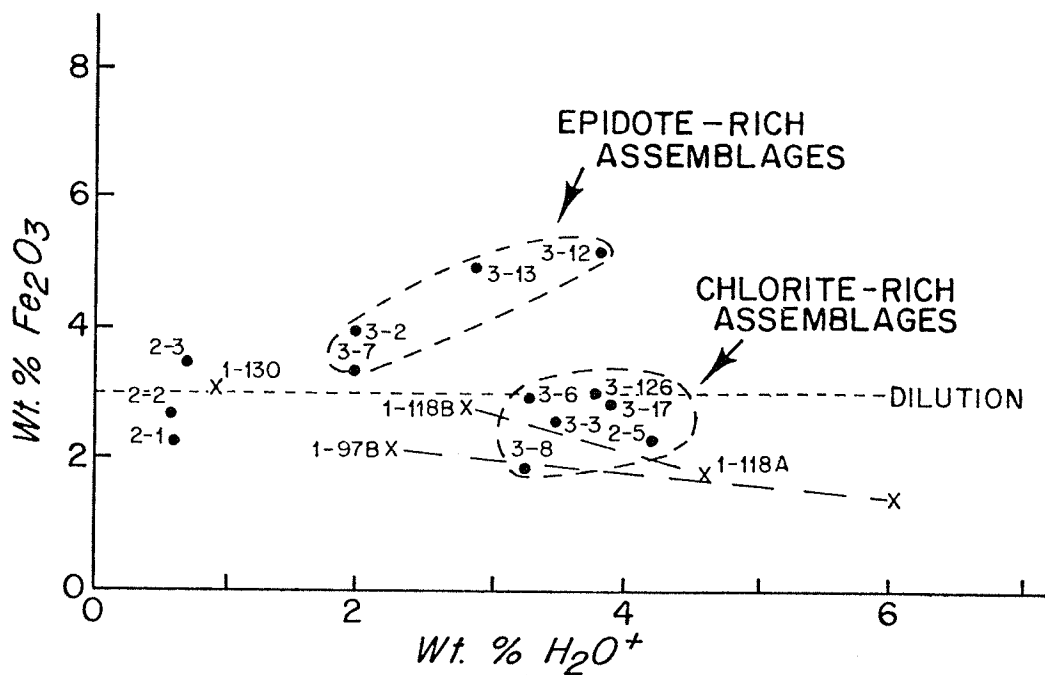
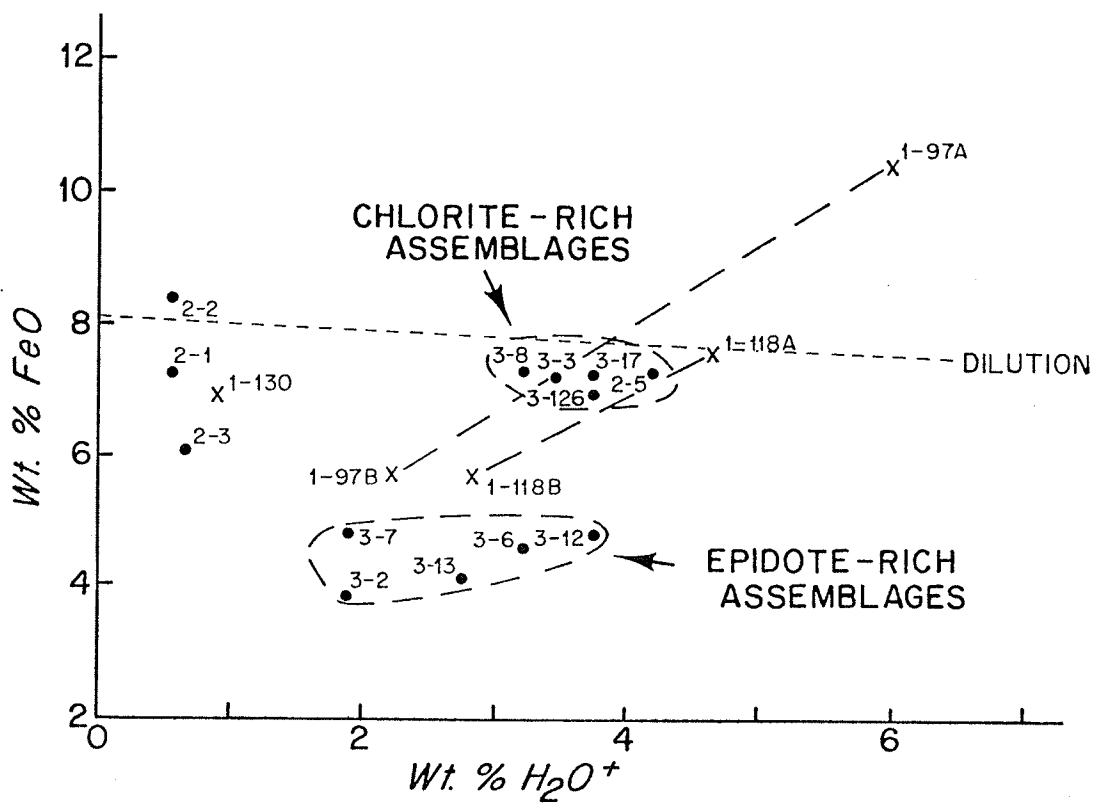


FIGURE 2-7.

Ferrous iron trends vs. water content for hydrothermally altered basalts showing separation of different mineral assemblages.

(Symbols as for previous Figures).

FIGURE 2-7.





( $^{22}\text{O}_2\text{S}$ ) samples show large increases in the FeO content and a smaller decrease in the  $\text{Fe}_2\text{O}_3$  content. These samples all contain pyrite, which suggests that they reacted with the circulating fluid under reducing conditions. In order for sulphate reduction to take place, the oxygen must have been removed from the fluid during previous basalt-seawater interactions. Since the total amount of iron in these samples also increases, an additional source of  $\text{Fe}^{2+}$  is also necessary; this could be provided by a fluid that had undergone previous reactions, during which iron had been leached from the rock.

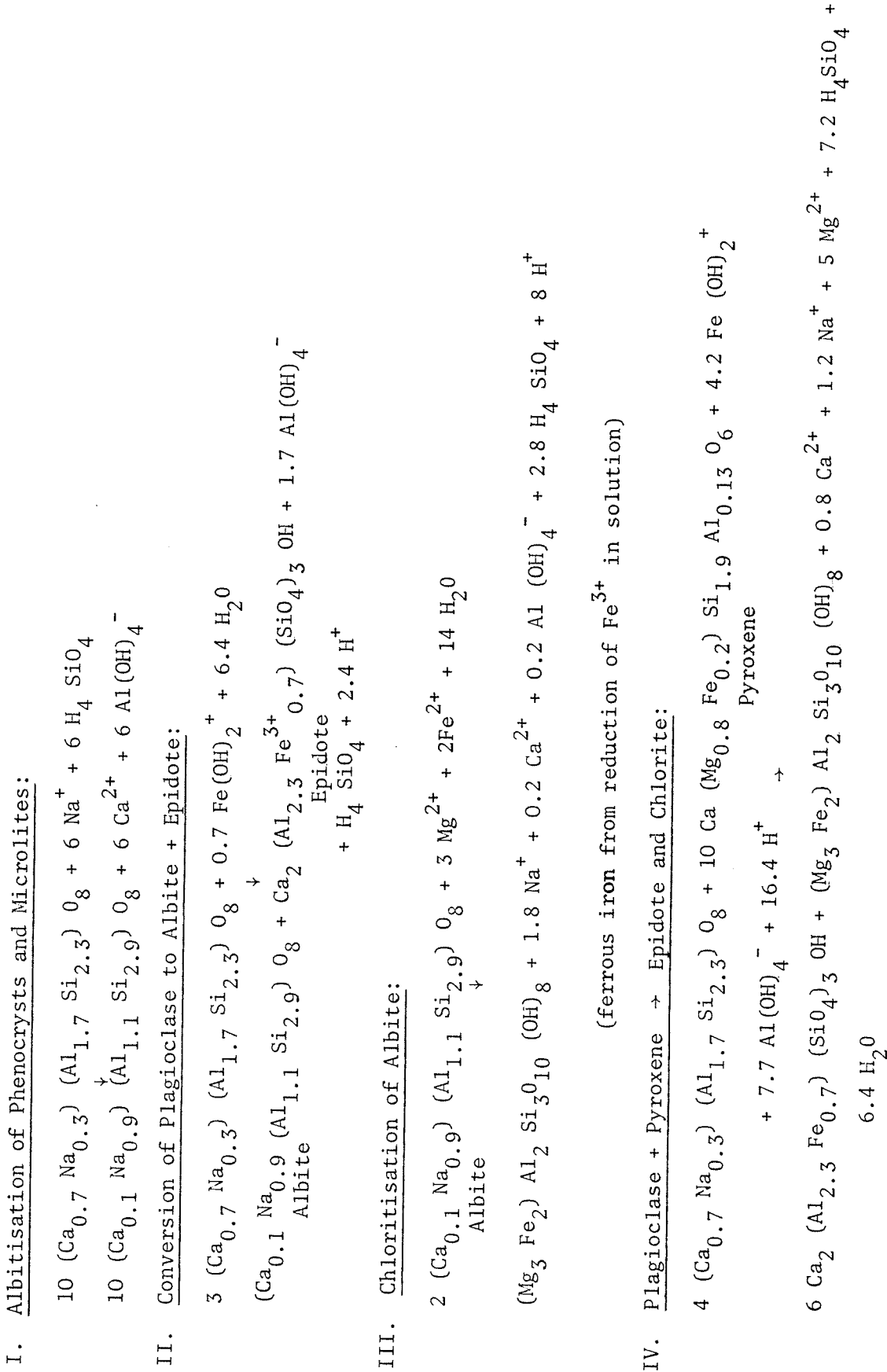
$\text{SiO}_2$  is generally removed into solution and most rocks show a loss of silica; however, the precipitation of quartz in veins occasionally gives a local increase. The concentrations of silica in solution is probably controlled by the solubility of quartz. This has been shown to be the case in the Reykjanes geothermal system (Arnorsson, 1970) and in laboratory experiments (Hajash, 1975).

## 2.4 MINERAL CONVERSIONS

### A. PLAGIOCLASE

Table 2-2 shows the reactions during hydrothermal alteration of plagioclase that are suggested from the mineralogical studies. The average compositions of the minerals are taken from electron microprobe analyses carried out on the fresh and altered samples (Tables AI-1 and AI-3). The speciation of dissolved iron in seawater is still controversial - the  $\text{Fe}(\text{OH})_2^+$  species used here is that suggested as the most probable by

TABLE 2-2. Reactions During Hydrothermal Alteration of Plagioclase.



Stumm and Brauner (1975). All the analyzed iron is assumed to be ferrous iron in actinolite and chlorite, and ferric iron in epidote, and the equations were constructed on the basis of conservation of charge.

The albitisation of the plagioclase microlites and phenocrysts (reaction I) is a simple ion exchange, with  $\text{Ca}^{2+}$  being replaced by  $\text{Na}^+$ . In order to conserve charge,  $\text{Al}^{3+}$  must be replaced by  $\text{Si}^{4+}$ ; this reaction will not alter the pH of the solution.

The conversion of plagioclase to albite and epidote, and the chloritisation of albite (reactions II and III) result in an increase in the activity of hydrogen ions in solution, while reaction IV, which was observed in only one or two samples, consume hydrogen ions. These three reactions all require a source of iron already present in the plagioclase structure. Reaction III necessitates a source of both magnesium and iron, both of which may be derived from the circulating fluid.

These reactions also demonstrate that when albite is chloritised, it releases the  $\text{Na}^+$  that was originally taken up during albitisation. Since the conversion of plagioclase to albite + epidote, which is the other principal reaction involving sodium, results in no exchange of sodium between solid and liquid phases, the overall effect of these reactions will be to show little change in the bulk rock analyses of sodium. The net flux of sodium will be determined by the extent of the initial albitisation of plagioclase, and the further chloritisation of the albite.

## B. OLIVINE AND PYROXENE

Alteration reactions involving olivine and pyroxene are listed in Table 2-3. Olivine has been observed to alter to chlorite, often with the production of euhedral pyrite. This conversion must involve a redox reaction. The only significant reducing agent in basalt is ferrous iron and this has the potential for reducing sulphate in seawater. Such a reduction may be via reaction V- a modification of a reaction suggested by Spooner and Fyfe (1973 - in which pyrite is formed, and the magnesium and silica released may then be used in the formation of chlorite. Reaction VI represents the simple conversion of olivine to chlorite.

Pyroxene microphenocrysts alter to amphibole by reaction VII. The amphibole composition is taken from the microprobe analyses (Table AI-6), with all the iron assumed to be  $Fe^{2+}$ . The other reaction, which has previously been discussed, is its conversion with plagioclase to epidote and chlorite.

These reactions result in the consumption of hydrogen ions and the release of magnesium and silica. The magnesium is then available for uptake in chlorite and actinolite during the alteration of the groundmass, and during the precipitation of chlorite in vesicles and veins. If the magnesium end member in the solid solution series for the composition of the secondary chlorite is considered then this reaction can be approximated by:

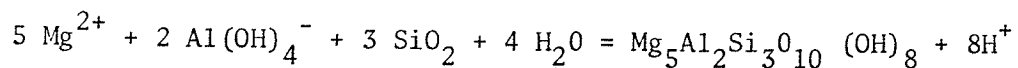
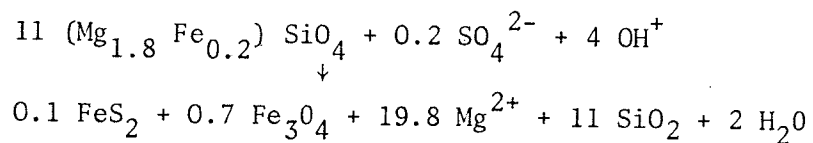
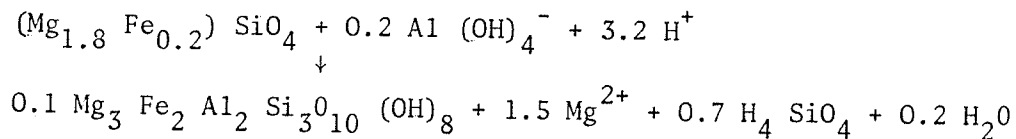


TABLE 2-3. Reactions During Hydrothermal Alteration of Olivine and Pyroxene.

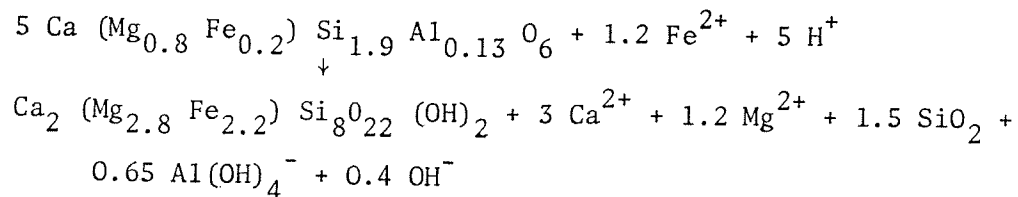
V. Redox Reaction:



VI. Olivine → Chlorite:



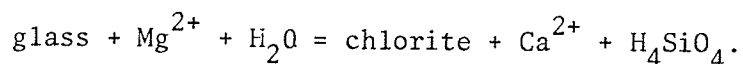
VII. Conversion of Pyroxene to Amphibole:



and demonstrates that magnesium and  $\text{OH}^-$  are extracted from seawater, so lowering the pH.

### C. ALTERATION OF THE GLASS MATRIX

Most of the samples consist of a few phenocrysts in a glassy matrix, which alters to chlorite commonly intergrown with actinolite. This reaction will release Ca,  $\text{SiO}_2$ , Fe, Mn, and possibly some of the trace elements, but  $\text{Mg}^{2+}$  will be removed from seawater and incorporated into the chlorite. In order to conserve charge,  $\text{OH}^-$  must also be removed from seawater, as shown in the equation above; this, together with the plagioclase alteration reactions, provide a mechanism for lowering pH, although subsequent reactions will offset some of this pH lowering. It is not possible to write a quantitative equation for this reaction because the stoichiometric composition of the glass is unknown. The overall reaction, without coefficients, can be represented by:



### 2.5. CONCLUSIONS

The results obtained from the petrographic observations, and the mineralogical and bulk chemical analyses are consistent with the following conclusions.

1) Greenschist facies metamorphism of oceanic basalts results in considerable mineralogical and chemical changes.

The major phenocryst transformations are:

- a) plagioclase → albite → chlorite  
                  <sup>x</sup>  
                  <sup>x</sup> albite + epidote
- b) plagioclase + pyroxene → chlorite + epidote
- c) olivine → chlorite (+ pyrite)
- d) pyroxene → actinolite

The groundmass alters to an intergrowth of chlorite and actinolite which may be accompanied by quartz and albite. Vein minerals include chlorite, actinolite, epidote, quartz, and Cu-Fe-Zn sulphides.

2) The rocks may be subdivided by their mineralogy into chlorite-rich (>15% chlorite and <15% epidote), and epidote-rich assemblages (>15% epidote and <15% chlorite). These divisions correlate with the bulk chemical trends observed. The chlorite-rich assemblage loses CaO and gains significant quantities of MgO due to the formation of chlorite, whereas the epidote-rich samples show only slight variation in either, the CaO being used in the formation of epidote, and the original MgO being retained in the actinolite. The epidote-rich rocks are more oxidized than their precursors, while the chlorite-rich rocks can be further subdivided into those that maintain the same proportions of ferrous and ferric iron, and those that show an increase in ferrous iron due to the precipitation of pyrite.

### 3. ELEMENTAL FLUXES DURING HYDROTHERMAL ALTERATION OF BASALTS.

#### 3.1. INTRODUCTION.

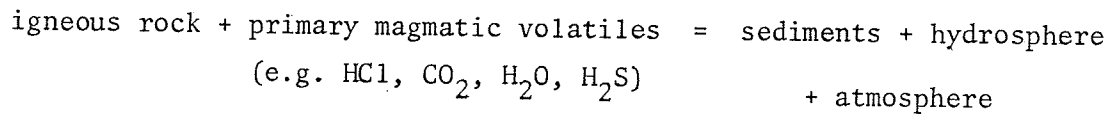
It is generally believed that the relative elemental abundances in the oceans has not varied markedly over a long period of time. This idea is based on palaeontologic, isotopic and geochemical evidence (for example, Garrels and Mackenzie, 1971), and the constancy in relative proportions is thought to extend back to at least the Cambrian.

There have been two approaches to the study of the global cycling of elements based on this premise. The first of these has been the application of chemical equilibrium models to the composition of seawater (Sillen, 1961; Garrels and Thompson, 1962; Lafon and Mackenzie, 1974). This method allows the time-invariant system to be modelled from the thermodynamic properties of the constituent phases. However, equilibrium between the rock and seawater is not reached during hydrothermal alteration. Petrographic observations and mineral analyses, discussed in Chapter 2, provide some information on reactions but the application of a chemical equilibrium model in this instance, is not feasible.

The alternative approach has been the construction of geochemical mass balances (for example, Goldschmidt, 1954; Horn and Adams, 1966; Mackenzie and Garrels, 1966; Garrels and Mackenzie, 1971). A steady-state system is assumed in which the only requirement is that the net input and output rates of each element are equal. The assumption is made that sedimentary rocks are the result of long-term weathering of the primary igneous rocks, and hence a balance exists between the average compositions and quantities of rocks, seawater and sediment.



A more sophisticated geochemical balance has been attempted by Li (1972), in which maintenance of the overall charge balance, and the mass balance of the stable isotopes in the system, are emphasized. These techniques produce a general mass balance equation in which:



Hydrothermal reactions between seawater and the oceanic crust represent a process, which incorporates the rocks derived from the mantle reservoir into the overall geochemical mass balances. This means that a more realistic steady-state mass balance can be constructed. When applied to sub-systems for individual elements, the steady-state model requires a knowledge of all the addition and removal mechanisms that affect the element. In this chapter, I calculate the elemental fluxes observed during hydrothermal alteration of oceanic igneous rocks, and discuss their significance for geochemical mass balances within the framework of a steady-state model.

### 3.2. MAJOR ELEMENT ANALYSES.

The major element analyses are reported in Appendix I, Table AI-7. In the following discussion, the observed concentrations will be compared with previously published data for greenschist facies metabasalts taken from Aumento and Loncarevic (1969), Cann (1969), Bonatti et al (1975), Chernyseva (1971), Hekinian and Aumento (1973), Melson and Van Andel (1966), Melson et al (1968), Ozima et al (1976), Shido et al (1974), and Thompson and Melson (1972).

#### A. SILICA.

The silica content of the altered rocks indicate that silica is mobilised during hydrothermal alteration (Fig. 3-1).  $H_2O^+$  has been used as an indication of the extent of alteration of various samples. The core-to-rim analyses generally show that alteration of the pillow margins results in a loss of  $SiO_2$ - a good example is shown by the core-to-rim  $SiO_2$  contents of sample AII-60 2-142, where three zones could be separated for analysis. However, a few samples, such as AII-42 1-96, show an increase in  $SiO_2$  in the rims, which is due to local precipitation of quartz in fine veinlets. The  $SiO_2$  contents of the altered pillow interiors are variable; in some samples  $SiO_2$  is lost, while in others, it is gained.

The previously published data also suggest variable  $SiO_2$  contents in hydrothermally altered basalts (Fig. 3-2). Alteration of two glassy basalts (with  $H_2O^+$  contents of 7.26 and 8.14%) to assemblages composed mostly of chlorite, results in a loss of silica, while alteration of holocrystalline basalts results in variable  $SiO_2$  contents.

FIGURE 3-1.

Silica concentration vs. water content.

- x - AII-42 samples
- - Ch-44 samples
- o - AII-60 samples
- x→x - core-to-rim analyses
- - DILUTION trend (indicates the apparent change in  $\text{SiO}_2$  concentration due to the addition of  $\text{H}_2\text{O}^+$ )

FIGURE 3-1.

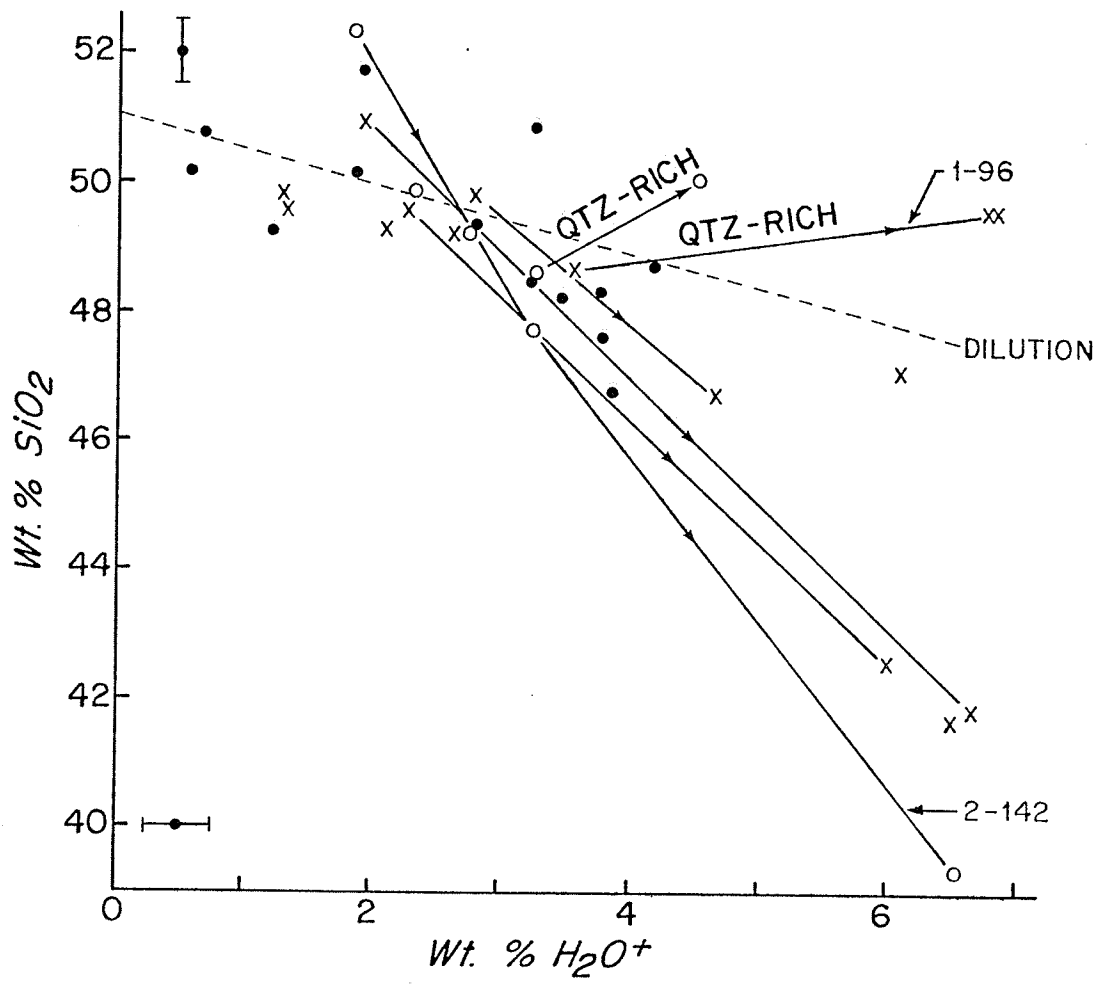
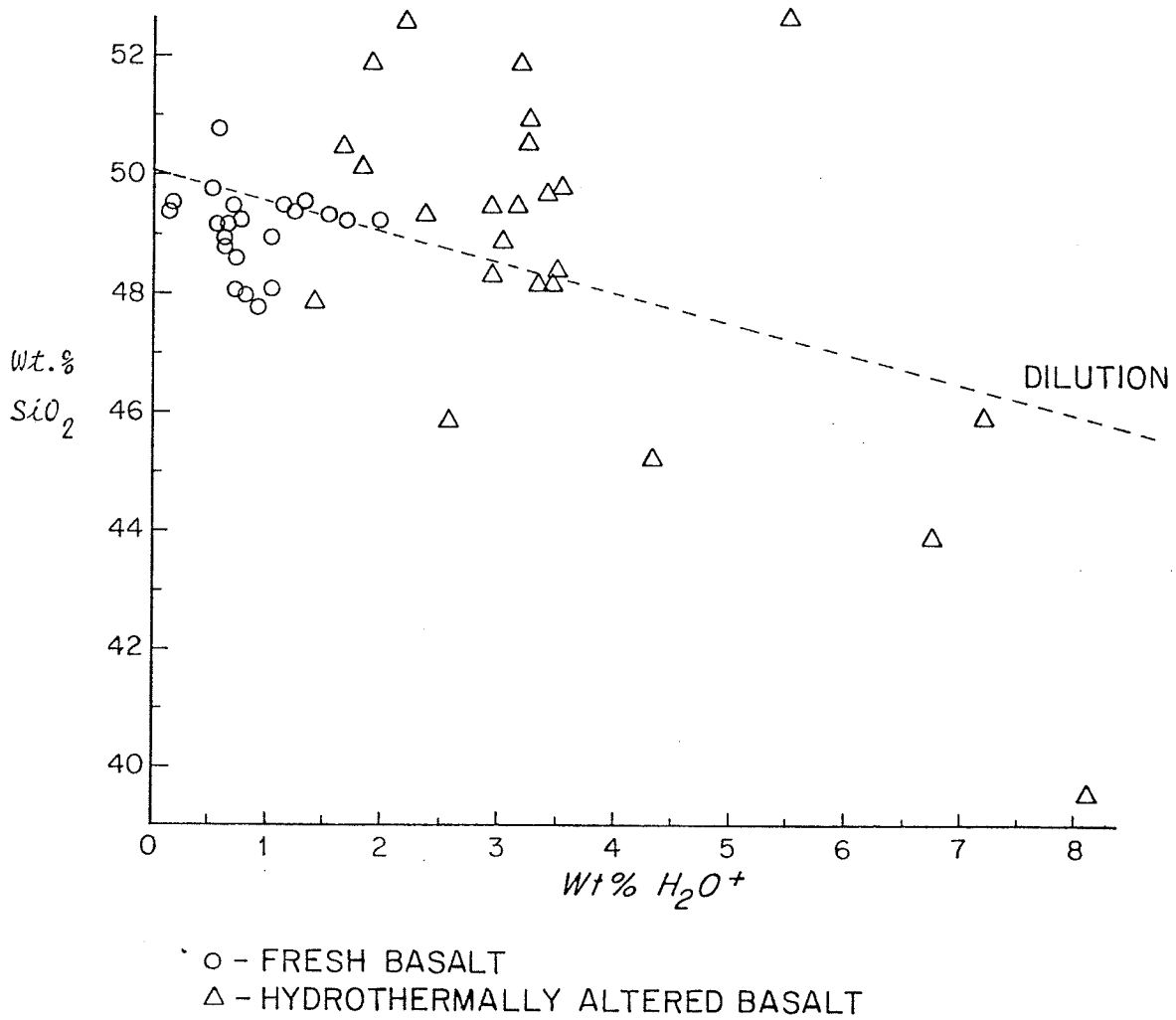


FIG. 3-2  $\text{SiO}_2$  TRENDS-PREVIOUSLY PUBLISHED DATA



## B. CALCIUM

The bulk rock CaO content also shows a linear decrease with increasing water content, with up to a factor of three change in concentration (Fig. 3-3). However, the mineral control on the calcium content is apparent. The CaO contents of the basalts decrease during alteration to epidote-rich assemblages, but after the altered sample contains more CaO than would be expected by assuming a linear relationship between CaO and  $H_2O^+$ . This is because some of the calcium released during albitisation of the plagioclase tends to be preserved in epidote, rather than being transported away in the circulating fluid. Alteration of both the pillow interiors and the rims to chlorite-rich assemblages results in loss of CaO.

The previously published data also indicate that the CaO content decreases linearly with increase in  $H_2O^+$  during hydrothermal alteration (Fig. 3-4). The sample showing a high CaO content (Hekinian and Aumento, 1973) contains calcite in veins and vesicles.

## C. MAGNESIUM

The magnesium content of the altered samples shows a positive correlation with  $H_2O^+$  as it is taken up from the circulating fluid as chlorite is formed (Fig. 3-5). This increase is also shown by the core-to-rim trends and, in the most altered samples, the MgO concentration increases by up to a factor of two. Again, mineral controls are seen, the epidote-rich assemblage showing a slight decrease in the MgO concentration compared with the fresh precursor.

An inverse correlation is also observed between CaO and MgO, as shown in Fig. 3-6, in which previously published data have been plotted in addition to the data presented in this study. This indicates that as

FIGURE 3-3.

CaO (wt.%) concentration vs. water content.

- x - AII-42 samples
- - Ch-44 samples: chlorite-rich assemblage
- ⊙ - Ch-44 samples: epidote-rich assemblage
- o - AII-60 samples
- x→x - core-to-rim analyses
- - DILUTION trend (represents apparent change  
in CaO concentration due  
to addition of  $H_2O^+$ )

FIGURE 3-3.

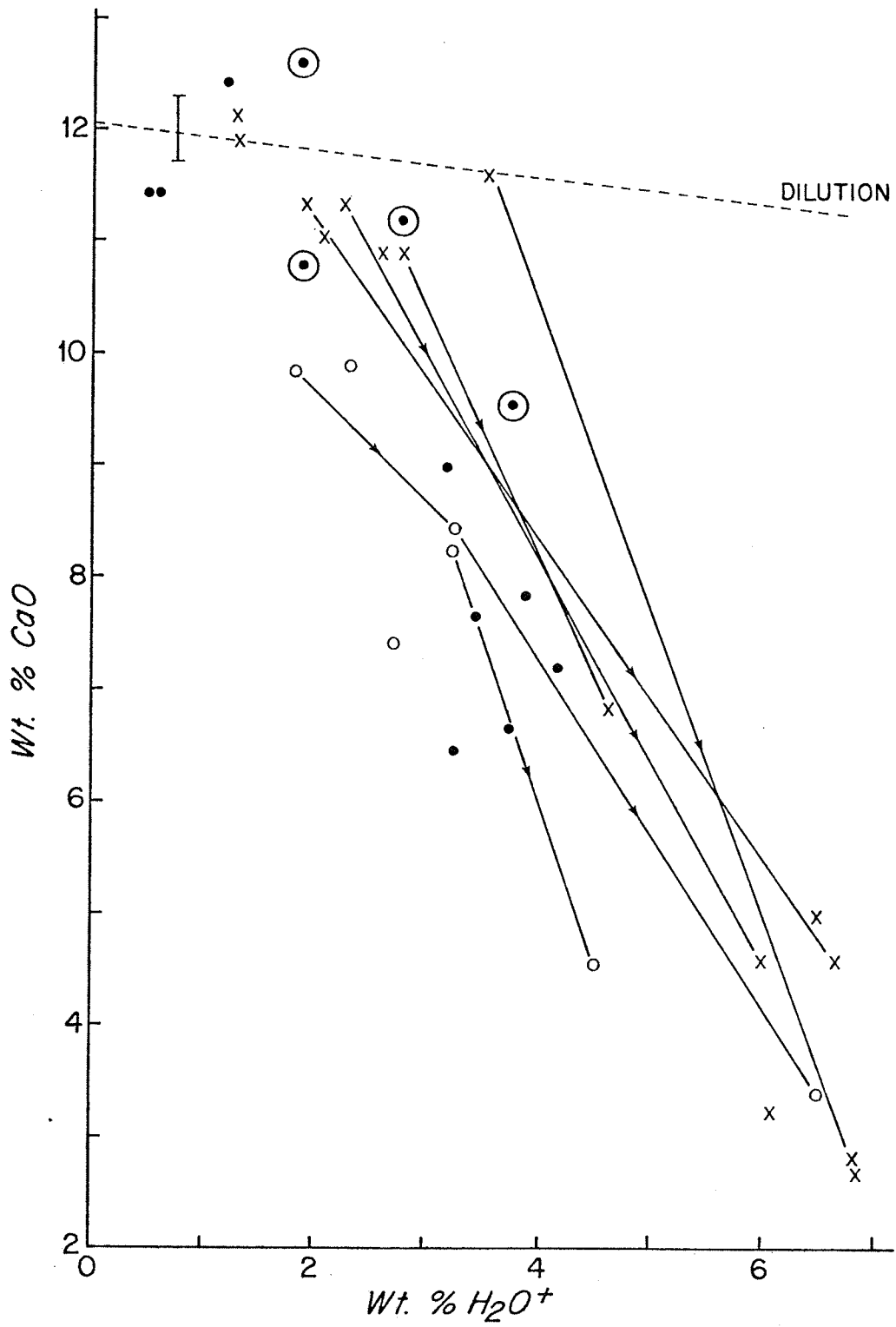




FIGURE 3-4.  
CaO concentrations- previously published data.

(Symbols as for Fig. 3-2)

FIGURE 3-4.

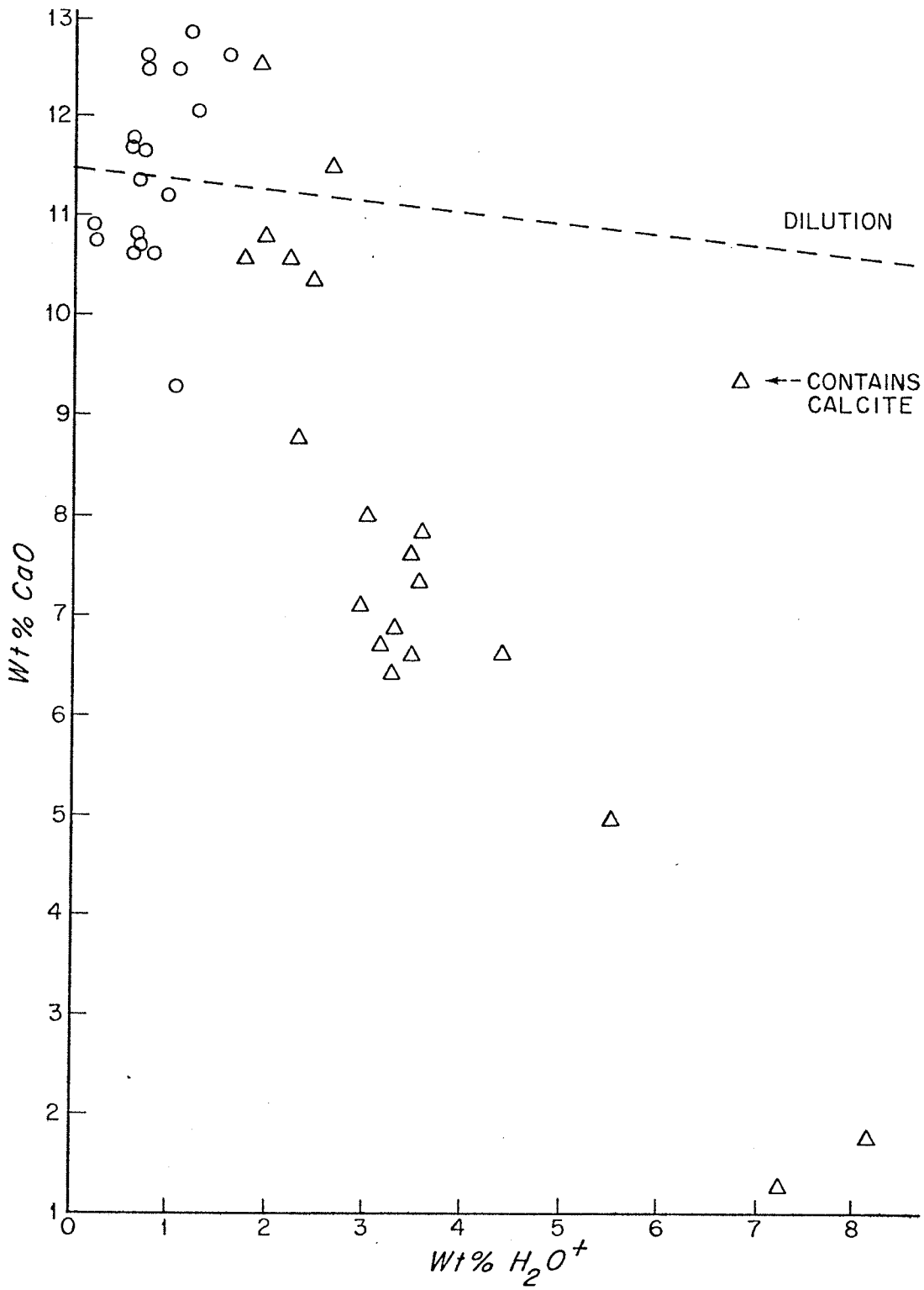


FIGURE 3-5.  
MgO concentrations vs. water content.

(Symbols as for Fig. 3-3)

FIGURE 3-5.

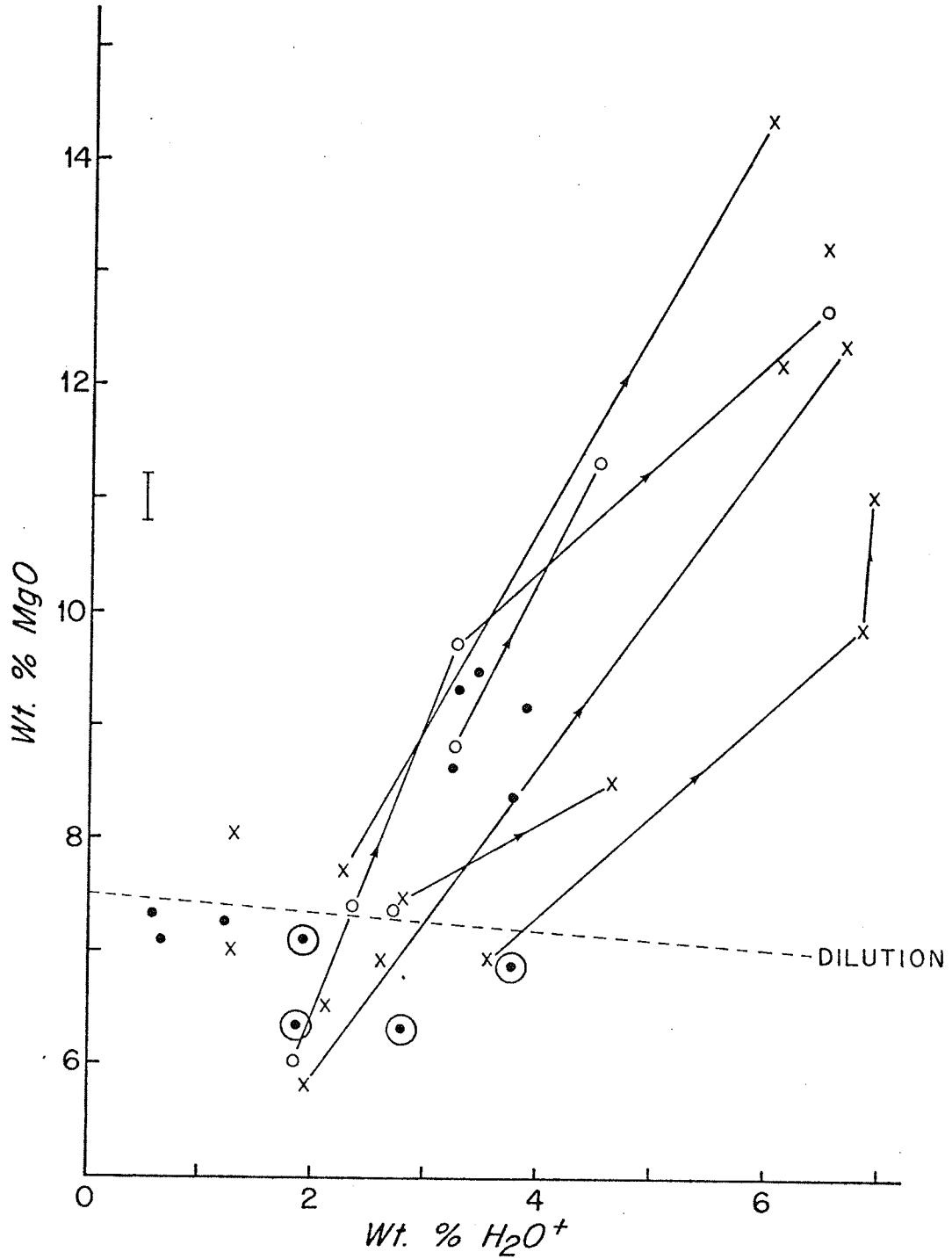
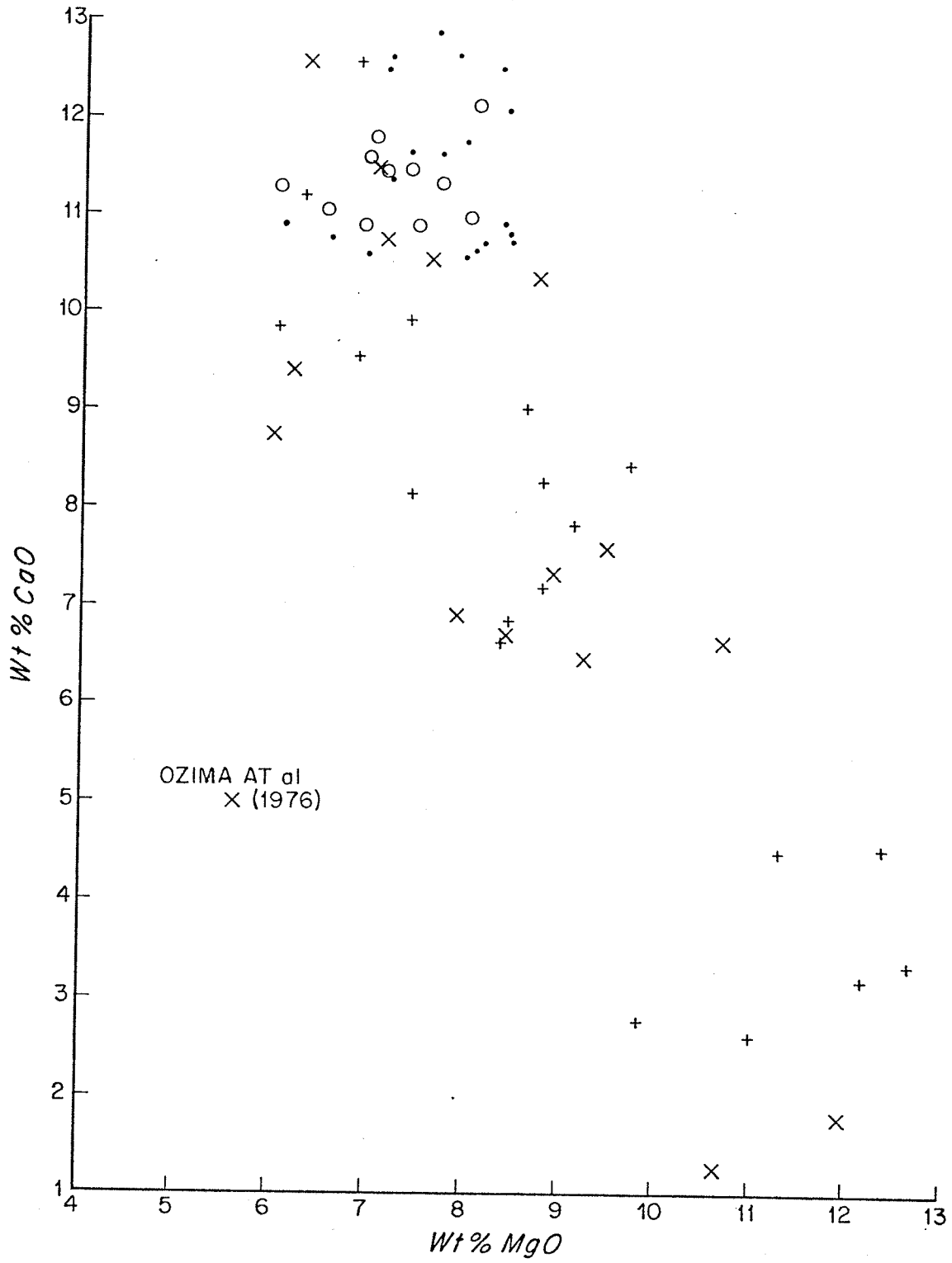


FIGURE 3-6.  
CaO vs. MgO contents for fresh and hydrothermally  
altered basalts.

- - fresh basalts        )
- x - altered basalts     ) previously published data
- o - fresh basalts        )
- + - altered basalts     ) this study

FIGURE 3-6.



the chlorite contents of the altered samples increase, as indicated by the MgO concentration, there is a concomitant decrease in CaO. One sample that does not lie on this trend is a greenschist facies metabasalt from the Mid-Atlantic Ridge at 30°N. Its mineral assemblage is apatite-haematite-ilmenite-albite-muscovite-epidote-chlorite-calcite-quartz, and it is postulated to have reacted with a solution coming from a continental mass (Ozima et al., 1976). If this is true, then it is not comparable with the greenschist facies metabasalts found on other parts of the ridge.

#### D. IRON

The correlation of the iron concentration with the mineralogy and  $H_2O^+$  content has been discussed in the previous chapter. The epidote-rich rocks lose iron, but the  $Fe_2O_3/FeO$  ratio increases. The chlorite-rich rocks that contain little or no pyrite also lose some iron, but their  $Fe_2O_3/FeO$  ratio stays relatively constant, while the remaining chlorite-rich samples gain iron and the  $Fe_2O_3/FeO$  ratio decreases, due to the precipitation of pyrite in veins or in the altered groundmass adjacent to veins.

The previously published data also suggest that iron is mobilized during hydrothermal alteration and, in general, the FeO content decreases while the  $Fe_2O_3$  concentration stays relatively constant (Figs. 3-7 and 3-8) although a few samples are highly oxidized. However, two chlorite-rich samples show an increase in total iron and in the FeO concentration. Since, in almost all cases, modal analyses have not been reported, it is not possible to divide them into chlorite-rich and epidote-rich assemblages but the trends are in general agreement with my studies.

FIG. 3-7 Fe<sub>2</sub>O<sub>3</sub> TRENDS- PREVIOUSLY PUBLISHED DATA

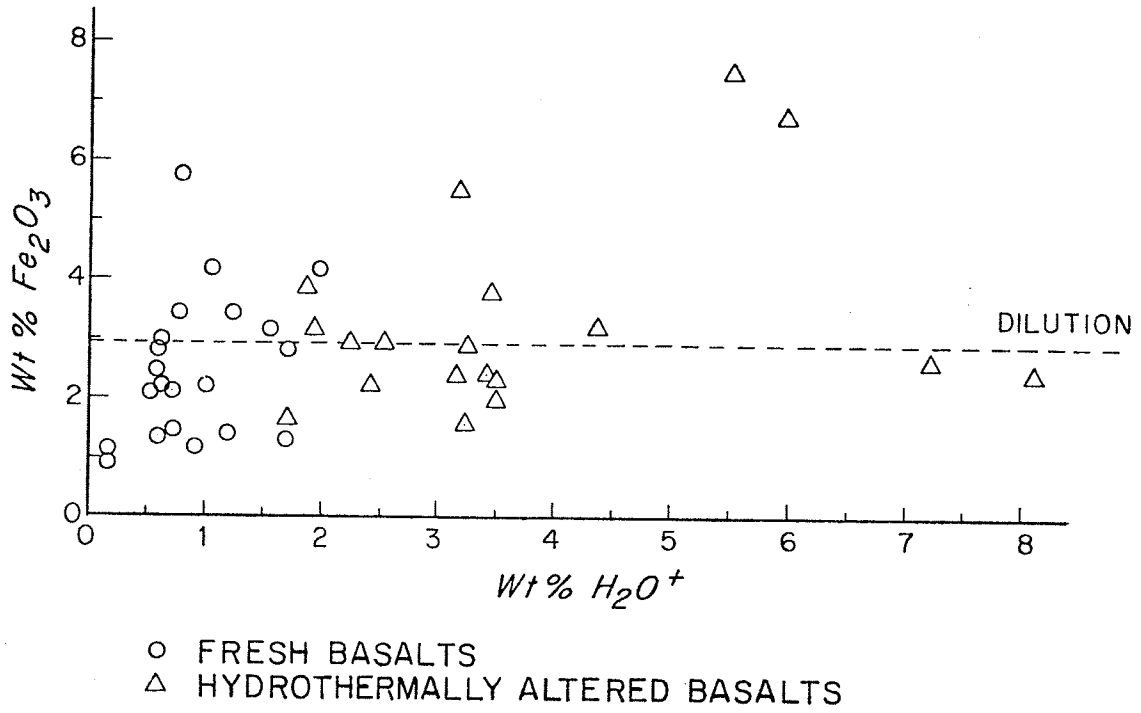
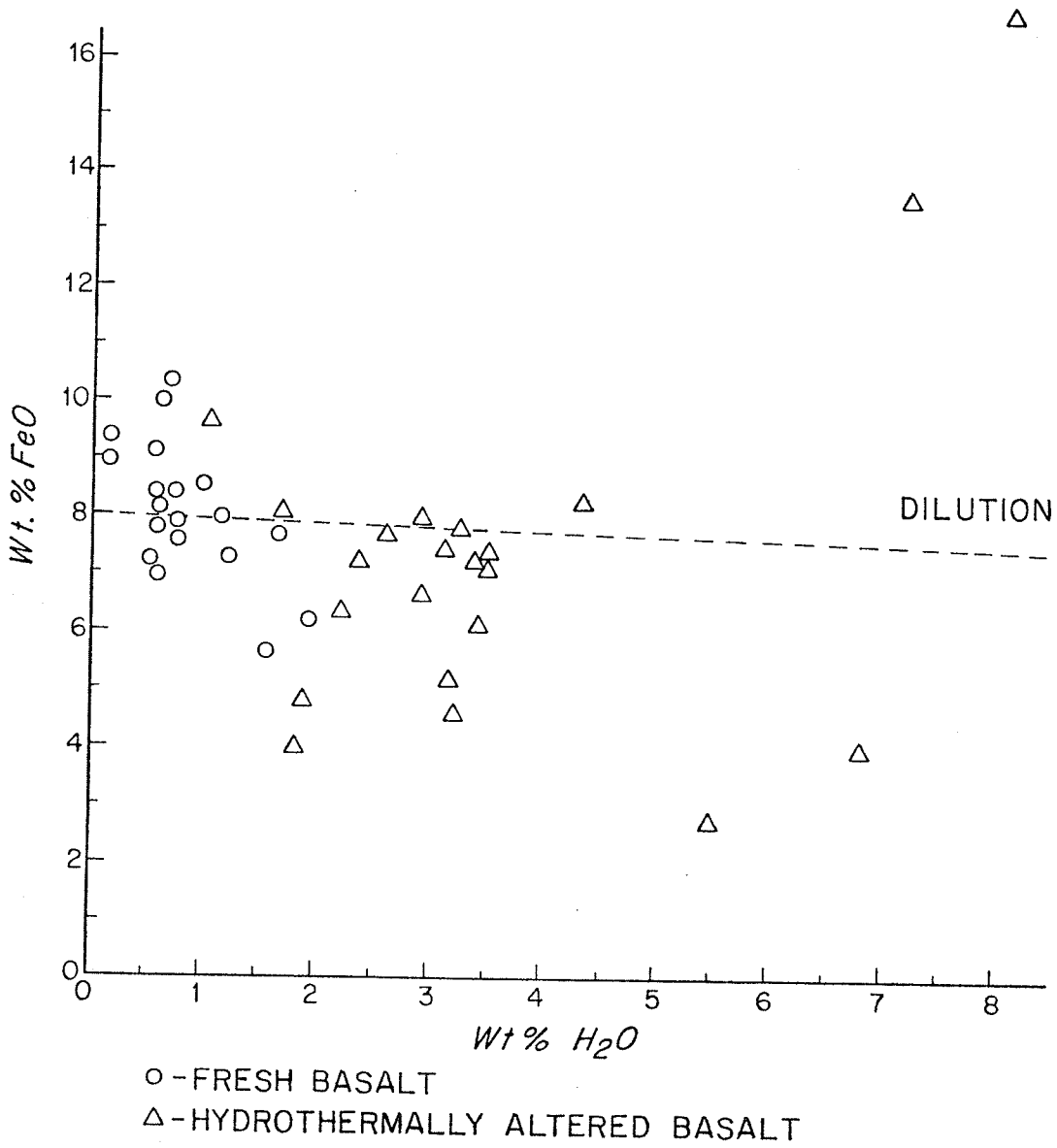




FIG. 3-8 FeO TREND—PREVIOUSLY PUBLISHED DATA



E. SODIUM AND OTHER MAJOR ELEMENTS.

Sodium varies somewhat between samples and from core-to-rim in individual samples, but no consistent trends can be seen in the data. Previous studies indicate that, in general, alteration of basalt to greenschist facies, and particularly to chlorite-rich rocks, results in no appreciable differences in the sodium concentration; although Cann (1969) observed a loss of  $\text{Na}_2\text{O}$  from glassy samples. However, Miyashiro et al (1971) noted uptake of Na O during zeolite facies metamorphism.

No consistent trends have been observed in the  $\text{K}_2\text{O}$  content of greenschist facies metabasalts, although Melson and Van Andel (1966) reported a decrease in  $\text{K}_2\text{O}$  concentration during alteration. This is contrasted with low temperature weathering during which  $\text{K}_2\text{O}$  is taken up by the rock (Hart, 1973; Thompson, 1973a).

Aluminium shows no consistent trends during hydrothermal alteration (Fig. 3-9), and shows very little change in concentration in the core-to-rim analyses. The variations shown in the graph are caused by the changes in concentrations of other elements. For example, in the core-to-rim analyses of AII-42 1-108, the leaching of CaO and uptake of MgO are approximately balanced. However, the concentration of  $\text{SiO}_2$  decreases by about 9% in the altered rim, while the  $\text{FeO}^*$  and  $\text{H}_2\text{O}^+$  contents increase by about 3 and 4.5% respectively. Hence, the  $\text{Al}_2\text{O}_3$  content will appear to increase by about 1.5% from its initial value of 15.31% to a value of about 16.8% in the outer rim.

FIGURE 3-9.  
 $\text{Al}_2\text{O}_3$  concentrations vs. water content.  
(Symbols as for Fig. 3-1)

FIGURE 3-9.

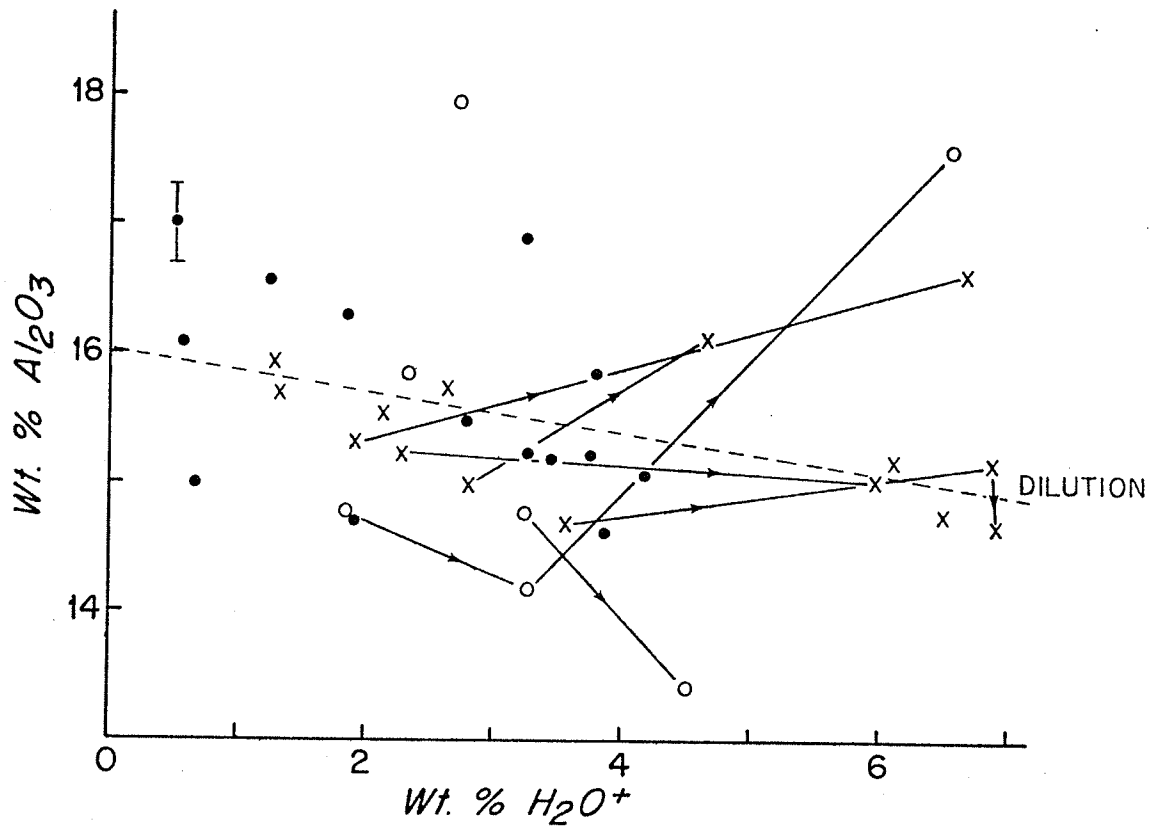


FIGURE 3-10.

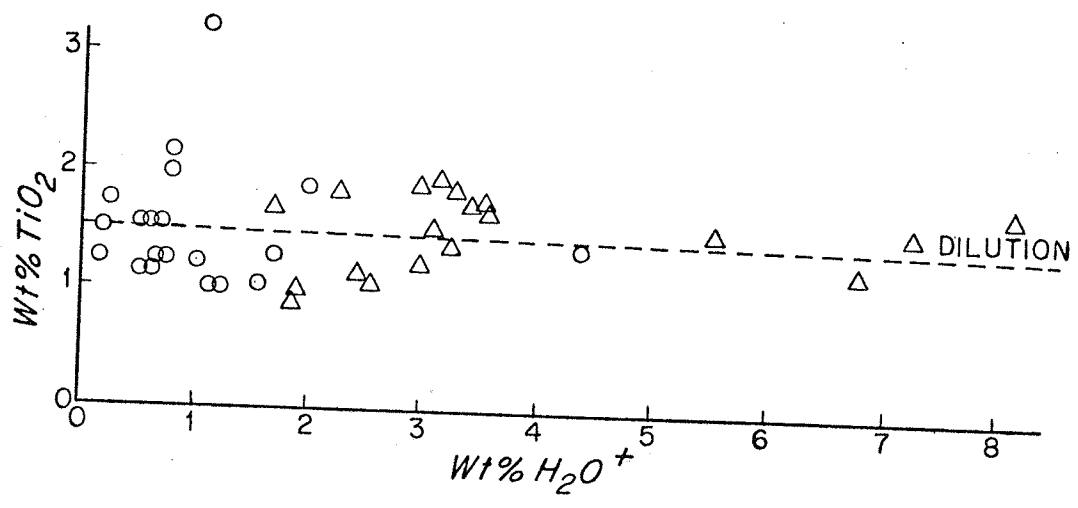
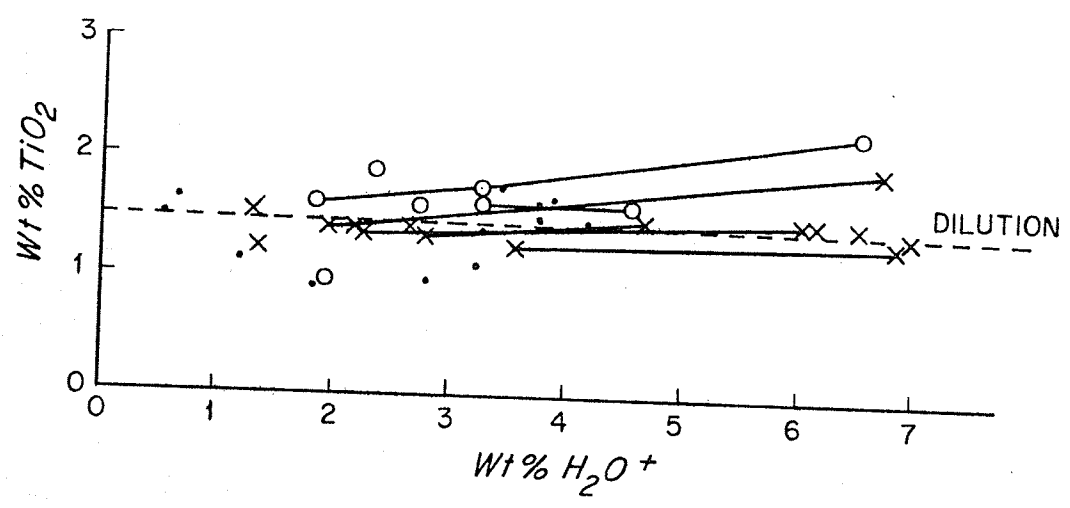
TiO<sub>2</sub> concentrations vs. water content

(Symbols as for Fig. 3-9)

FIGURE 3-11

TiO<sub>2</sub> concentrations- previously published data

(Symbols as for Fig. 3-8)



Titanium shows no marked changes in concentration during hydrothermal alteration, although the core-to-rim analyses do suggest that there may be higher concentrations in the rims than in the interiors (Fig. 3-10). Previously published data (Fig. 3-11) are difficult to assess, since the precursors are unknown, however, only small variations in the  $TiO_2$  concentrations are observed.

### 3.3 MASS BALANCES DURING ALTERATION

In order to test the hypothesis that hydrothermal reactions lead to significant chemical exchange between the hydrosphere, lithosphere and upper mantle, the mass balances of the elemental losses and gains by the rock are required. In order to determine these mass balances, the data can be normalized to some element. The aluminum contents of basalts show no marked changes during subaerial weathering of basalt (Goldich, 1938). As discussed in the previous section, aluminum also exhibits no trends or major changes during hydrothermal alteration of submarine basalts. The mineral reactions suggested in the previous chapter indicate that there is some local exchange of aluminum during the formation of new mineral phases; however, bulk analyses suggest that there is no overall migration.

Table 3-1 shows the absolute elemental fluxes during hydrothermal alteration. For the samples in which core-to-rim analyses were available, the chemical composition of the altered outer zone was recalculated assuming that the concentration of aluminum in the fresh interior has been maintained during alteration.

TABLE 3-1.

Gains and Losses During Hydrothermal Alteration in  
g. oxide/ 100 cm<sup>3</sup> rock.

+: Element gained by rock.

-: Element lost from rock.



Gains (+) and Losses (-) During Hydrothermal Alteration of Basalt Assuming Constant Aluminum

(g/100 cm<sup>3</sup>)

Altered Sample or Outer Rim	AII-42 1-96A	AII-42 1-96B	AII-42 1-97A	AII-42 1-108A	AII-42 1-118A	AII-42 1-99	AII-42 1-106	Ch-44 2-5	Ch-44 3-12	Ch-44 3-17
Compared With										
Fresh Sample or Pillow Interior	AII-42 1-96C	AII-42 1-96C	AII-42 1-97B	AII-42 1-108B	AII-42 1-118B	AII-42 Average*	AII-42 Average	Ch-44 Average (2)	Ch-44 Average (2)	Ch-44 Average (2)
SiO <sub>2</sub>	+ 2.86	+ 3.56	-19.61	-23.58	- 6.57	- 8.21	-23.96	- 4.97	- 6.98	-11.18
CaO	-24.92	-24.45	-18.92	-18.56	-10.90	-23.06	-18.28	-11.27	- 4.51	- 9.67
MgO	+11.41	+ 8.23	+18.40	+18.96	+ 3.15	+14.13	+16.82	+ 3.44	- 1.82	+ 4.22
H <sub>2</sub> O*	+ 9.32	+ 9.40	+10.42	+13.48	+ 5.27	+12.71	+13.76	+ 9.89	+ 8.93	+ 9.03
FeO	+ 4.46	+ 2.52	+11.56	+ 8.19	+ 2.92	+ 3.08	+10.53	- 1.77	- 0.73	0.0
FeO	+ 7.36	+ 3.06	+13.52	+12.64	+ 5.32	+ 6.21	+13.07	- 0.13	- 6.72	- 0.32
Fe <sub>2</sub> O <sub>3</sub>	- 3.21	- 0.66	- 2.19	- 4.92	- 2.65	- 3.47	- 2.80	- 1.21	+ 6.66	+ 0.36
Na <sub>2</sub> O	+ 0.86	+ 3.27	- 1.16	- 1.89	+ 2.65	- 3.50	- 3.25	- 0.33	+ 2.91	+ 1.15
K <sub>2</sub> O	+ 0.03	+ 0.09	0.0	- 0.07	+ 0.09	+ 0.08	+ 0.22	- 0.39	- 0.39	+ 0.27
TiO <sub>2</sub>	+ 0.39	+ 0.22	+ 0.24	+ 1.63	+ 0.56	+ 0.17	+ 0.07	- 0.46	- 0.36	+ 0.04
P <sub>2</sub> O <sub>5</sub>	+ 0.03	- 0.25	+ 0.05	- 0.19	- 0.02	0.0	+ 0.08	+ 0.13	+ 0.06	+ 0.19
MnO	- 0.06	- 0.05	+ 0.17	+ 0.12	+ 0.12	- 0.14	+ 0.05	- 0.06	+ 0.06	- 0.04

\*\* Average (2) - refers to average of samples Ch-44 2-1, 2-2 and 2-3.

\* Average - refers to average of all samples from same dredge haul with H<sub>2</sub>O < 2%.

Table 3-1 (Continued)

Altered Sample or Outer Rim Compared With	Ch-44		Ch-44		Ch-44		Ch-44		Ch-44		Ch-44		AII-60		AII-60	
	3-126	3-13	3-2	3-3	3-6	3-7	3-8	2-141A	2-142A	2-142C	Average (2)	Average (2)	Average (2)	Average (2)	2-142A	2-142B
Fresh Sample or Pillow Interior	Average (2)	Average (2)	Average (2)	Average (2)	Average (2)	Average (2)	Average (2)	Average (2)	Average (2)	Average (2)	Average (2)	Average (2)	Average (2)	Average (2)	Average (2)	Average (2)
SiO <sub>2</sub>	- 5.87	- 2.52	+ 1.06	- 6.39	+ 1.24	+ 2.71	- 2.62	+ 1.92	- 32.48	- 13.83						
CaO	- 12.77	- 0.09	+ 4.14	- 10.09	- 13.22	- 1.50	- 5.75	- 10.21	- 17.76	- 4.16						
MgO	+ 2.23	- 3.50	- 3.21	+ 5.22	+ 4.82	- 1.39	+ 1.92	+ 6.38	+ 19.74	+ 10.01						
H <sub>2</sub> O <sup>+</sup>	+ 8.77	+ 6.12	+ 3.56	+ 7.90	+ 7.38	+ 3.65	+ 7.45	+ 3.18	+ 13.68	+ 3.81						
FeO*	- 0.26	- 4.36	- 5.88	- 0.50	- 6.95	- 5.64	- 6.20	- 3.21	+ 13.88	+ 3.51						
FeO	- 0.93	- 8.68	- 9.07	- 0.16	- 7.46	- 6.93	- 4.36	+ 0.07	+ 8.01	- 0.10						
Fe <sub>2</sub> O <sub>3</sub>	+ 0.72	+ 4.79	+ 3.53	- 0.37	+ 0.56	+ 1.42	- 2.06	- 3.64	+ 6.58	+ 4.12						
Na <sub>2</sub> O	+ 1.60	+ 1.10	+ 0.41	+ 0.74	+ 4.11	+ 2.57	+ 1.92	- 0.17	- 0.38	- 0.76						
K <sub>2</sub> O	- 0.31	- 0.17	- 0.39	- 0.53	- 0.56	- 0.48	- 0.36	+ 0.47	- 0.01	- 0.01						
TiO <sub>2</sub>	- 0.06	- 1.89	- 2.00	+ 0.27	- 0.73	- 1.83	- 1.47	- 0.07	+ 1.95	+ 0.30						
P <sub>2</sub> O <sub>5</sub>	+ 0.16	+ 0.17	- 0.08	- 0.06	- 0.20	- 0.26	+ 0.06	- 0.01	- 0.01	- 0.06						
MnO	- 0.06	- 0.20	- 0.22	- 0.09	- 0.09	- 0.23	- 0.28	- 0.17	- 0.07	- 0.11						

Table 3-1 (Continued)

Altered Sample or Outer Rim Compared With	AII-60 2-14	AII-60 2-143
Fresh Sample or Pillow Interior	AII-60 2-142C	AII-60 2-142C
SiO <sub>2</sub>	- 5.12	- 6.16
CaO	+ 0.48	- 3.59
MgO	+ 4.11	+ 4.87
H <sub>2</sub> O <sup>+</sup>	+ 1.48	+ 2.82
FeO*	+ 1.50	+ 0.57
FeO	- 0.55	- 0.16
Fe <sub>2</sub> O <sub>3</sub>	+ 2.31	+ 0.83
Na <sub>2</sub> O	+ 0.93	+ 2.32
K <sub>2</sub> O	+ 0.71	- 0.13
TiO <sub>2</sub>	+ 0.73	+ 0.06
P <sub>2</sub> O <sub>5</sub>	+ 0.32	- 0.09
MnO	- 0.28	+ 0.05

The normalized data for the outer rim were then compared with the analyses of the fresh interior, and the density measurements (Table AI-7) used to calculate the elemental fluxes in terms of mass of oxide in  $\text{gm}/100 \text{ cm}^3$  rock. For those samples where the precursor was unknown, the composition of the original rock had to be estimated. Although the composition of fresh oceanic basalt does not vary greatly, and the estimation of the original rock composition was based on fresh rock analyses from the same area, and usually from the same dredge haul, this method may introduce slight errors into the absolute values of the fluxes. Completely altered samples from AII-42 were compared with an average of all analyses from the same dredge haul in which the  $\text{H}_2\text{O}^+$  content was less than 2%, and the altered samples from Ch-44 were compared with an average of the available fresh rock analyses: 2-1, 2-2, and 2-3. A similar calculation has been carried out, assuming that the concentration of  $\text{TiO}_2$  remains constant during hydrothermal alteration, and hence normalizing to  $\text{TiO}_2$ . This results in fluxes which are in very good agreement with those calculated assuming constant  $\text{Al}_2\text{O}_3$ .

The fluxes shown by the completely altered samples fall into the same pattern as the core-to-rim fluxes, which indicates that large errors in estimation of fluxes are not introduced by assumptions regarding the composition of the precursor. Examples of the fluxes for each of the mineral groups: chlorite-rich containing pyrite, chlorite-rich with no pyrite, and epidote-rich assemblages, are shown as bar diagrams in order of increasing  $\text{H}_2\text{O}^+$  uptake in Figs. 3-12 and 3-14. From these figures, it can be seen that, with increasing  $\text{H}_2\text{O}$  uptake, the absolute fluxes for some of the elements increases. In addition, the fluxes are larger in the chlorite-rich rocks than in the epidote-rich rocks. During the formation of chlorite,  $\text{MgO}$  is taken up to the extent of over  $15 \text{ g}/100 \text{ cm}^3$

FIGURES 3-12 to 3-14.

Examples of mass fluxes during hydrothermal alteration of basalts (g. oxide/ 100 cm<sup>3</sup> rock) assuming constant aluminium.

+ - element gained by rock  
- - element lost from rock

1-118A cf 1-118B - altered zone (1-118A) compared with fresh interior (1-118B).

Fig. 3-12 - chlorite-rich, pyrite containing assemblage

Fig. 3-13 - chlorite-rich, with no pyrite

Fig. 3-14 - epidote-rich assemblage

FIGURE 3-12.

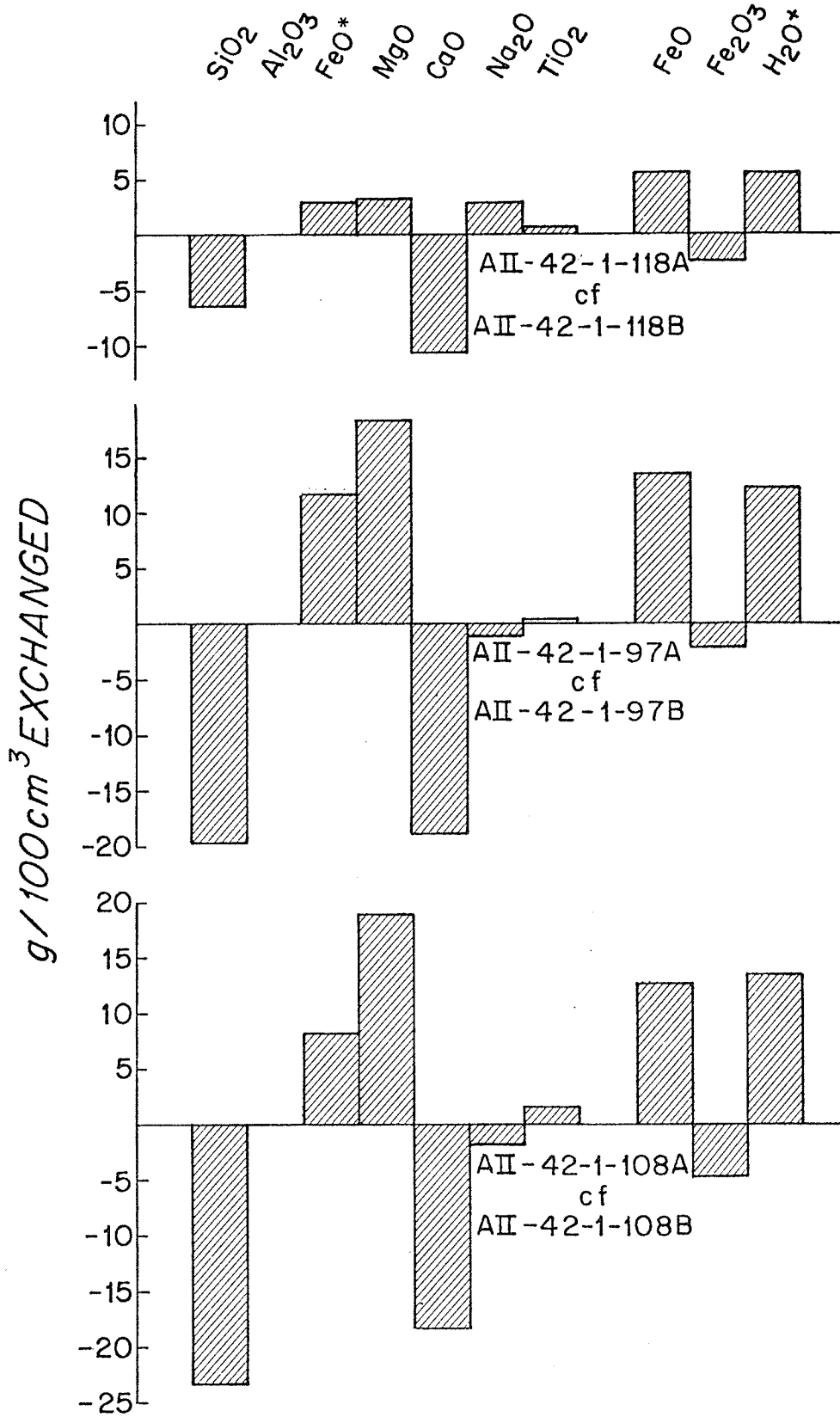


FIGURE 3-13

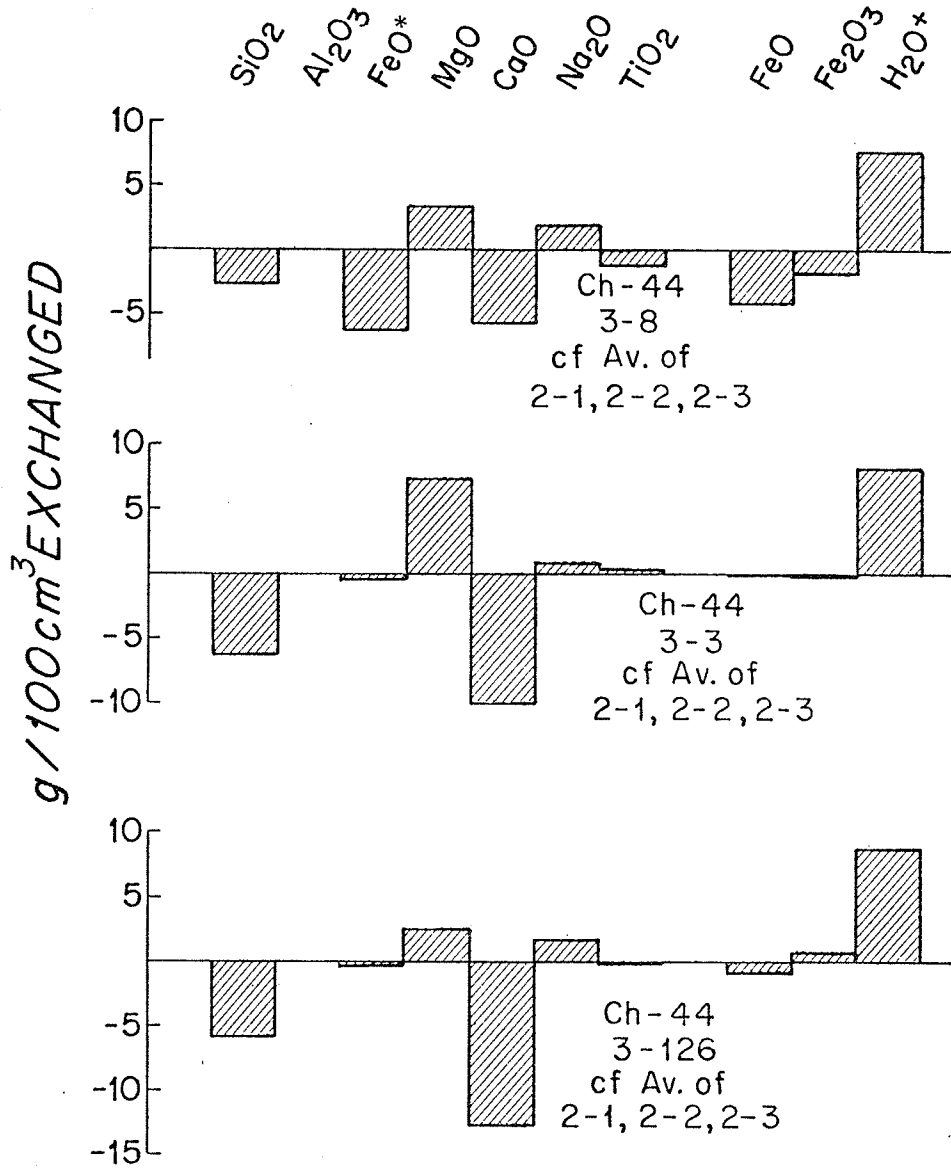
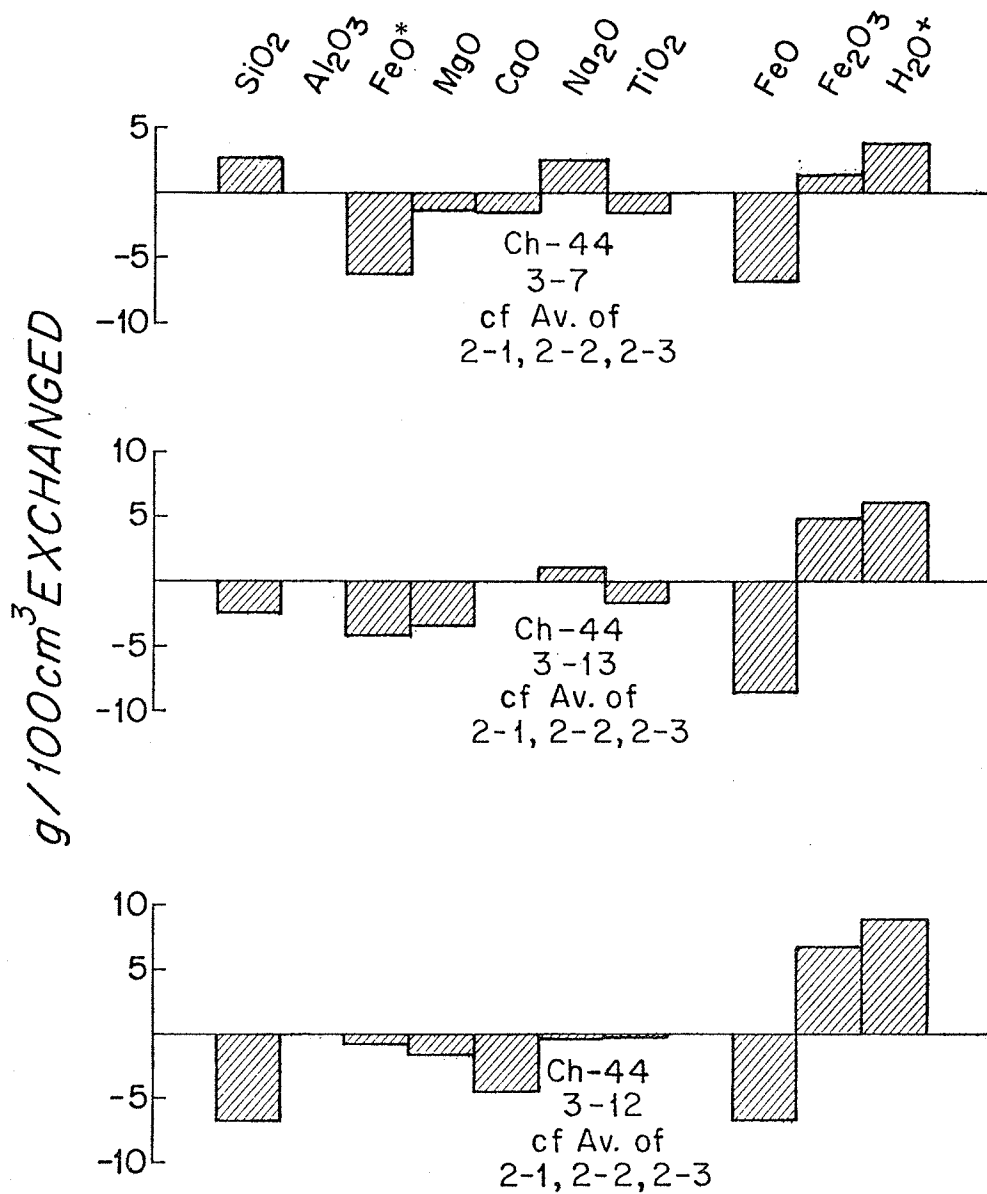


FIGURE 3-14.





in the most altered samples. However, in the epidote-rich rocks, very small amounts of MgO (less than 5 g/100 cm<sup>3</sup>) are leached from the rock. CaO is lost from all the samples, usually in about a 1:1 ratio with MgO, except for the smaller fluxes due to the formation of epidote in the epidote-rich assemblages. A decrease in iron is observed in all samples, except for those in which pyrite has been precipitated. One interpretation of this is that the iron was initially leached from the rock, but the concentration is high due to the precipitation of pyrite. This is supported by the fact that Fe<sub>2</sub>O<sub>3</sub> decreases in all the samples, suggesting that some iron has been lost but total iron increased by the influx of ferrous iron. Na, K and Ti are variable, and show no consistent trends.

The range of elemental fluxes due to hydrothermal alteration of basalts are summarized in Table 3-2, together with fluxes calculated from changes in fluid composition during experimental studies (Mottl, 1976), and those calculated by Wolery and Sleep (1976) from consideration of the convective heat removal requirements. The flux of SiO<sub>2</sub> calculated from the analyses of the dredged basalts is higher than Wolery and Sleep's estimate because solubility constraints have not been considered in the former calculation; this will be discussed in a later section. For calcium, the agreement between the estimates is good, but the Mg flux calculated by Wolery and Sleep is higher than suggested by either the experimental data or the analyses of the dredged metabasalts.

TABLE 3-2.

Comparison of Estimates of Major Element Fluxes During Hydrothermal Alteration of Basalts.

	*Elemental Fluxes (g/100 cm <sup>3</sup> rock)		
	<sup>1</sup> Hydrothermally altered basalts (this study)	<sup>2</sup> Experimental system	<sup>3</sup> Experimental and heat flow estimates
	Range	Average	
SiO <sub>2</sub>	-5 to -20	-10	-0.99 to -2.96
Ca	-0.7 to -7.0	-3.6	-2.15 to -4.44
Mg	+0.6 to +6.0	+3.0	+5.74 to +11.5
Na	-2.6 to +3.1	-	---
K	-0.4 to +0.6	-	---

\* +- element gained by the rock  
 -- element lost from rock

1- estimates from Table 3-1.

2- from Mottl (1976). Calculated from experimental elemental fluxes assuming 1 km. cumulative thickness of greenstone (see Table 13, Mottl (1976)), and assuming density of basalt = 2.9 g/cc.

3- from Wolery and Sleep (1976). Calculated from consideration of heat exchange and flow rate of water through the rock, and experimental elemental changes. Converted to g/100 cm<sup>3</sup> rock by same technique as for Mottl (1976).

### 3.4. MAGNITUDES OF FLUXES AND SIGNIFICANCE IN MASS BALANCES.

In testing the original hypothesis, the mass balances of the rocks and the directions of elemental fluxes during hydrothermal alteration have been estimated. It is now feasible to assess their possible significance for the cycling of elements through the oceans. There are, however, several problems associated with such calculations. The first problem is that the extent of alteration in the oceanic crust is unknown. This is dependent upon two factors: the depth of water penetration and the permeability of the rock. Estimates of the depth of penetration have ranged up to 10 km; however, based on the heat flow data explained in the Introduction, a depth of penetration of 2 - 4 km. is more likely. The amount of rock that comes into contact with the circulating seawater is related to the permeability. The basalts extruded on to the sea floor will contain numerous micro-cracks caused by stress during quenching and contraction, and this will allow circulation of seawater to be pervasive throughout the upper layers of the fresh rock. However, as these cracks are closed by precipitation of vein minerals or by expansion of the rock during the formation of hydrated alteration products, hydrothermal circulation will then be controlled by the major faults and fractures in the rock. At this time, the only rock that will be altered by reaction with seawater will be adjacent to the flow path of the fluid. Since these processes are both time-dependent, it is extremely difficult to estimate the amount of rock that is hydrothermally altered. Thus, in my calculations, I shall use the amount of rock that is hydrothermally altered as a variable to test maximum and minimum values, and to put constraints on the significance of these fluxes for geochemical mass balances.

The second problem is that the degree of metamorphism and the mineral assemblage has to be estimated. One of the principal variables affecting this is temperature, which may range from a few hundreds of degrees to ambient bottom water temperatures. These temperature changes severely affect the magnitudes and directions of elemental fluxes. For example, during weathering at ambient bottom water temperatures, Ca, Mg, and Si are lost from the basalt, while H<sub>2</sub>O and K<sub>2</sub>O increase (e.g. Hart, 1970, 1973; Thompson, 1973a). However, the directions of fluxes shown by the experimental work (Bischoff and Dickson, 1975; Hajash, 1975; Npntl, 1974, 1976), and in the Reykjanes geothermal system (Bjornsson et al., 1972) are those noted in this work for the chlorite-rich assemblages, even though they represent zeolite facies metamorphism.

Chemical analyses and mass balances of dredged metamorphic rocks also indicate the rock types that are of importance in elemental changes. As far as can be assessed from published data, zeolite and greenschist facies metabasalts show the same directions of elemental fluxes (Aumento et al., 1971; Miyashiro et al., 1971). The few reported analyses of amphibolites (Aumento et al., 1971; Cann and Funnell, 1967; Miyashiro et al., 1971) suggest that, apart from water, the chemical composition does not change during alteration to amphibolites. Hence, in terms of geochemical mass balances, zeolite and greenschist facies metabasalts are probably the most significant.

The frequency of metamorphic rock types dredged from the ocean floor can be used as an indication of abundance. There are a few reported occurrences of amphibolites, as shown in Table 2-1; however, the number of chlorite-rich greenschist facies metabasalts that have been reported

far exceeds the number of amphibolites. Of the greenschist facies metabasalts, chlorite-rich rocks have been described from the Carlsberg Ridge (Cann and Vine, 1966; Cann, 1969; Hekinian, 1968) and from the Arabian-Indian Ridge (Chernyseva, 1971; Rozanova and Baturin, 1971) in the Indian Ocean. Many occurrences of chlorite-rich rocks from the Mid-Atlantic Ridge have been reported including 53°N (Hekinian and Aumento, 1973), 45°N (Aumento and Loncarevic, 1969; Aumento et al., 1971), 30°N (Quon and Ehlers, 1963), 24 and 30°N (Miyashiro et al., 1971), 30°N (Ozima et al., 1976), 22°N (Melson and Van Andel, 1966; Melson et al., 1968), 11°N (Melson and Thompson, 1971), 10°N to 3°S (Bonatti et al., 1971, 1975), 1°S (Bogdanov and Ploshko, 1967), 4°S (Thompson and Melson, 1972), and Palmer Ridge (Cann and Funnell, 1967; Cann, 1971). Other dredge hauls in the W.H.O.I. collection that contain abundant chlorite-rich rocks have been recovered from the FAMOUS area, the Vema and Romanche Fracture Zones, and King's Trough. These occurrences suggest that these rocks are ubiquitous, and are the predominant metamorphic rock type in the upper 2-3 km of oceanic crust, which have been sampled by dredging. The Deep Sea Drilling Project has not recovered many hydrothermally altered basalts, however, most holes have penetrated only a few meters of the crust. The deep hole of Leg 37 at 36°N in the Atlantic penetrated 500 meters with no significant recovery of metabasalts. We are as yet uncertain how typical or representative of the crust this hole is, but certainly the statistics of dredge recoveries suggest hydrothermally altered basalts are reasonably common.

Hence, in my calculations, I shall use the elemental fluxes calculated previously for the chlorite-rich assemblages. In order to take into account

the observation that the fluxes are larger during alteration of the outer rims than from pillow interiors, I shall use a range of values for the elemental fluxes calculated in the previous section, and summarized in Table 3-2.

### 3.5 WATER TO REACTED ROCK RATIO

The fluxes of Mg and Ca listed in Table 3-2 can be used to calculate two independent water-to-reacted rock ratios within the hydrothermal system. This calculation is shown in Table 3-3. The change in composition of the circulating fluid has been approximated using the chemical analyses of drill-hole water from Reykjanes (Bjornsson et al., 1972). The range of water-to-reacted rock ratios calculated from magnesium and calcium are 5-47: 1 and 5-57: 1 by volume respectively. These are in good agreement with Wolery and Sleep (1976) who estimated the ratio to be 13-40 cm<sup>3</sup> water to 1 cm<sup>3</sup> basalt by using heat flow data to estimate a fluid flow rate.

The use of the Iceland water compositions is justified for two reasons. The composition of the Reykjanes drillhole water used for this calculation has probably not been affected by boiling. Secondly, laboratory experiments using water-to-rock ratios of  $\leq 10:1$ , have shown similar elemental concentrations in the reacted fluid. It can also be seen from the calculation that an error of several hundred ppm in the concentration in the circulating fluid will not radically change the water-to-rock ratio, since the fluxes of Mg and Ca to and from the basalt are so large.

### 3.6 GEOCHEMICAL BUDGETS

The fluxes of elements during hydrothermal alteration may now be assessed in terms of geochemical budgets. The budgets of magnesium, calcium, silica, water, sulphate and oxygen will be considered. Specific

TABLE 3-3.

Calculation of Water-to-Reacted Rock Ratios in the Hydrothermal System.

	Concentrations in ppm.	
	Mg	Ca
FLUID.		
1. Seawater	1282	386
2. Hydrothermal fluid (Iceland)	<u>10</u>	<u>1600</u>
Amount exchanged (2 - 1)	<u>-1272</u>	<u>1214</u>
BASALT.		
Exchange based on fluxes in Table 3-2	6,000 - 60,000	7,000 - 70,000
WATER TO REACTED ROCK RATIO	5 - 47: 1	5 - 57: 1

parameters which are used throughout these calculations are listed in Table 3-4. The total length of the ridge system has been taken from Sverdrup, Johnson and Fleming (1942), and agrees well with an estimate by Williams (1974) of  $5.37 \times 10^4$  km  $\pm$  5%. Williams (1974) also estimated an average half spreading rate of 2.74 cm/yr  $\pm$  5%, and so the average spreading rate for all oceanic spreading centres has been taken to be 5 cm/yr. Hence, the surface area of new ocean floor created each year is 2.75 km<sup>2</sup>, which is in reasonable agreement with estimates by Deffeyes (1970) of 2.5 km<sup>2</sup>/yr, and by Williams and Von Herzen (1974) of 2.94 km<sup>2</sup>/yr.

#### A. MAGNESIUM.

The geochemical budget of magnesium is not balanced. The amount of dissolved magnesium delivered to the oceans annually via the rivers is estimated to be about  $1.3 \times 10^{14}$  g/yr. (Garrels and Mackenzie, 1971). If the assumption is made that the oceans are in a steady state with respect to magnesium, then the outputs are insufficient to balance the river input. Drever (1974) has extensively discussed the Mg problem, a summary of which is shown in Table 3-5. This indicates that the discrepancy is  $0.69 \times 10^{14}$  g/yr, i.e. about 50% of the annual river input. Low temperature weathering of submarine basalts may provide an additional source of magnesium of about  $1 \times 10^{-9}$  g/cm<sup>3</sup>/yr (Hart, 1973; Thompson, 1973a), which would make the difference between the inputs and outputs even larger. This discrepancy suggests that either the input is wrong or there is another sink for magnesium. Drever dismissed the possibility the seawater reacts with basalt to form chlorite, because there was no obvious mechanism for the circulation of seawater through the crust,



TABLE 3-4.

General Parameters For Mass Balance Calculations.

Length of ridge system:	$5.5 \times 10^4$ km.	(1)
Average spreading rate:	5 cm/yr.	
Hence,		
surface area of basalt intruded annually:	$2.75 \text{ km}^2/\text{yr.}$	
Volume of basalt intruded annually:	$27.5 \text{ km}^3/\text{yr.}$	(2)

(1)- from Sverdrup, Johnson and Fleming (1942)

(2)- assumes a thickness of oceanic crust of 10 km.

TABLE 3-5.

The Magnesium Budget. (Adapted from Drever, 1974).

INPUT:

River flux of dissolved  $Mg^{2+}$ :  $1.31 \times 10^{14}$  g/yr.

OUTPUTS:

( $\times 10^{14}$  g/yr.)

1. Carbonate formation: 0.075
  2. Ion exchange: 0.097
  3. Glauconite formation: 0.039
  4. Mg-Fe exchange in sediments: 0.29
  5. Burial of interstitial water: 0.11
- Total outputs: 0.61

Outputs = ~50% of the annual river input.

and also the reaction had not been observed.

The alteration of oceanic basalts to secondary mineral assemblages containing abundant chlorite, and the concomitant uptake of magnesium from seawater, has now been confirmed. Fig. 3-15 illustrates the dependence of the amount of Mg removed from seawater during hydrothermal alteration on the volume of rock that is altered, for a range of fluxes taken from the chlorite-rich data, as discussed in the previous section. This shows that, in order to account for the unbalanced magnesium, it is necessary to alter between 1.1 and 11 km<sup>3</sup> of basalt for the fluxes illustrated, i.e. about 4 - 40% of the annual amount of basalt intruded.

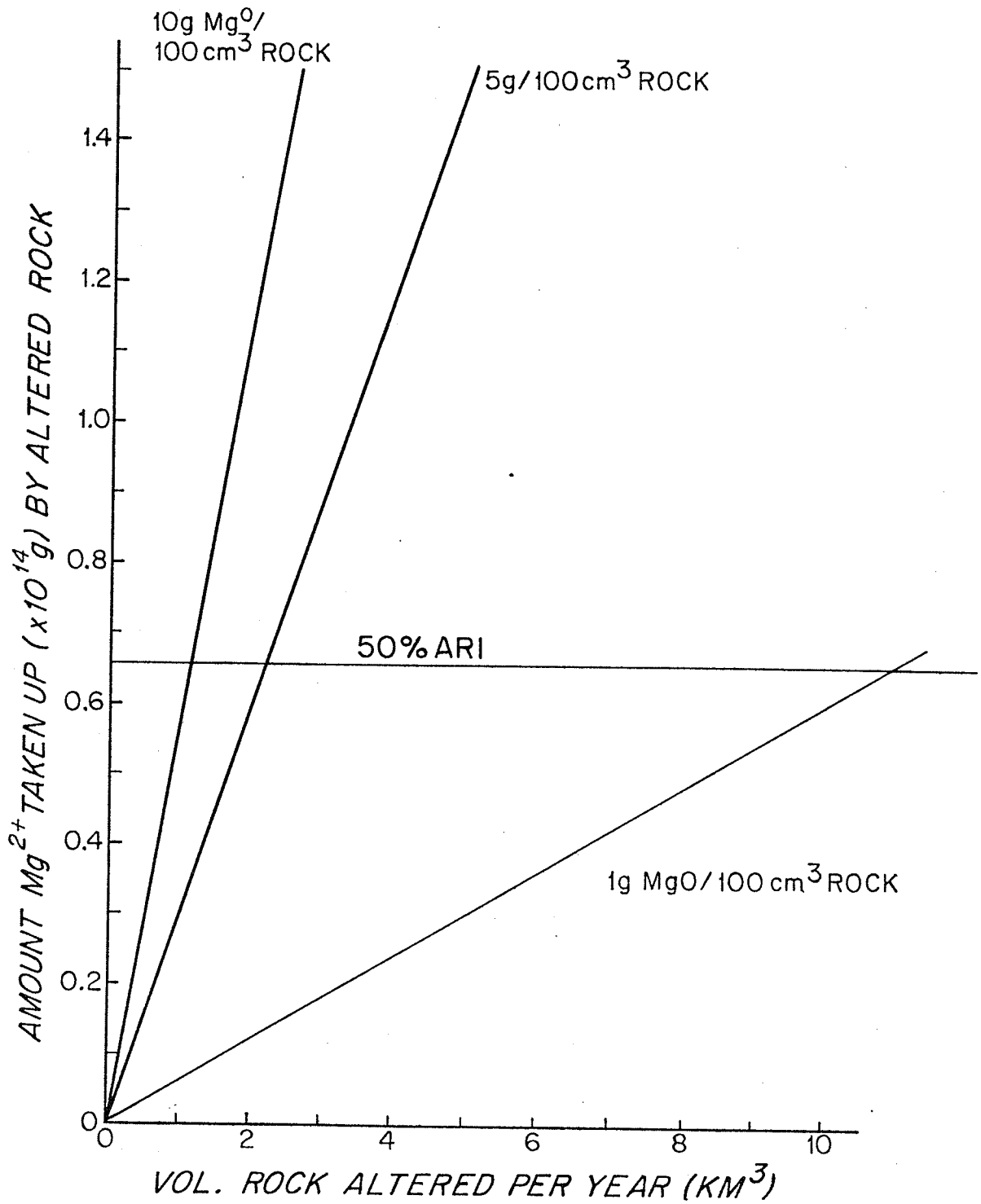
An alternative approach can be used for this calculation. Laboratory experiments (Bischoff and Dickson, 1975; Hajash, 1975; Mottl et al, 1974, Mottl, 1976) suggest that nearly all of the Mg is removed from seawater during interaction with basalt. Hence, using the water-to-rock ratio calculated in the previous section, a second estimate of the volume of rock to be altered can be made. If the assumption is made that all of the Mg is removed from seawater, then  $5.4 \times 10^{16}$  cm<sup>3</sup> of seawater must react with basalt in order to remove all the excess Mg. Taking the water-to-rock ratio to be between 5 and 47, then the volume of rock to be altered is 1 - 10 km<sup>3</sup>, which is consistent with the previous calculation. If it is now assumed that all of the excess Mg (i.e.,  $0.69 \times 10^{14}$  g/yr) can be accounted for by uptake during hydrothermal alteration, the percentage change in the concentration of Mg in the basalt can be estimated. For depths of penetration of between 1 and 5 km., the percent change in the concentration of Mg in the basalt is 0.02 to 1.1%, assuming that all of the rock is altered.

FIGURE 3-15.

Amount of  $Mg^{2+}$  taken up by hydrothermally altered basalt:  
vs. the volume of rock altered per year, for uptake rates of  
1, 5 and 10 g.MgO/ 100 cm<sup>3</sup> rock.

50% ARI- mass of  $Mg^{2+}$  equivalent to 50% of the annual river input.

FIGURE 3-15



Wolery and Sleep (1976) calculated a flux of Mg from the oceans into the basaltic crust of  $3.9 \times 10^{14}$  g/yr. This is a factor of six greater than that required to balance the Mg, and the calculation was based on an extremely high flow rate of seawater through the hydrothermal system.

However, most of the annually intruded basalt is unavailable for alteration because the depth of penetration is only 2 - 5 km. It is therefore more meaningful to consider the percentage of 'available' crust that must be altered to account for 50% of the annual river input. This is shown in Fig. 3-16, where the amount of 'available' crust, which is dependent on the depth of penetration, that must be altered to balance the magnesium is plotted for different uptake rates. Assuming an average uptake rate of 5 g MgO/100 cm<sup>3</sup> rock then, for a depth of penetration of between 2 and 5 km., the amount of 'available' crust that must be altered to account for all the excess magnesium ranges from 20 - 50%. This suggests that hydrothermal alteration of submarine basalts provides a very important sink for magnesium, and should be taken into account in geochemical mass balances because it has the capability of solving the excess magnesium problem.

#### B. CALCIUM.

Garrels and Mackenzie (1971) modelled the production of sediments from the weathering of igneous rock, and found that there is more sedimentary calcium in the stratigraphic column than would be predicted from the simple weathering model. They proposed that this excess calcium could be derived from weathering of volcanic material on the sea floor. The amount of calcium leached from the basalt

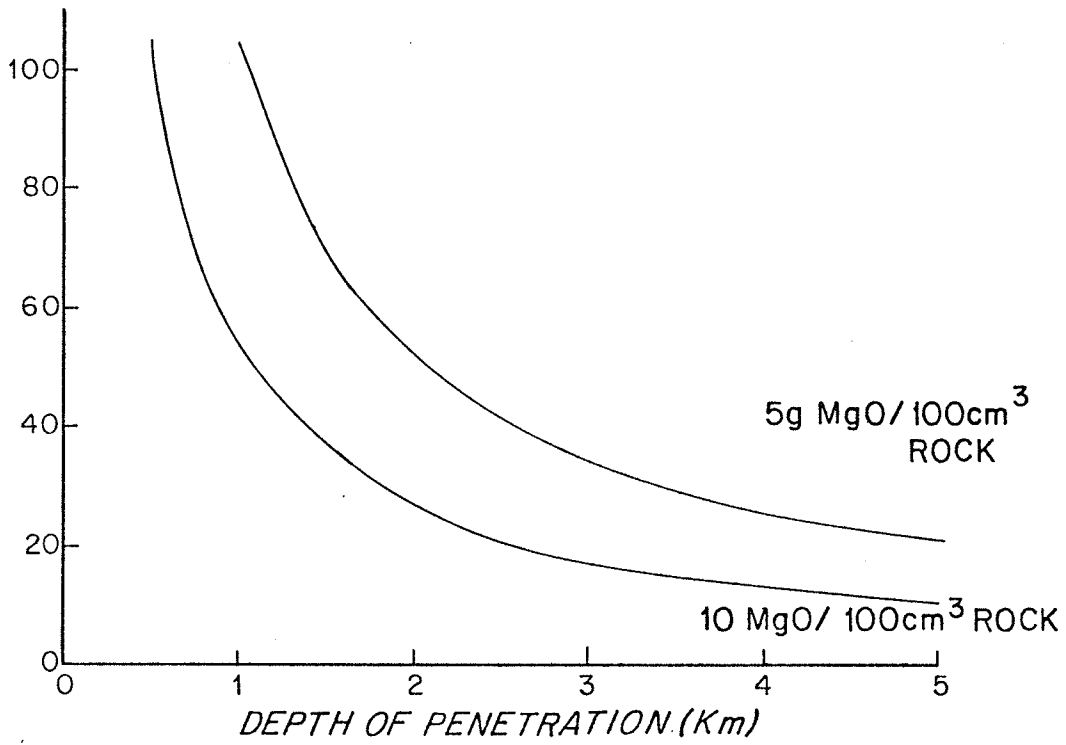
FIGURE 3-16.

Percent of 'available' crust to be altered to account for the excess Mg vs. depth of penetration, for uptake rates of 5 and 10 g.MgO/ 100 cm<sup>3</sup> rock.

'Available' crust = length of ridge x average spreading rate  
x depth of penetration

FIGURE 3-16

% "AVAILABLE" CRUST TO BE ALTERED TO ACCOUNT  
FOR DISCREPANCY IN ANNUAL RIVER INPUT OF  $Mg^{2+}$



'AVAILABLE' CRUST CALCULATED AS LENGTH OF RIDGE X  
AV. SPREADING RATE X DEPTH OF PENETRATION



during hydrothermal alteration largely balances the uptake of magnesium; hence, a calculation, similar to that for magnesium, can be made from my data, to determine the amount of  $\text{Ca}^{2+}$  leached from a given volume of rock (Fig. 3-17). Hydrothermal alteration provides an additional source of calcium for the geochemical budget. In order for fluxes of 5 and 10 g  $\text{CaO}/100 \text{ cm}^3$  rock to provide a source equivalent to the river input ( $4.88 \times 10^{14}$ ; Garrels and Mackenzie, 1971). between 6.8 and  $13.5 \text{ km}^3$  of basalt would have to be altered depending on the flux. This is 25 - 50% of the annual amount of basalt intruded, which suggests that, although this is an important source, the river input is still the most significant source of Ca. In addition, some Ca will be locally precipitated as carbonates and so will not become part of the sedimentary record.

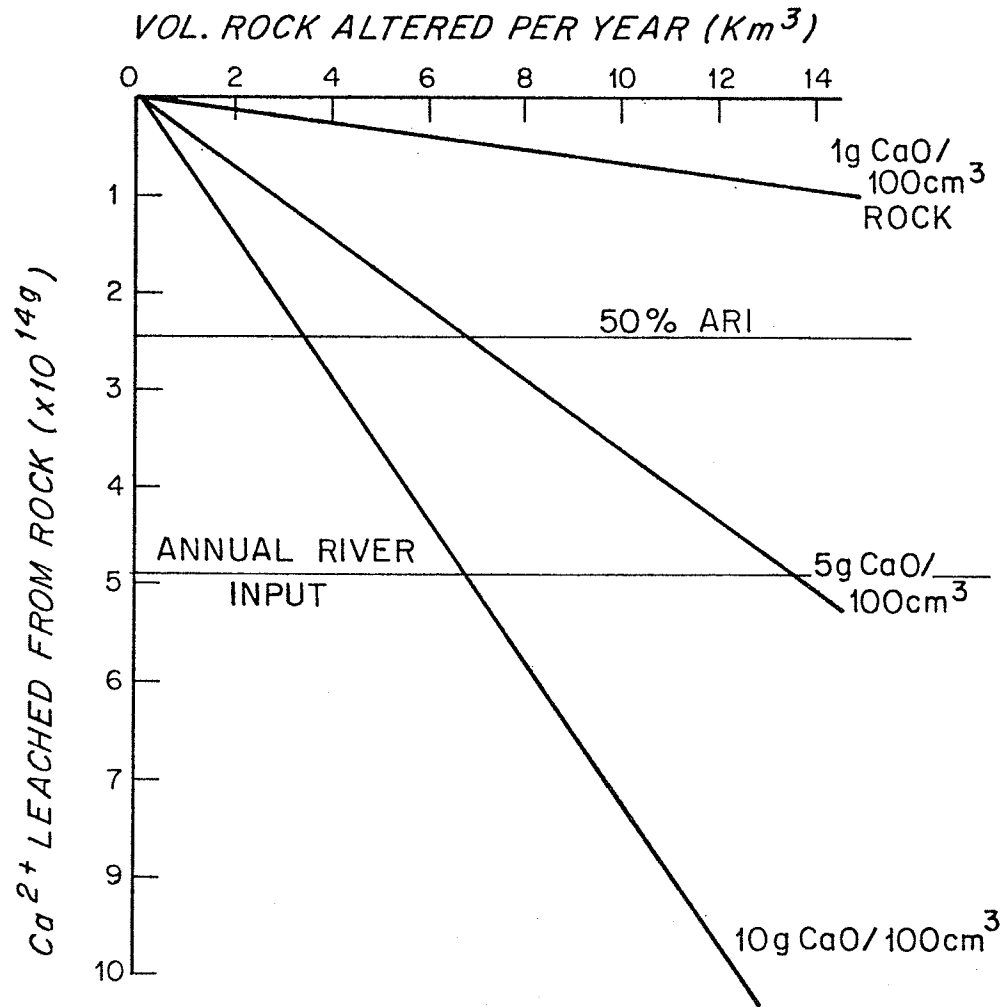
Wolery and Sleep (1976) calculated that, in order to account for the excess sedimentary calcium, a flux of  $0.34 \times 10^{14}$  g/yr. is required over 3500 myr. of earth history. This would require alteration of 0.3-1  $\text{km}^3$  of rock per year, and so hydrothermal circulation has the potential for solving the excess sedimentary calcium problem. This conclusion is also supported by the calcium fluxes of  $1 - 3 \times 10^{14}$  g/yr. calculated from experimental data (Mottl, 1976).

The precipitation of  $\text{CaCO}_3$  that may occur when the hydrothermal fluid mixes with seawater will provide an additional source of hydrogen ions, that would help balance the excess bicarbonate that is added to the oceans by the rivers. Thus, if 20% of this calcium flux is precipitated as carbonate, then a flux of  $7 \times 10^{12}$  g. of hydrogen ions will be produced.

FIGURE 3-17.

Amount of  $\text{Ca}^{2+}$  leached from basalt during hydrothermal alteration  
vs. the volume of rock altered.

FIGURE 3-17.



C. SILICA.

The petrographic observations and chemical analyses confirm that during hydrothermal alteration, silica is generally mobilised, but may be subsequently precipitated in veins and vesicles. The annual river input of silica is  $4.26 \times 10^{14}$  g. (Garrels and Mackenzie, 1971). This can be compared with the flux from hydrothermal alteration calculated from my data, as shown in Fig. 3-18. This shows that between 2.1 and 8.5 km<sup>3</sup> of basalt must be altered to constitute a source equivalent to the annual river input (i.e. 8 - 30% of the annual amount of basalt intruded), and hence hydrothermal alteration is potentially an important source.

However, the actual input of silica into seawater can be further constrained because the concentration of silica in the circulating fluid is controlled by the solubility of quartz. As the seawater, which initially contains about 6 ppm. SiO<sub>2</sub>, circulates through the rock and heats up, it will gain SiO<sub>2</sub> as the solubility of quartz increases with temperature. However, as the circulating fluid rises and cools, it will lose a considerable portion of its silica as quartz precipitates.

In order to obtain a maximum estimate of the input of silica from hydrothermal circulation, an equilibration temperature of 200°C. is assumed, for which the concentration of silica in seawater in equilibrium with quartz is about 240 ppm (Kennedy, 1950). The seawater-to-rock ratio has been previously calculated to be between about 5 and 50; hence, it is possible to calculate the amount of SiO<sub>2</sub> that can be removed at 200°C. for varying volumes of altered rock- this is shown in Table 3-6. This illustrates that the amount of SiO<sub>2</sub> removed by the circulating fluid is less than the amounts of silica lost from the rock that were calculated from the absolute fluxes. This means that a considerable amount of

FIGURE 3-18.

Amount of  $\text{SiO}_2$  released from basalt during hydrothermal alteration vs. the volume of rock altered per year.

FIGURE 3-18.

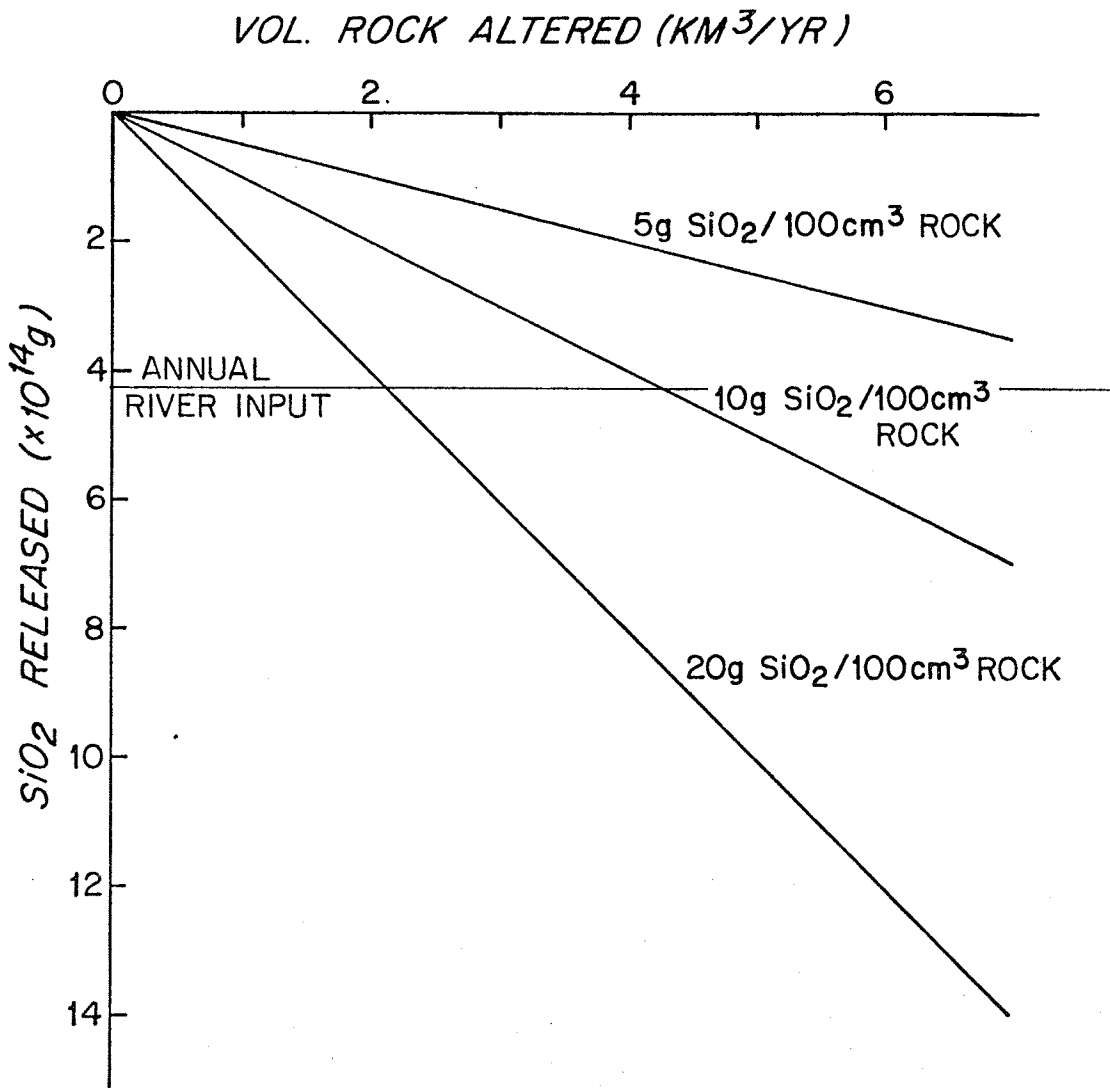


TABLE 3-6.

Silica Flux Calculations.

Vol. Rock Altered (km <sup>3</sup> )	Amount Water Reacted (x 10 <sup>12</sup> l.)	Amount of SiO <sub>2</sub> Removed in the Fluid at 200°C. (x 10 <sup>12</sup> g.)
1	5 - 50	1.2 - 12
2	10 - 100	2.4 - 24
5	25 - 250	6 - 60

redistribution of the silica takes place with some being reprecipitated within the basaltic pile and so not influencing the geochemical budget.

#### D. SULPHATE.

The annual river input of sulphate to the oceans is  $3.67 \times 10^{14}$  g/yr (Garrels and Mackenzie, 1971), and the dissolved sulphate in the oceans comprises one of the major oxidant reservoirs. There are two known processes by which sulphate can be removed from the oceans. Firstly, sulphate can be removed by the precipitation of calcium sulphate. This process may have been important in the geological past, but the present oceans contain no quantitatively significant evaporite basins. The other removal mechanism, and probably the most important in the present ocean, is by bacterial reduction of sulphate in sediments. In areas where the accumulation rate of organic material is larger than its destruction rate, the pore waters can become anaerobic and, under these conditions, bacterial reduction of sulphate occurs. The amount of sulphate removed by this mechanism can be estimated. Most sediments are deposited near-shore and contain about 0.3% sulphur as sulphide. Assuming a present-day sediment flux of  $250 \times 10^{14}$  g/yr (Garrels and Mackenzie, 1971), the rate of loss of sulphur is  $0.75 \times 10^{14}$  g/yr. This corresponds to about  $2.25 \times 10^{14}$  g/yr of sulphate, i.e. 61% of the annual river input.

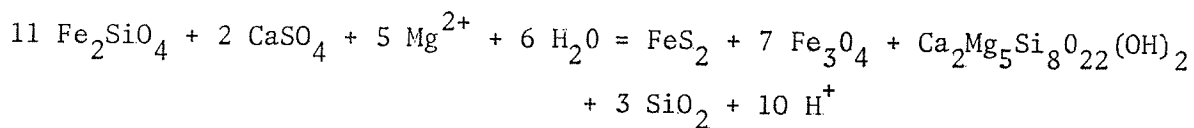
Experimental studies (Mottl, 1976) have indicated that a large amount of sulphate is reduced during basalt-seawater interactions. The amount of reduced sulphur, in many cases, exceeds the total available from the seawater, indicating that sulphur is also supplied from the



basalt. An estimate of the sulphur that can be removed from seawater by the reduction of seawater sulphate to form sulphides can be based upon the mineralogical observations. The amount of pyrite present in the samples studied ranges up to 5% by volume, so an average value of pyrite of 2% is assumed. The density of pyrite is  $5 \text{ g/cm}^3$ , giving a concentration of pyrite of  $0.1 \text{ g/cm}^3$ , and hence of sulphur of  $0.05 \text{ g/cm}^3$ . Therefore, alteration of  $1 \text{ km}^3$  of rock to an assemblage containing 2% pyrite requires  $5 \times 10^{13} \text{ g}$  sulphur. If a sulphur content in oceanic basalts of 0.1% is assumed, then this will provide  $0.28 \times 10^{13} \text{ g}$  sulphur. Therefore, about  $4.7 \times 10^{13} \text{ g}$  sulphur are required. This is equivalent to  $1.4 \times 10^{14} \text{ g SO}_4^{2-}$  (i.e. 38% of the annual river input).

This is likely to be a maximum estimate since the formation of pyrite will be limited to specific areas where conditions of low  $\text{O}_2$  fugacity and high S fugacity prevail; however, it appears that a source of sulphur other than the basalt is necessary for the formation of the observed quantities of pyrite.

Sulphate reduction by the oxidation of ferrous iron may take place by reduction of sulphate directly from seawater, or by a reaction involving anhydrite:



However, this reaction may not apply to the subsea floor system where anhydrite has not been observed. A simple calculation demonstrates that, if sulphate was being removed from seawater as anhydrite, then a considerable amount of anhydrite should be present. Assume that all of the seawater sulphate (2640 ppm) is removed during hydrothermal alteration by precipitation of anhydrite, and that the water-to-rock ratio is 5-50:1. Then, for every  $\text{km}^3$  of rock altered,  $17-170 \times 10^{12} \text{ g}$

$\text{CaSO}_4$  would be precipitated. In addition, the kinetics of the reaction suggest that sulphate reduction may also be extensive only in localities where there is a heat source (Wolery and Sleep, 1976). Although sulphate reduction occurs in the system, the absence of anhydrite in dredged oceanic metabasalts cannot be due entirely to this process. Mottl (1976) has suggested that a more plausible explanation is that anhydrite is subsequently redissolved by seawater circulating at lower temperatures.

Sulphur isotope studies (Fields et al, 1976) on samples from the DSDP show that there is a large isotopic variation ( $\delta\text{S}^{34} = -24.2$  to  $+23.0$  ‰) which means that the isotopic chemistry and source of the sulphur cannot yet be defined.

#### E. WATER.

Hydrothermal alteration results in a small proportion of the water that is circulating being retained in the crust. The quantity of water involved is extremely small in comparison with the masses of water within the other reservoirs of the hydrosphere.

A calculation to estimate the maximum uptake of water during hydrothermal alteration can be made assuming a depth of penetration of the circulating fluid of between 1 - 5 km. Taking an uptake of water of 1- 10 g/100 cm<sup>3</sup> from my data, and assuming that all of the freshly intruded crust to that depth of penetration is altered, then the total annual uptake of water can be calculated; the results are shown in Table 3-7. The mass of water delivered to the oceans annually from continental runoff and groundwater influx is  $32.5 \times 10^{18}$  g. (Garrels and Mackenzie, 1971), and so this means that the water fixed in the crust during hydrothermal circulation is negligible in terms of the mass

TABLE 3-7.

Water Flux During Hydrothermal Alteration.

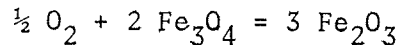
Depth of Penetration. (km)	Vol. Rock Altered. (km <sup>3</sup> )	Amount of H <sub>2</sub> O Gained Assuming Flux of 1-10g H <sub>2</sub> O/ 100 cm <sup>3</sup> (x 10 <sup>13</sup> g.)
1	2.75	2.75 - 27.5
2	5.50	5.50 - 55.0
5	13.75	13.75 - 135.0

balance of water, but it may be important for melting conditions at the subduction zones.

F. OXYGEN.

Garrels and Perry (1974) have suggested that the atmospheric oxygen reservoir has been fairly constant for 600 myr., and furthermore, that the present state is maintained in a near steady state condition by a balance between the production of oxygen by photosynthesis and its consumption by respiration, decay, and weathering of organic matter.

The oxidation- reduction system of oceanic basalt is represented by the following reaction:



Helgeson (1969) has estimated that, for this reaction,  $\log K = 18.95$  at  $200^\circ C.$ , and so it will proceed until  $f_{O_2} = 10^{-37.9}$ . The concentration of dissolved oxygen in the seawater entering the sub-sea floor system is about  $2 \times 10^{-4}$  moles/l., and, for the sake of simplicity in calculating removal of oxygen, it is assumed that all of this oxygen is removed during reaction with basalt. Then, for varying depths of penetration and assuming a water-to-rock ratio of 5 - 50: 1, the number of moles of oxygen removed can be calculated (Table 3-8). This amount can then be converted into a percentage of the annual net photosynthetic production ( $3.5 \times 10^{12}$  moles/yr; Garrels et al, 1976), and this is shown in the last column of Table 3-8. This indicates that even by altering large amounts of rock intruded, the amount of oxygen removed as  $Fe_2O_3$  is a very small percentage of the annual production of oxygen by photosynthesis. This confirms that hydrothermal alteration is not at all significant in its consumption of oxygen, and does not affect the present near steady state condition of oxygen.

TABLE 3-8.

Oxygen Consumption During Hydrothermal Alteration of Basalts.

Depth of Penetration (km.)	Vol. Rock Altered (x 10 <sup>15</sup> cm <sup>3</sup> )	Vol. Water Reacted (x 10 <sup>12</sup> l.)	No. Moles O <sub>2</sub> Removed. (x 10 <sup>8</sup> moles)	% of Net Annual Photosynthetic O <sub>2</sub> Production.
1	2.75	13.75 - 137.5	27.5 - 275	0.08 - 0.8
2	5.50	27.5 - 275.0	55 - 550	0.16 - 1.6
5	13.75	68.75 - 687.0	137.5 - 1375	0.39 - 3.9

3-7. CONCLUSIONS.

Considerable chemical changes occur during hydrothermal alteration of basalts at mid-ocean ridges. Application of a steady-state approach to the geochemical mass balances of those elements for which major changes are observed lead to the following conclusions:

- 1) Magnesium is taken up by the rock during hydrothermal alteration in the formation of chlorite. In general, fluxes range from 1 - 10 g MgO/ 100 cm<sup>3</sup> of rock, depending on the degree of alteration. This provides a significant sink for Mg, which is extremely important in the geochemical mass balance. In addition, a water-to-rock ratio of 5- 47: 1 is suggested from the chemical analyses.
- 2) The amount of calcium that is leached from basalt varies between 1 - 10 g.CaO/ 100 cm<sup>3</sup> of rock, and this flux has the potential to solve the excess sedimentary calcium problem pointed out by Garrels and Mackenzie (1971). Hydrothermal alteration provides a source of Ca which could be important in geochemical budgets; however, some of this will be locally precipitated as carbonates, but the amount is not yet certain. The water-to-rock ratio of 5- 57: 1 calculated from the CaO data is consistent with the ratio obtained from the MgO analyses.

An additional source of hydrogen ions to the oceans is provided by the precipitation of CaCO<sub>3</sub> that occurs when the hydrothermal fluid mixes with seawater.

- 3) Silica is generally leached from basalt during hydrothermal alteration, but a considerable portion of it is redistributed within the basaltic pile. The input of SiO<sub>2</sub> via this mechanism is controlled by the

solubility of quartz in the circulating fluid, and by the volume of water that passes through the system. Under this control, the input of silica into the oceans via hydrothermal circulation is of minor importance compared with the annual river input.

4) The changes in the redox conditions during hydrothermal alteration do not affect the present day oxidation states of the atmosphere and hydrosphere. The removal of seawater sulphate by reduction is probably a minor sink in the unbalanced sulphate budget, and is probably limited in extent by kinetics to higher temperature localities. Although oxygen is consumed during hydrothermal alteration, and removed from the system as  $\text{Fe}_2\text{O}_3$ , the quantities involved only make up a small fraction of the amount of oxygen produced by photosynthesis.

The hypothesis set up in the Introduction was that hydrothermal circulation could lead to significant chemical exchange between reservoirs, and could be an important factor in elemental cycles in the oceans. The chemical analyses and results presented in this chapter have established the importance of hydrothermal alteration in the geochemical mass balances of Mg and Ca. In addition, interaction between basalt and seawater at high temperatures provides a source of hydrogen ions which will assist in balancing the excess bicarbonate brought into the oceans by the rivers. The sulphate and oxygen consumed during these reactions are minor, and will have no effect on the oxidation state of the atmosphere.

It has also been possible to put some constraints on the elemental fluxes into the oceans so that flux ranges could be suggested. However, the absolute fluxes of these elements must await further geophysical

information in order to put limits on the volume of basalt that is subject to hydrothermal alteration.



#### 4. TRACE ELEMENT DISTRIBUTION IN HYDROTHERMALLY ALTERED BASALTS.

##### 4.1. INTRODUCTION.

Hydrothermal alteration of freshly intruded basalt at the mid-ocean ridges has been invoked to explain the occurrences of metal-enriched deposits found in the ocean and in oceanic crustal sequences.

Metalliferous sediments in the deep sea are generally associated with active oceanic ridges, and it has been proposed that they originate by hydrothermal alteration of oceanic basalts (Arrhenius and Bonatti, 1965; Bonatti and Joensuu, 1966; Bostrom and Peterson, 1966; Skorniyakova, 1964). The concept of sea-floor spreading requires that these sediments move away from the ridge and are gradually overlain by pelagic sediments. This leads to the formation of a metal-enriched basal sediment layer which has been sampled in several areas of the ocean by the Deep Sea Drilling Project (von der Borch and Rex, 1970; von der Borch et al, 1971; Cronan et al, 1972; Cronan, 1973; Horowitz and Cronan, 1976). A few examples of the chemical composition of these sediments are listed in Table 4-1. They are depleted in Al relative to pelagic sediments, and the Si/Al ratio tends to be higher than in authigenic ferromanganese deposits and deep-sea sediments. Iron and manganese are the two major components of these sediments, but their ratios are highly variable. These sediments also tend to be enriched in Cu, Ni, Zn, Ba, U and Hg.

Metalliferous sediments are also found in ophiolite complexes, which are distinct rock sequences believed to represent slices of oceanic crust that have been obducted on to the continent (for example, Moores

TABLE 4-1. Trace Element Analyses of Metalliferous Sediments.  
(on a CaCO<sub>3</sub>- free basis).

	Wt. %				ppm				
	Fe	Mn	Si	Al	Cu	Ni	Zn	Co	Cr
DSDP sites (#37, 38, 39)	23.6	6.66	7.11	2.39	1070	630	600	86	16 (1)
Crest of EPR (12°-14°S.)	18.0	6.00	6.10	0.5	730	430	380	105	55 (2)
Mid-Atlantic Ridge (26°N.)	0.01	39.2	-	-	12	100	-	18	- (3)
Av. composition pelagic clay	6.50	0.67	25.0	8.4	250	225	165	74	90 (4)

- (1) Dymond et al (1973)
- (2) Bostrom and Peterson (1966)
- (3) Scott et al (1974a)
- (4) Turekian and Wedepohl (1961)

and Vine, 1971; Robertson and Hudson, 1973). The chemical composition of these sediments, and their stratigraphic position within the ophiolitic unit, are consistent with their formation at mid-ocean ridges. In addition, sulphide ore deposits are also widespread within the basaltic unit both as massive ore bodies and as disseminated mineralisations (Spooner and Fyfe, 1973; Bonatti et al, 1976; Fryer and Hutchinson, 1976). These deposits are also believed to be an expression of leaching of trace metals from basalt by circulating seawater, and the subsequent precipitation of sulphides under conditions of low oxygen fugacity.

A consequence of these models for metalliferous sediment and ore deposit formation is that the hydrothermally altered basalt should be depleted in iron, manganese, and some trace elements. Keays and Scott (1976) examined the gold, silver, sulphur, silica, iron and manganese contents of pillow lavas from the Mid-Atlantic Ridge, and attributed the lower concentrations found in the interiors, relative to the rims, to leaching of the interiors by the interaction of basalt with hot seawater.

In this chapter, I present trace element analyses of the suite of hydrothermally altered basalts from 22°S., 4°S., and 22°N., to further test the original hypothesis that hydrothermal reactions result in chemical exchange between rock and seawater, and also to test the hypothesis for the formation of metalliferous sediments and ore deposits. Analyses of the trace elements, except for Mn, were carried out by G. Thompson using optical emission spectrometry; manganese was determined using plasma spectrophotometry. Full details of the methods, together with their precision and accuracy, are given in Appendix II. The chemical analyses are reported in Tables AI-9 and AI-10 of Appendix I.

#### 4.2. RESULTS AND DISCUSSION.

Fresh basalts show a wide range in trace element compositions (Melson et al, 1968; Thompson et al, 1972b). This variation is a function of the source composition, degree of partial melting, and the subsequent fractional crystallisation within the magma before final eruption. For ocean floor basalts, these effects give rise to a depletion in the Cr, Ni and Co contents with increasing fractional crystallisation, while the concentrations of elements such as Zr, Ba, Sr, V, and Y will increase (Thompson et al, 1972b). Hence, the assessment of compositional changes produced by hydrothermal alteration requires a good knowledge of the precursor. In my study, I have used carefully selected samples from areas where fresh samples from the same dredge haul were available, in addition to those samples for which core-to-rim analyses could be carried out. For each of the trace elements, the results presented here are compared with previously published analyses of fresh and altered basalts taken from: Aumento and Loncarevic, 1969; Bonatti et al, 1975; Cann, 1969; Melson et al, 1968; Melson and Thompson, 1971; Nicholls and Islam, 1971; Thompson and Melson, 1972.

##### A. BORON.

Boron shows a positive correlation with  $H_2O^+$  content (Table AI-9, Fig. 4-1), and the core-to-rim analyses indicate that the concentration can increase by up to a factor of two. Previous studies of boron in oceanic basalts (Thompson and Melson, 1970) suggested that low temperature weathering, at ambient bottom water temperatures, resulted in uptake of boron, but that hydrothermally altered basalts may be depleted in this

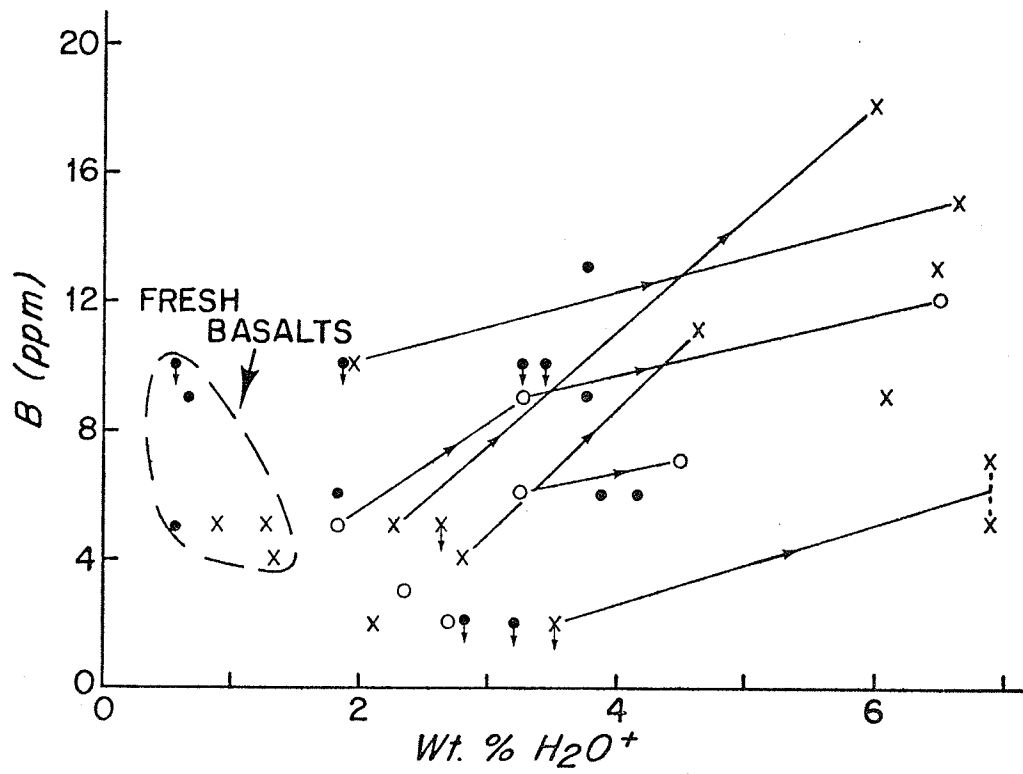
FIGURE 4-1.

Boron concentrations (ppm) vs. water content (wt.%).

- x - AII-42 samples
- - Ch-44 samples
- o - AII-60 samples
- x→x - core-to-rim analyses
- ↓ - analyses recorded as less than the plotted value.

(Precision discussed in the text)

FIGURE 4-1.



element. This latter conclusion was based on the analyses of the cores of some altered basalts from the Ch-44 (22<sup>o</sup>N.) collection. My analyses indicate that most of the cores are depleted or similar to fresh basalts in boron concentration, but the outer rims are enriched. (At the 5 ppm. level, the precision of the analyses is only  $\pm 50\%$ ; at the 10 ppm. level, it is  $\pm 20\%$ , so that significant differences are only seen in a few cases).

There is very little other previous data for comparison. An average value for fresh basalts of  $7 \pm 3$  ppm. was suggested by Melson and Thompson (1971). Apart from the metamorphosed basalts at 22<sup>o</sup>N. that contain less than 10 ppm. of boron, Bonatti et al (1975) and Thompson and Melson (1972) have reported greenschist facies metabasalts containing 15 ppm. boron, suggesting some uptake during hydrothermal alteration.

#### B. LITHIUM.

The concentration of lithium in the fresh rocks and cores is fairly constant at 4-6 ppm (Fig. 4-2). During hydrothermal alteration, lithium is apparently mobilised and the concentration can reach up to 20 ppm. The core-to-rim trends also show enrichment as observed for boron. Previous work (Melson et al, 1968; Thompson et al, 1972; Thompson, 1973a) suggested that, like boron, lithium is gained during low temperature weathering, but no trends were observed during hydrothermal alteration. However, the data from Melson et al (1968) include two altered samples with Li concentrations of 20 and 22 ppm. A metabasalt from 4<sup>o</sup>S. also had a high concentration of Li of 12 ppm (Thompson and Melson, 1972). In addition, mobilisation of Li is also indicated in some

FIGURE 4-2.

Li concentrations (ppm) vs. water content.

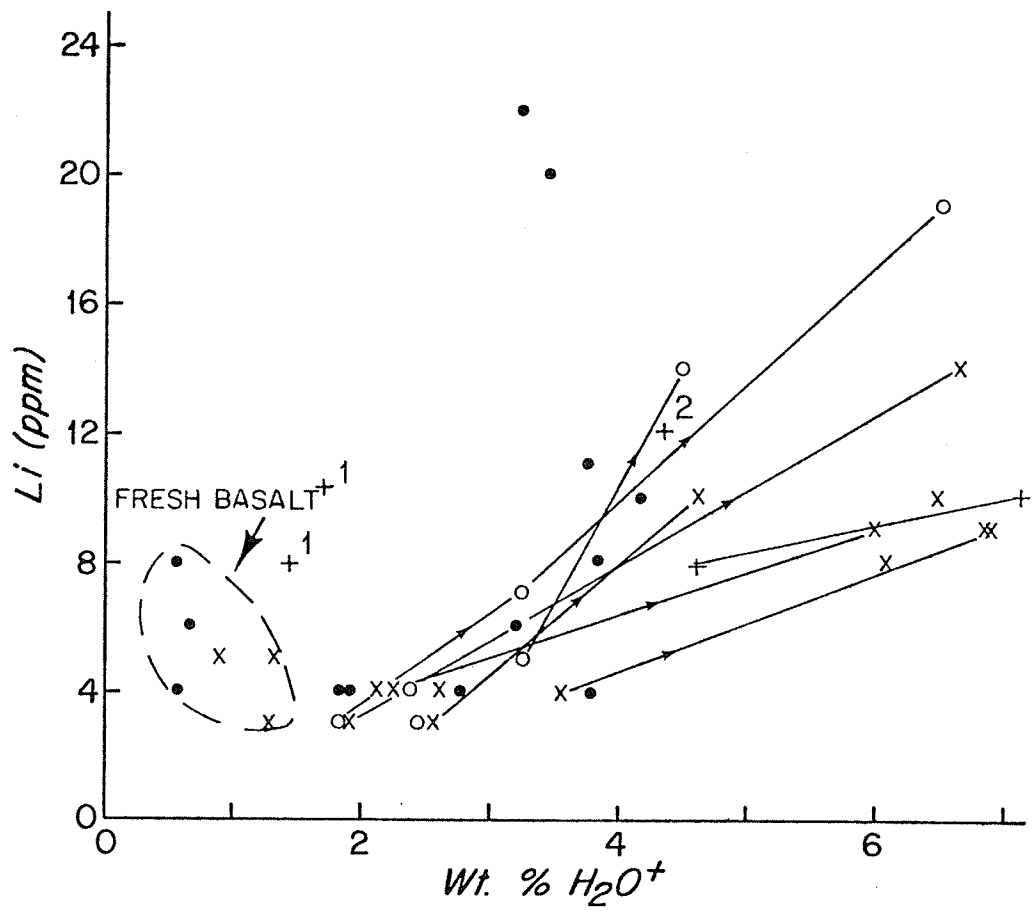
(Symbols as for Fig. 4-1)

+<sup>1</sup> - data from Vallance (1974)

+<sup>2</sup> - data from Thompson and Melson (1972)



FIGURE 4-2.



continental greenschist facies metabasalts (Vallance, 1974), which have Li concentrations of 8-10 ppm., compared with concentrations of about 3 ppm. in the fresh precursors.

My data also indicate that there is a correlation between boron and lithium ( $r = 0.57$ ; 95% confidence limits of 0.51 and 0.62). The precision for Li is  $\pm 10\%$  at the 4 ppm. level, so that the differences observed are significant. Thus, like boron, enrichment of lithium in the outer rims with some depletion in the cores provides evidence for mobilisation.

#### C. STRONTIUM.

The concentrations of strontium in fresh basalts generally fall in the range 90 - 190 ppm. (Engel et al, 1965; Aumento, 1968; Melson et al, 1968). Strontium is apparently mobilised and its concentration has previously been observed to decrease in sympathy with calcium (Cann, 1969; Melson et al, 1968). My analyses (Table AI-9, Fig. 4-3) indicate that the relation is more complex. In the epidote-rich assemblages, uptake of strontium from seawater is indicated (Fig. 4-3a). This is in agreement with Melson et al (1968) who noted that epidote-rich rocks are marked by higher Sr contents. Compared with the fresh samples, the concentrations increase by a factor of two.

Alteration of pillow interiors to chlorite-rich assemblages results in very little change in the Sr concentrations compared with the fresh rocks. Nicholls and Islam (1976) also concluded that, in general, there is no noticeable change in concentration; however, Cann (1969) and Melson et al (1968) observed a slight Sr depletion accompanying the decrease in CaO (Fig. 4-4).

FIGURE 4-3.

Sr concentrations vs. water content.

Fig. 4-3 a): Ch-44 (22°N.) samples

b): AII-42 (4°S.) and AII-60 (22°S.) samples, showing  
core-to-rim trends.

(Symbols as for Fig. 4-1)

FIGURE 4-3 a)

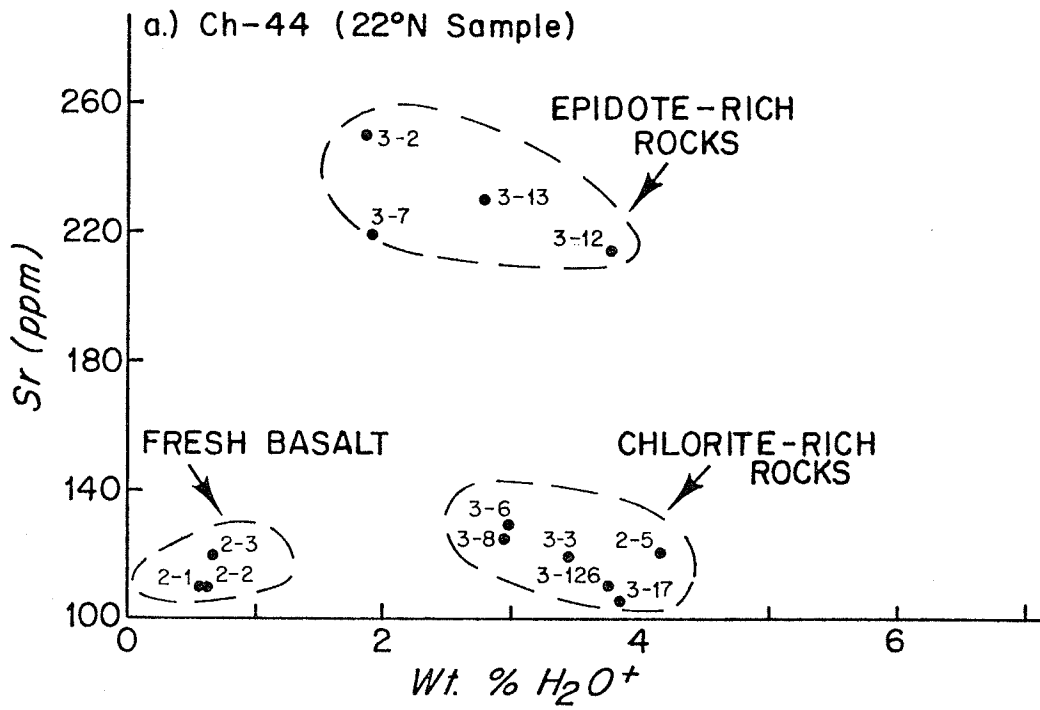


FIGURE 4-3 b)

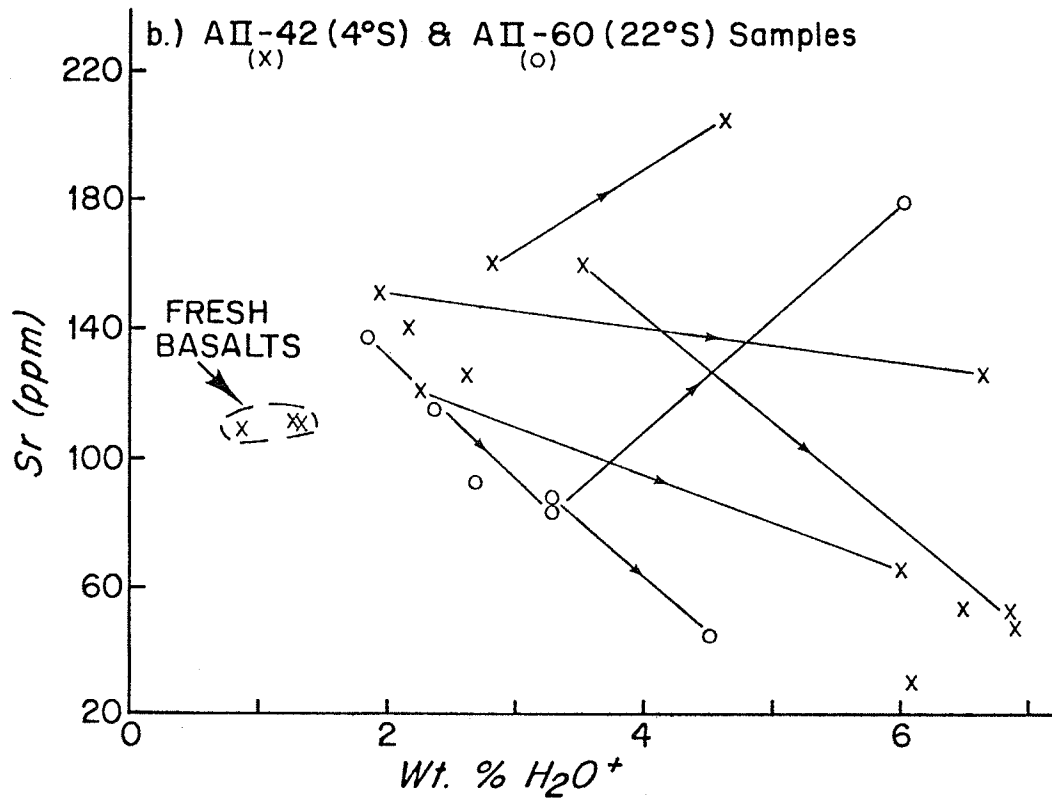
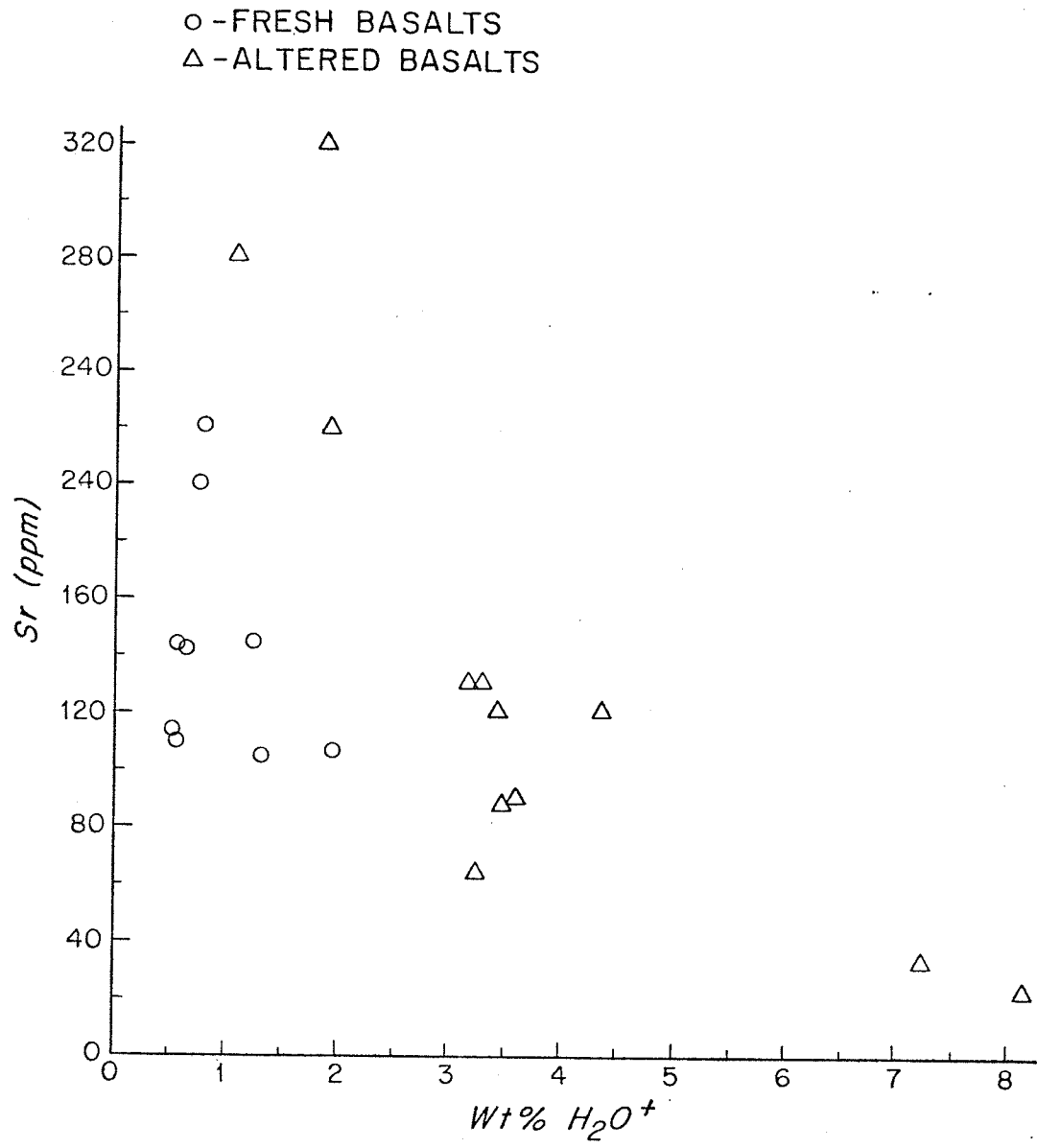


FIGURE 4-4.

Sr concentrations (ppm) vs. water content-  
previously published data.

FIGURE 4-4.



The core-to-rim trends of the altered pillows (Fig. 4-3b) indicate that loss of Sr occurs with the loss of Ca, although there are two exceptions- AII-42 1-118 and AII-60 2-142. Analyses of two glassy basalts that had been altered to dominantly chlorite (samples with  $H_2O^+$  contents of 7.62% and 8.14% in Fig. 4-4), also suggest a loss of Sr during alteration of the outer pillow margins (Cann, 1969).

Fig. 4-5 shows the correlation between Sr and CaO contents for the analyses presented here, together with the previously published data. The epidote-rich rocks fall on a line with a slope (0.08) similar to that for the chlorite-rich assemblage (0.06). If the two exceptions mentioned above are omitted from the calculation of the least squares fit line to the chlorite-rich data, then the correlation is good ( $r = 0.75$ ), and suggests that the Sr concentrations are dominantly controlled by the same chemical processes as calcium.

#### D. BARIUM.

Barium is present in very low concentrations in the fresh basalts studied (less than 5 ppm.). In the hydrothermally altered basalts, no differences can be seen between the two mineral assemblage types (epidote-rich or chlorite-rich); however, there appears to be a slight increase in barium concentration in the altered pillow interiors compared with the fresh rock (Fig. 4-6). However, this is not unequivocal since the concentration of Ba in the fresh basalts from a single area can vary by a factor of three (for example, Melson et al, 1968). The core-to-rim compositional trends, however, indicate some mobilisation of Ba with a decrease in the outer rim, except for AII-42 1-118 and AII-60 2-142, that showed a slight increase in Sr content in the outer margins.



FIGURE 4-5.

Correlation between Sr and CaO contents of fresh and hydrothermally altered basalts.

- x - AII-42 samples
- - Ch-44 samples
- o - AII-60 samples
- x→x - core-to-rim analyses
- Δ - previously published data
- - least squares fit line for my data, omitting epidote-rich rocks, and the two core-to-rim trends discussed in the text.

FIGURE 4-5.

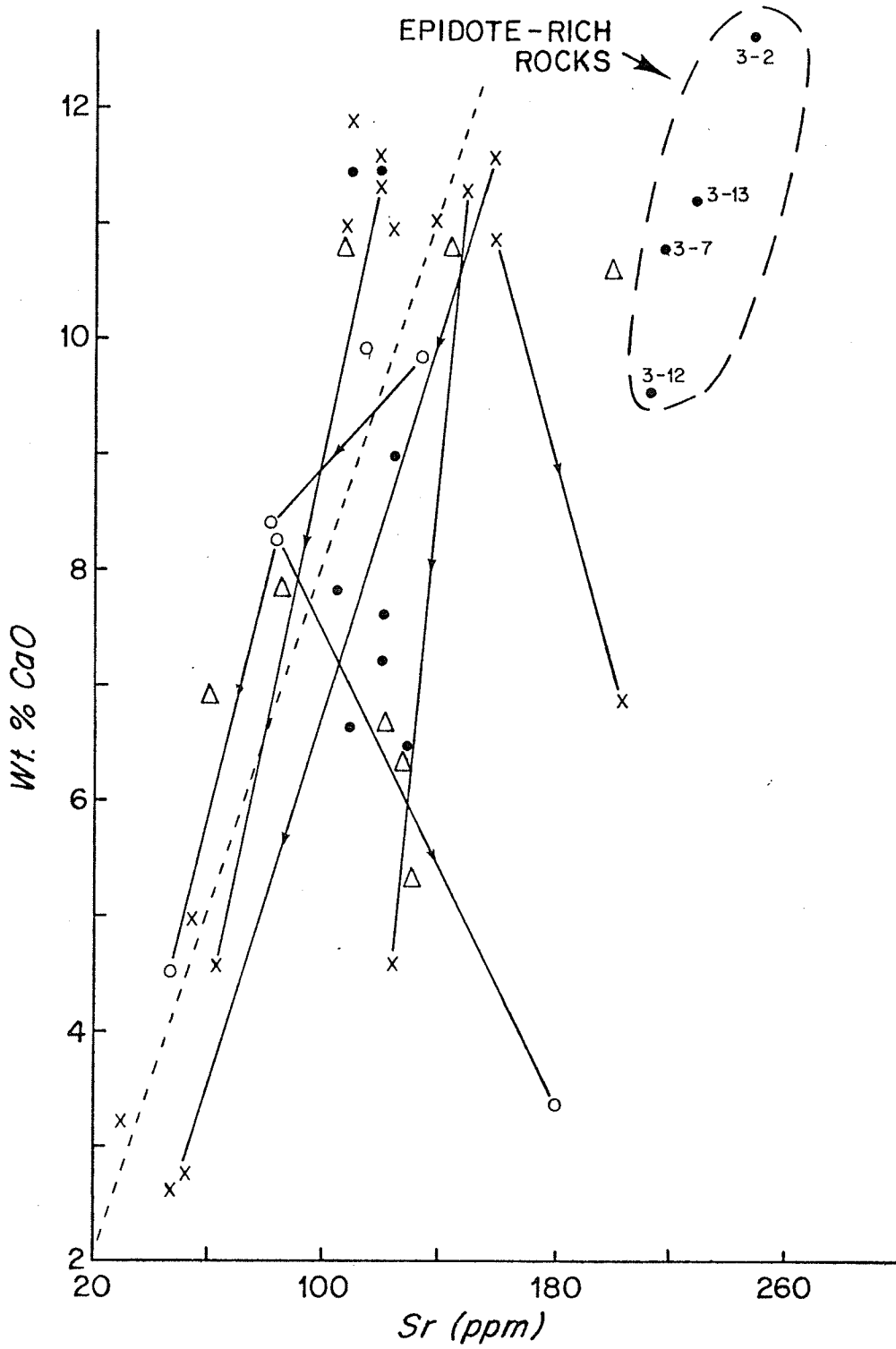


FIGURE 4-6.

Barium concentrations (ppm) vs. water content.

(Symbols as for Fig. 4-1)

Fig. 4-6 a): fresh rocks compared with altered pillow interiors

Fig. 4-6 b): core-to-rim trends.

FIGURE 4-6.a)

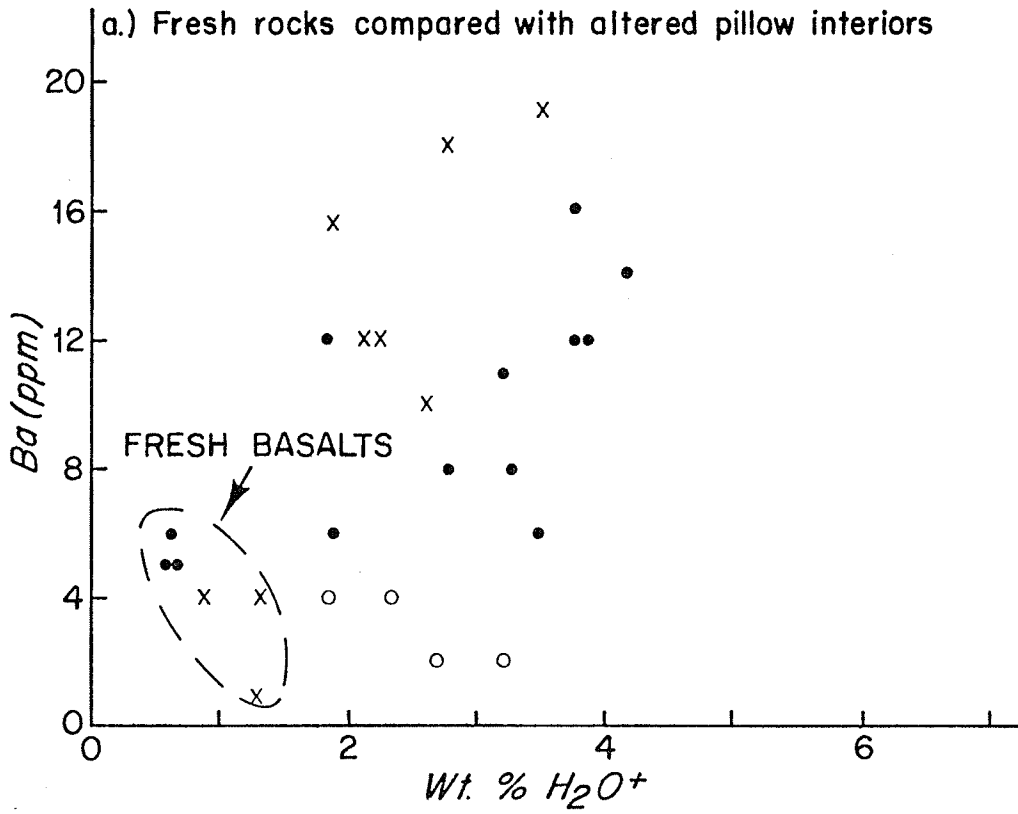
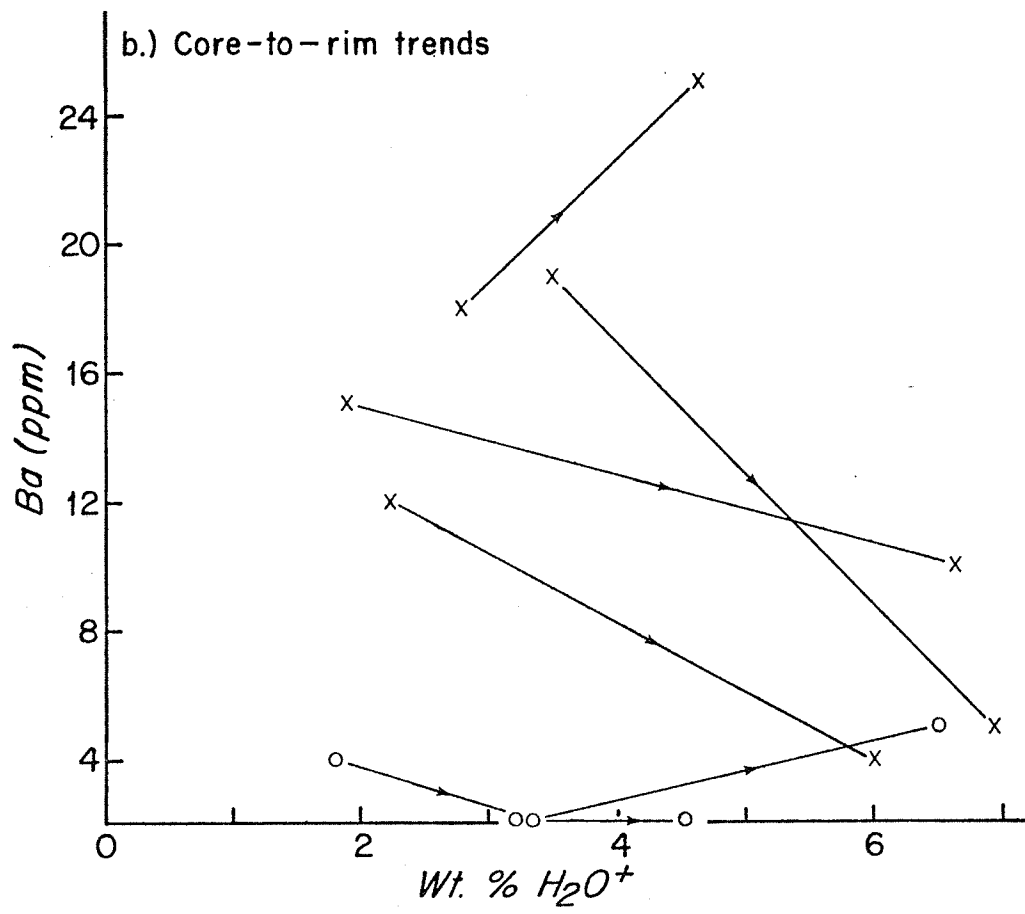


FIGURE 4-6 b)



Published data (Fig. 4-7) show very little variation apart from one of the chlorite-rich samples that has a barium concentration of 22 ppm (Cann, 1969). However, in general, the barium concentrations are apparently not greatly affected by hydrothermal alteration, although the Ba concentrations in the highly altered rims provide evidence of some mobilisation.

#### E. NICKEL AND COBALT.

The variations in concentrations of Co and Ni in fresh oceanic basalts are apparently controlled by olivine fractionation. For example, the Ni concentrations in the fresh basalts studied vary between 75 - 140 ppm., and are correlated with the magnesium concentration.

Alteration of the pillow interiors has no detectable major effect on the concentrations of Ni and Co (Figs. 4-8 and 4-9). The core-to-rim trends for both Ni and Co show higher concentrations in the rim, although several of these trends are within the precision of the analytical technique ( $\pm 10\%$ ). The high concentrations of Ni in the outer margins of AII-42 1-108 and AII-60 2-142, are probably due to the partitioning of Ni into vein sulphides, which are abundant in these samples. This suggests that there is some mobilisation of these elements during hydrothermal alteration.

Previously published data (Figs. 4-10 and 4-11) also indicate some mobilisation, particularly in the alteration of glassy basalts. No definite trends are observed in the alteration of holocrystalline basalts.

Overall, hydrothermal alteration shows no major effects on the concentrations of these elements. However, the concentrations of Ni in the pyrite-rich rocks suggest that there is some leaching and mobilisation of the elements.

FIG. 4-7 BA-PREVIOUSLY PUBLISHED DATA

○ - FRESH BASALTS  
△ - ALTERED BASALTS

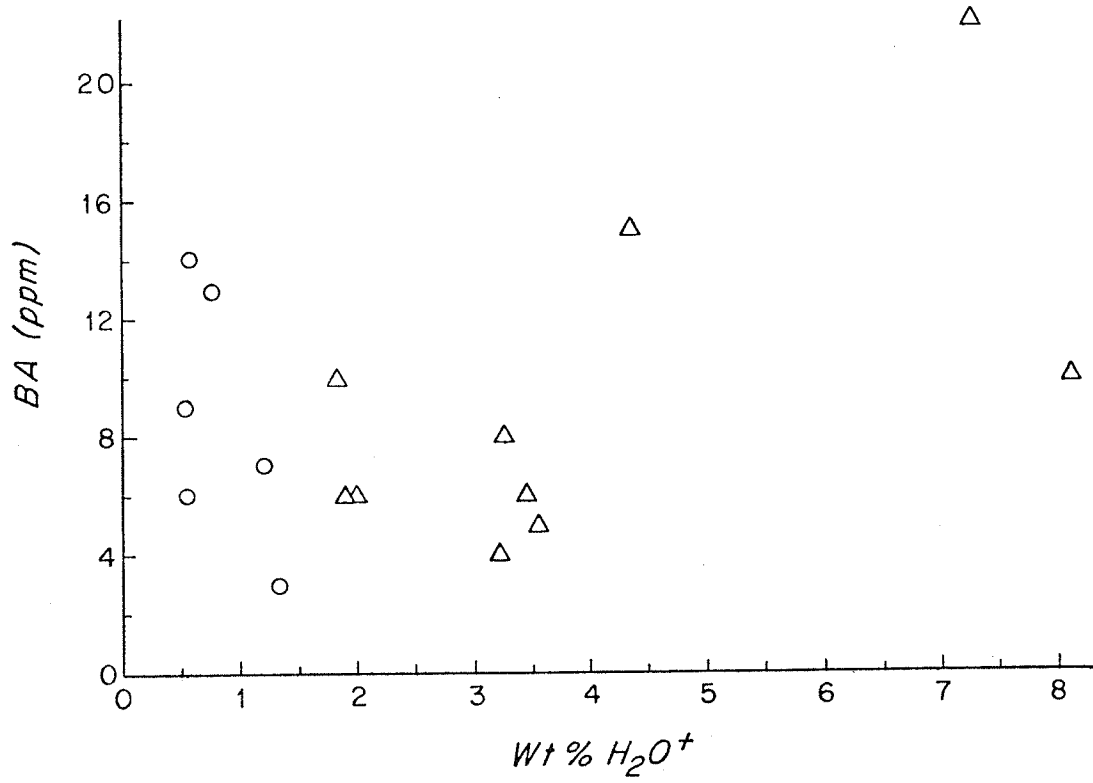


FIGURE 4-8.

Nickel concentrations (ppm.) vs. water content.

(Symbols as for Fig. 4-1)



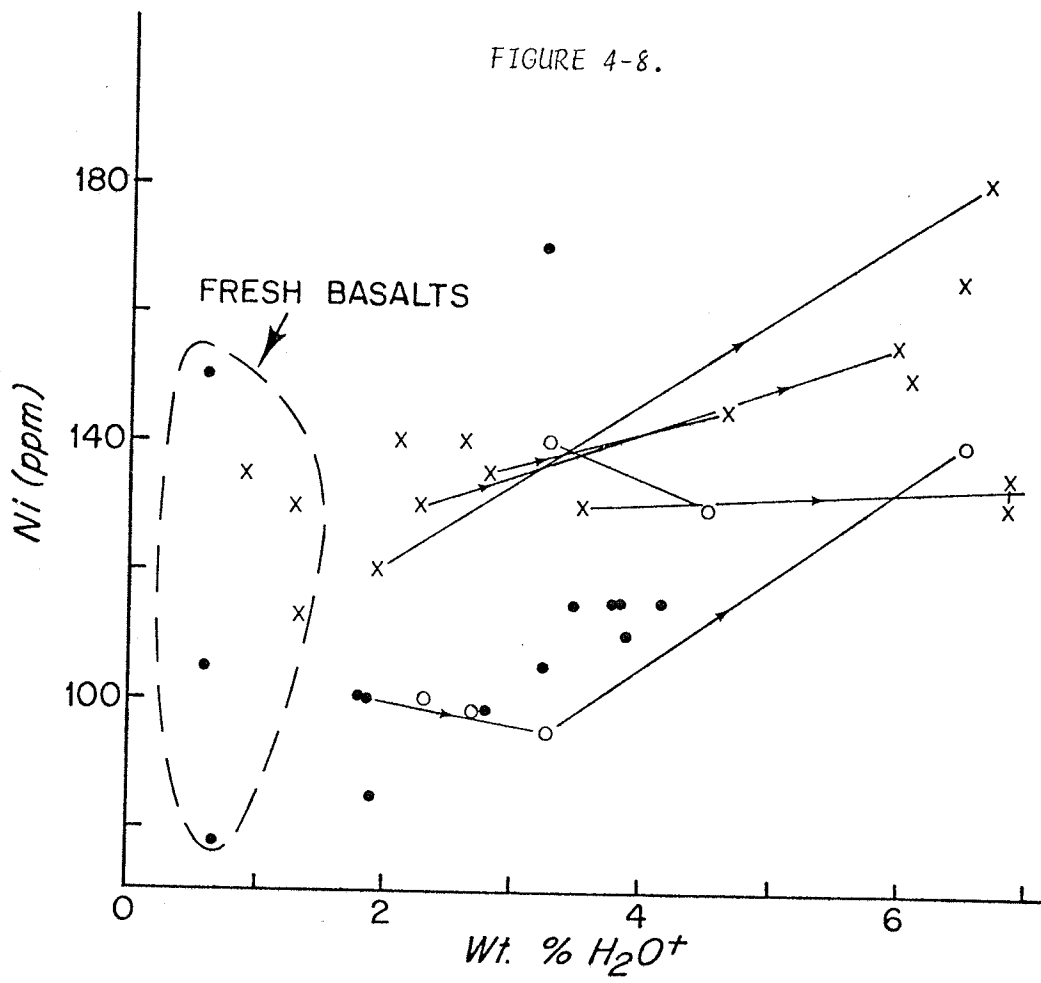


FIGURE 4-9.  
Cobalt concentrations (ppm.) vs. water content.

(Symbols as for Fig. 4-1)

FIGURE 4-9.

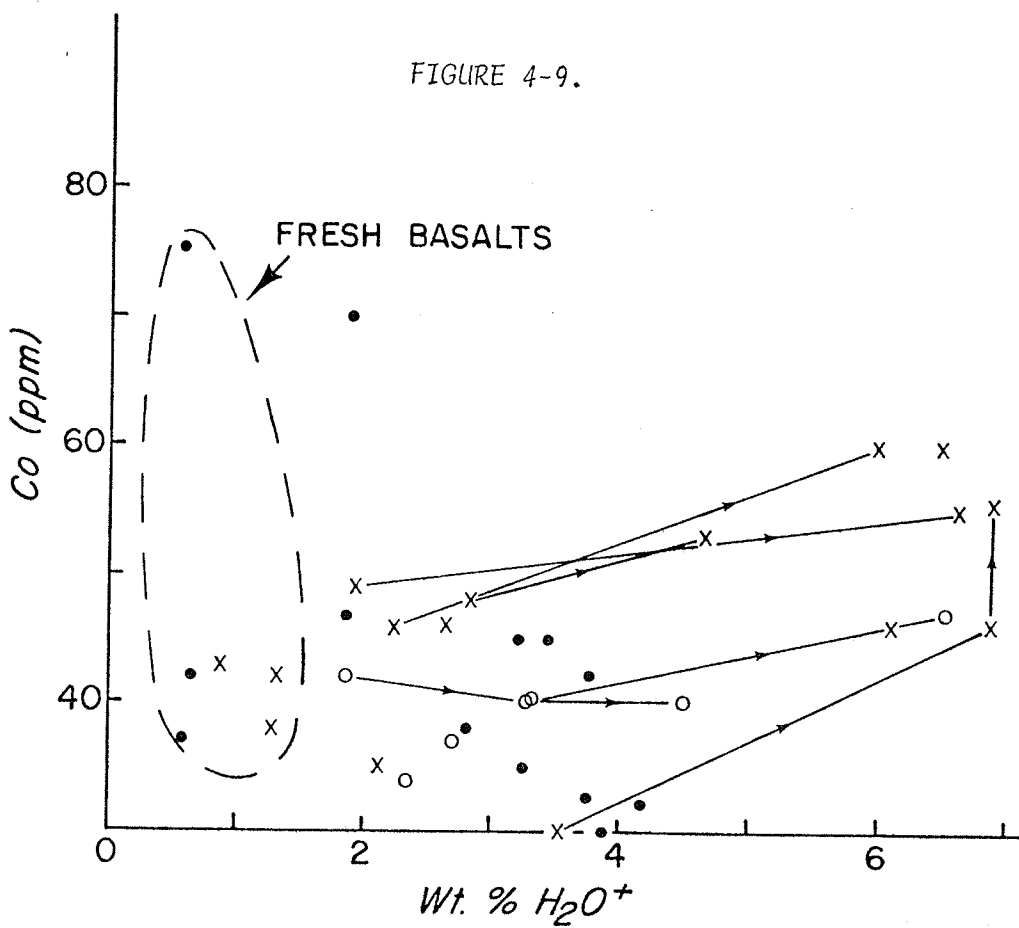


FIGURE 4-10.

Nickel concentrations- previously published data.

FIGURE 4-11

Cobalt concentrations- previously published data.

o - fresh basalts

Δ - altered basalts

FIGURE 4-10

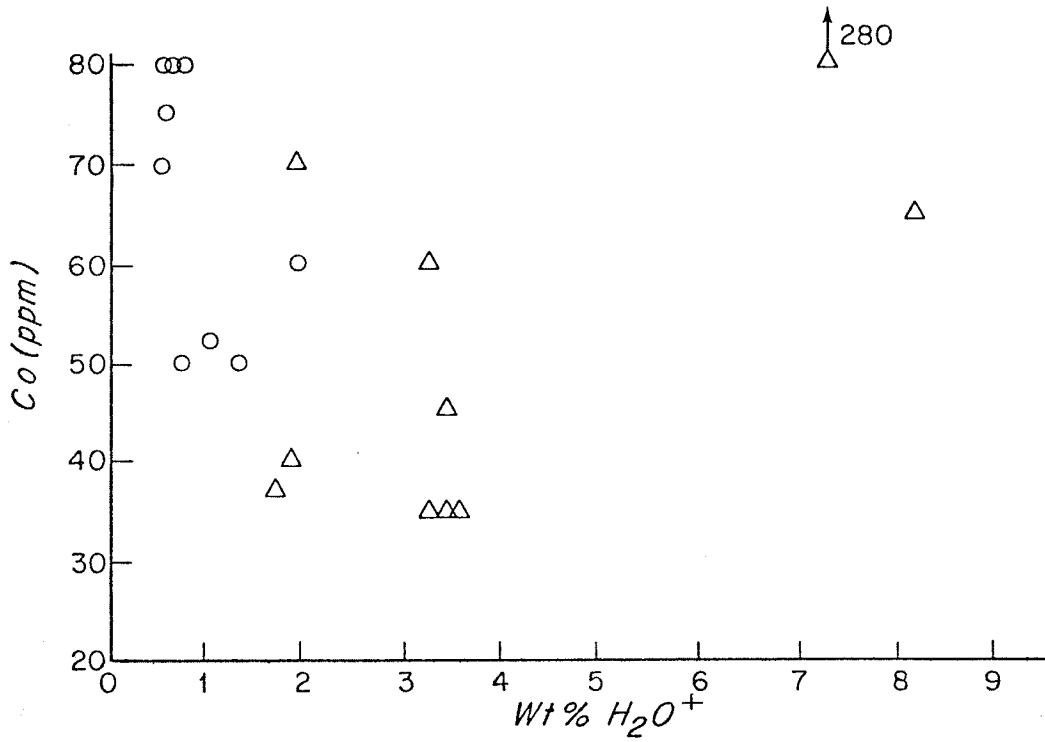
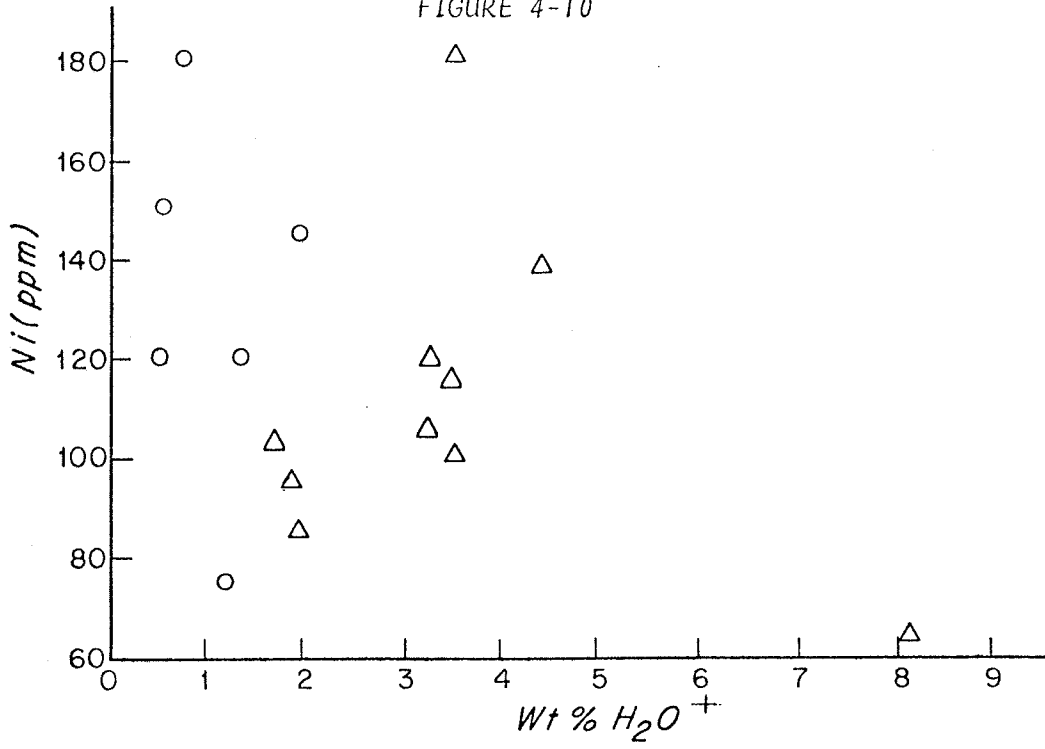


FIGURE 4-11

F. VANADIUM.

The concentration of V in the fresh basalts analysed is between 245 and 290 ppm. The alteration of the pillow interiors results in no major changes in the V content (Fig. 4-12). The core-to-rim trends also suggest that there is no significant mobilisation of V during alteration; all the variations observed are within the precision of the analytical technique ( $\pm 10\%$ ).

Previously published data (Fig. 4-13) have shown much more variation in the concentration of V in both the fresh basalts and hydrothermally altered basalts. However, in general, no significant trends can be seen, suggesting that V is not affected, to any great extent, by hydrothermal alteration.

G. CHROMIUM.

The wide variability in the concentration of Cr in the fresh samples (from 280-550 ppm.) is due to the effect of fractional crystallisation and the degree to which spinel and olivine have crystallised. This wide variation in concentration makes changes due to hydrothermal alteration extremely difficult to observe. The core-to-rim concentrations of Cr show no consistent trends and, apart from AII-42 1-108 and AII-60 2-142, which show marked Cr concentrations in the rims (370 ppm. compared with 300 ppm., and 405 ppm. compared with 230 ppm. respectively), the concentration of Cr stays constant within the precision of the analytical method.

Other analyses of Cr in oceanic basalts also indicate wide variability in the Cr contents of both fresh basalts (100 - 500 ppm.) and greenschist facies metabasalts (70 - 400 ppm.), but no consistent

FIGURE 4-12.

Vanadium concentrations vs. water content

(Symbols as for Fig. 4-1)

FIGURE 4-13.

Vanadium concentrations- previously published data.

(Symbols as for Fig. 4-11)

FIGURE 4-12.

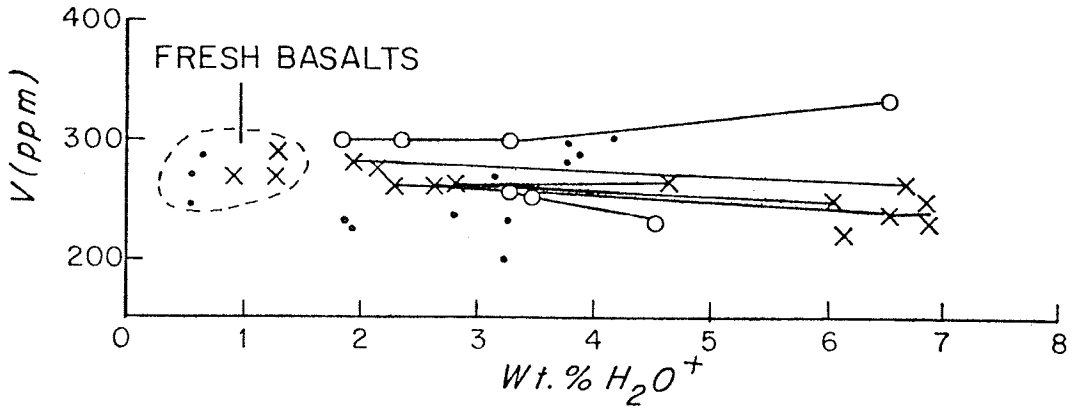
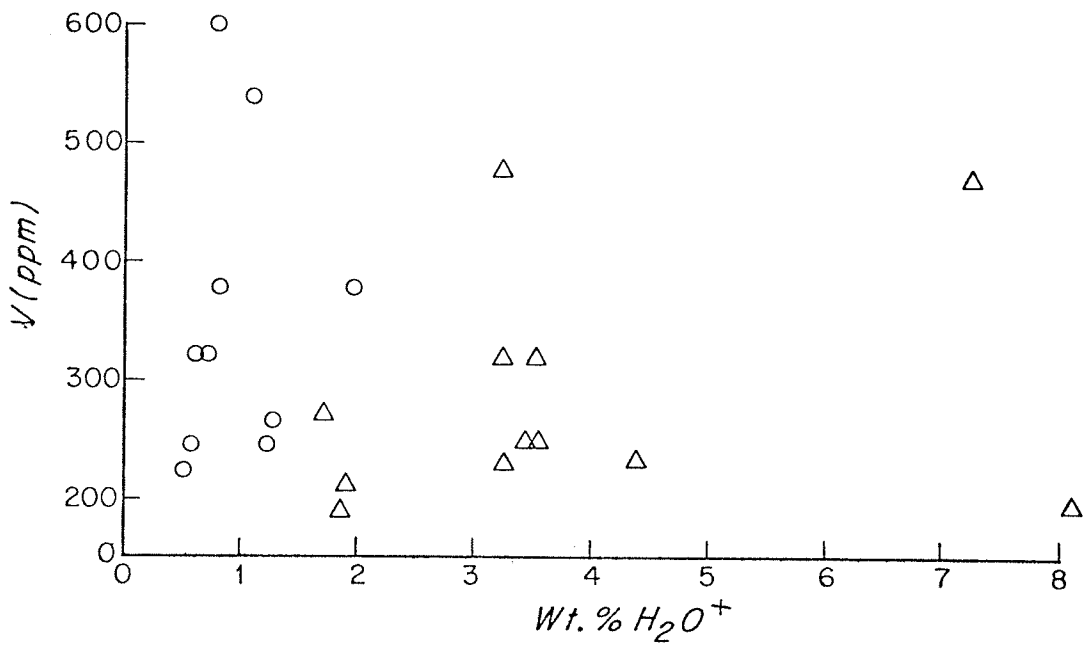


FIGURE 4-13.





trends during alteration are observed.

#### H. COPPER.

The concentration of Cu in the fresh samples analysed is quite variable, ranging from 48 - 155 ppm. Alteration of the pillow interiors to both chlorite-rich and epidote-rich assemblages results in leaching of the Cu into the circulating fluid, with a resultant decrease in the copper concentrations (Fig. 4-14). Several of the core-to-rim trends also indicate a lower concentration of copper in the outer margins; however, others show marked increases in the concentration of copper in the outer rims, as do a few other altered samples where core-to-rim analyses were not possible. These samples are those containing vein sulphides, so clearly there is partitioning of the Cu with these secondary deposits.

Fig. 4-15 shows previously published data which, although not as convincing, do suggest mobilisation of Cu during hydrothermal alteration, with a concomitant decrease in the Cu concentration of the basalt. These observations lead to the conclusion that hydrothermal alteration results in mobilisation and enrichment of Cu in the circulating fluid, with local precipitation when environmental conditions compatible with sulphide precipitation are encountered.

#### I. MANGANESE.

The results of the Mn analyses are reported in Table AI-10, and are plotted against  $H_2O^+$  in Fig. 4-16. The variability in concentrations suggests that Mn is mobilised during hydrothermal alteration, and migrates in the circulating fluid. The Mn concentrations in the altered samples are extremely variable, and no consistent trends can be seen during

FIGURE 4-14.

Copper concentrations (ppm.) vs. water content.

(Symbols as for Fig. 4-1)

FIGURE 4-15.

Copper concentrations- previously published data

(Symbols as for Fig. 4-11)

FIGURE 4-14

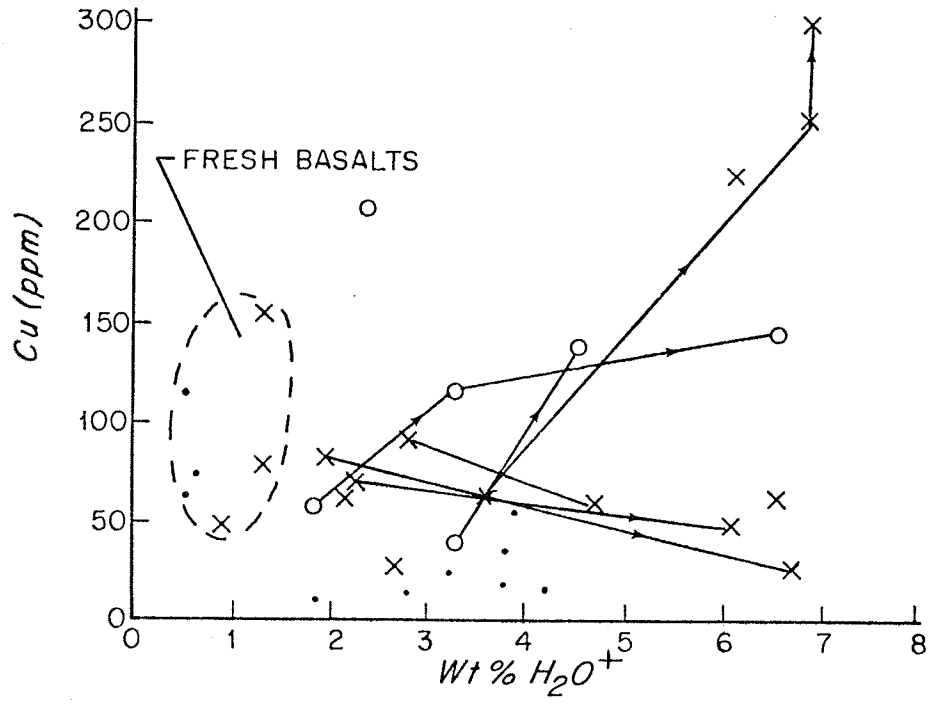


FIGURE 4-15

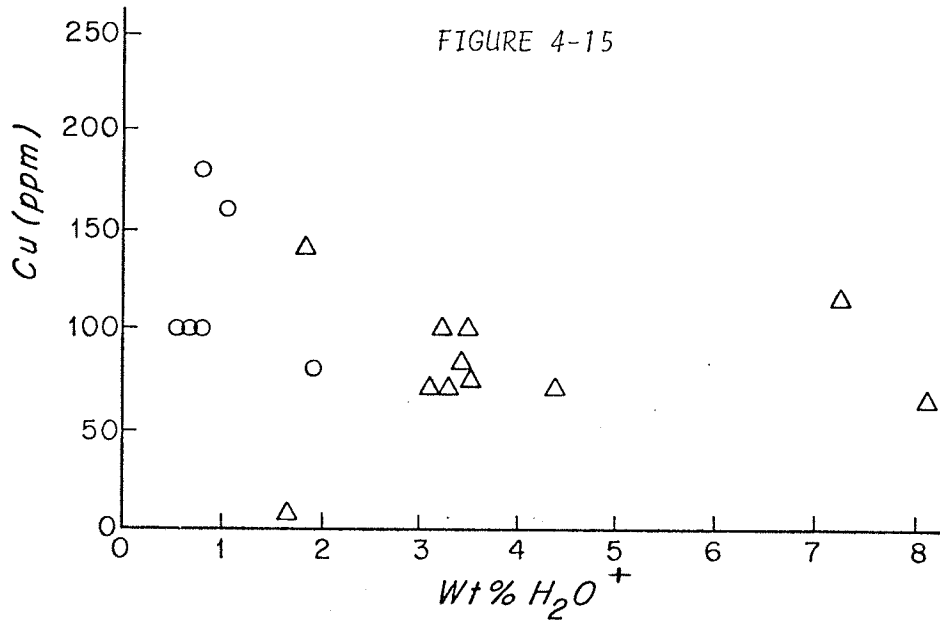


FIGURE 4-16.

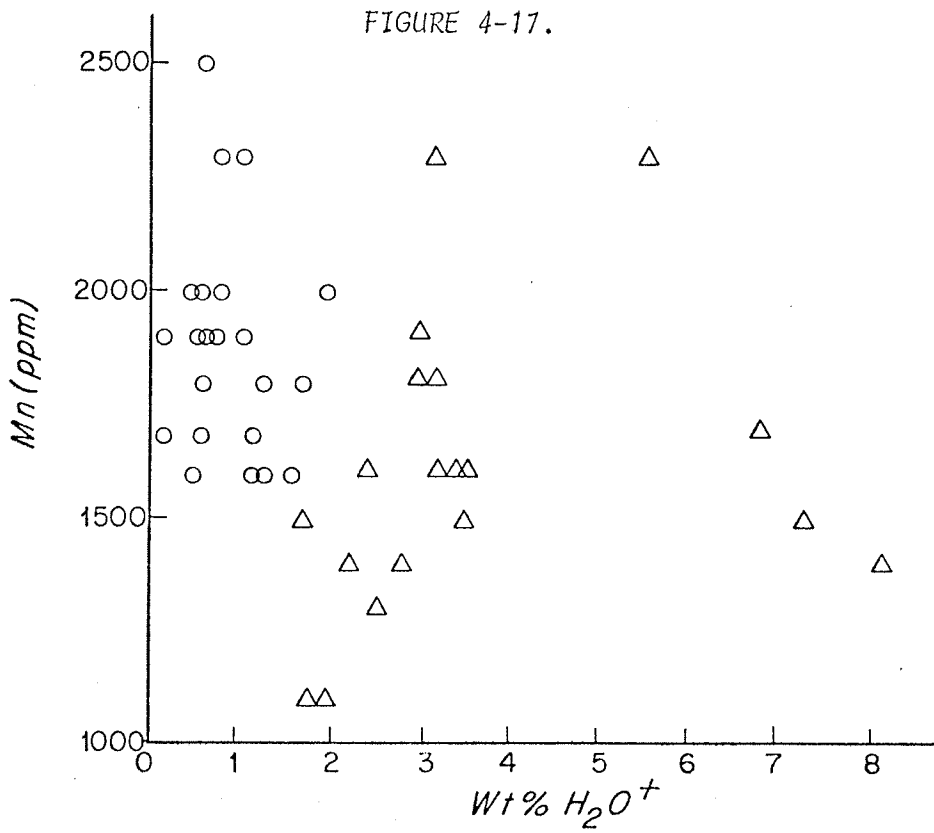
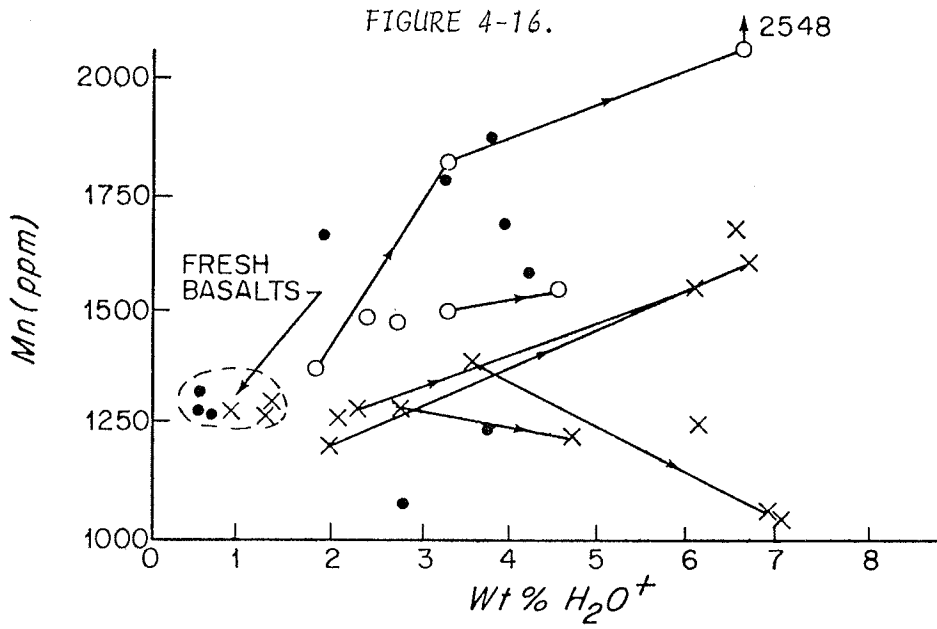
Manganese concentrations vs. water content.

(Symbols as for Fig. 4-1)

FIGURE 4-17.

Manganese concentrations- previously published data.

(Symbols as for Fig. 4-11)



alteration of either the pillow interiors or the outer margins. Keays and Scott (1976) observed Mn enrichment in the rims of pillow basalts from the Mid-Atlantic Ridge, and attributed it to loss of Mn from the interiors during hydrothermal alteration.

Other published data are plotted in Fig. 4-17. The Mn concentrations have been taken from the major element analyses presented in the references listed in Chapter 3, section 3.2. The Mn concentrations are extremely variable in both the fresh and altered basalts, and no consistent trends are observed. However, the data do suggest that Mn is mobilised during hydrothermal alteration. Its migration will be dependent on the prevailing Eh and pH conditions, since these determine the concentration of Mn in solution.

#### J. YTTRIUM AND ZIRCONIUM.

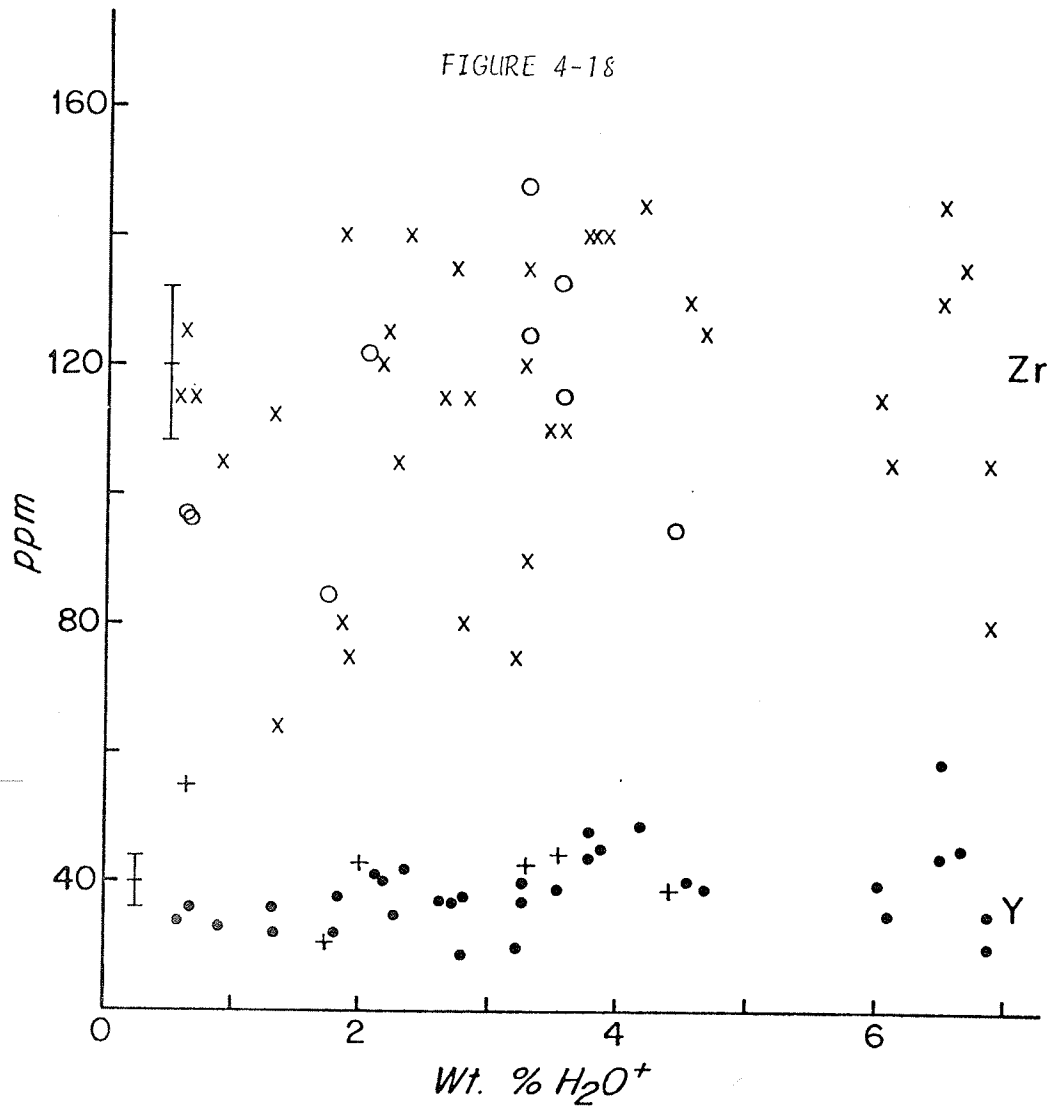
Yttrium and zirconium are concentrated in the residual liquid during fractional crystallisation; thus, fresh basalts show a range in concentration dependent on the amount of crystal precipitation before eruption. Hydrothermal alteration apparently has little effect on the concentration of these elements (Fig. 4-18). Most of the observed variation can be explained by density changes during alteration.

This constancy during alteration is of particular interest due to the recent use of these elements, together with titanium, for the identification of the original tectonic setting of basic volcanic rocks (Pearce and Cann, 1971; Frey et al, 1976). These workers have compared the trace element concentrations in rocks from known tectonic settings with those whose origin is unknown. The success of this method obviously requires that secondary processes, such as hydrothermal

FIGURE 4-18.

Concentrations of yttrium and zirconium vs. water content.

- x - Zr concentrations - this study
- o - Zr concentrations - previously published data
  
- - Y concentrations- this study
- + - Y concentrations - previously published data





alteration, do not markedly affect the concentrations of these elements. My study confirms this assumption as shown in Fig. 4-18. Pearce and Cann (1973) also suggested that distinction between ocean floor basalts, low-K tholeiites from oceanic islands, and calc-alkali basalts from island arcs, is possible using a discriminant function for Ti and Zr. A plot of Ti vs. Zr is shown in Fig. 4-19 for the data from my analyses, together with published data from basalts from other tectonic situations. I have used the Ti data normalised to constant Al for my data since, although the concentration of Ti may remain constant during alteration, changes in the concentrations of other elements may cause changes in the Ti values in the bulk composition analyses. The hydrothermally altered samples fall into the same field as the ocean floor basalts indicating that the Ti and Zr remain constant during hydrothermal alteration, as previously noted. The separation between the compositional fields is quite good, although there is a slight overlap at high and low titanium values. A better separation is achieved in a Zr-Y plot (Fig. 4-20), where a small field overlap occurs between the volcanic arc and ocean floor basalts, but the island basalts fall into a well-defined separate field. This suggests that for basalts that have been subject to hydrothermal alteration, consideration of the Zr-Y relation may provide a more reliable way of predicting the original tectonic setting than consideration of Ti-Zr relations.

FIGURE 4-19.

Relation between Ti and Zr contents for basalts from different tectonic settings.

- - hydrothermally altered basalts (this study)
- - fresh ocean floor basalts (this study and Pearce and Cann, 1973)
- x - volcanic arc rocks (Pearce and Cann, 1973)
- + - ocean island basalts (Pearce and Cann, 1973)

FIGURE 4-19

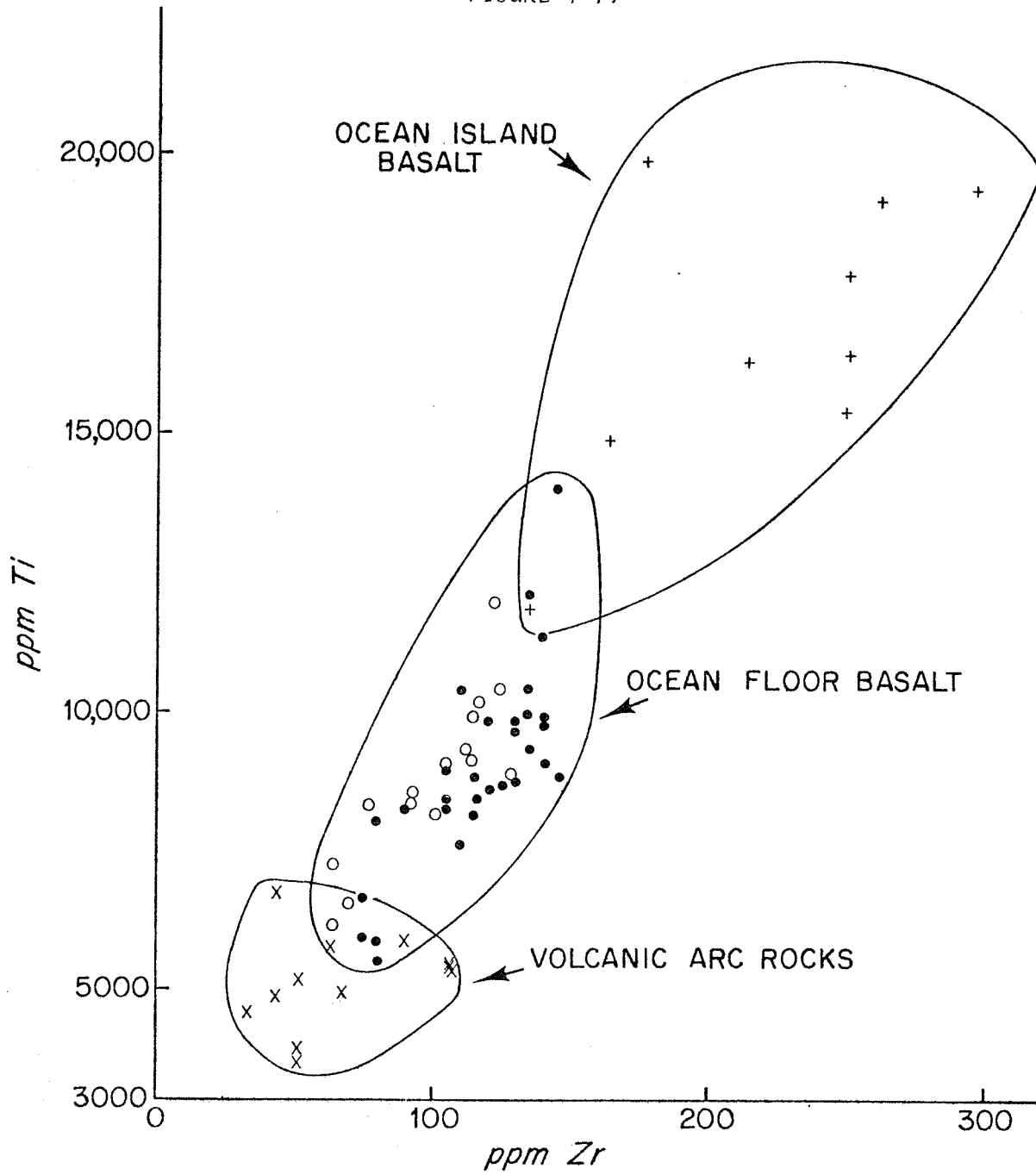
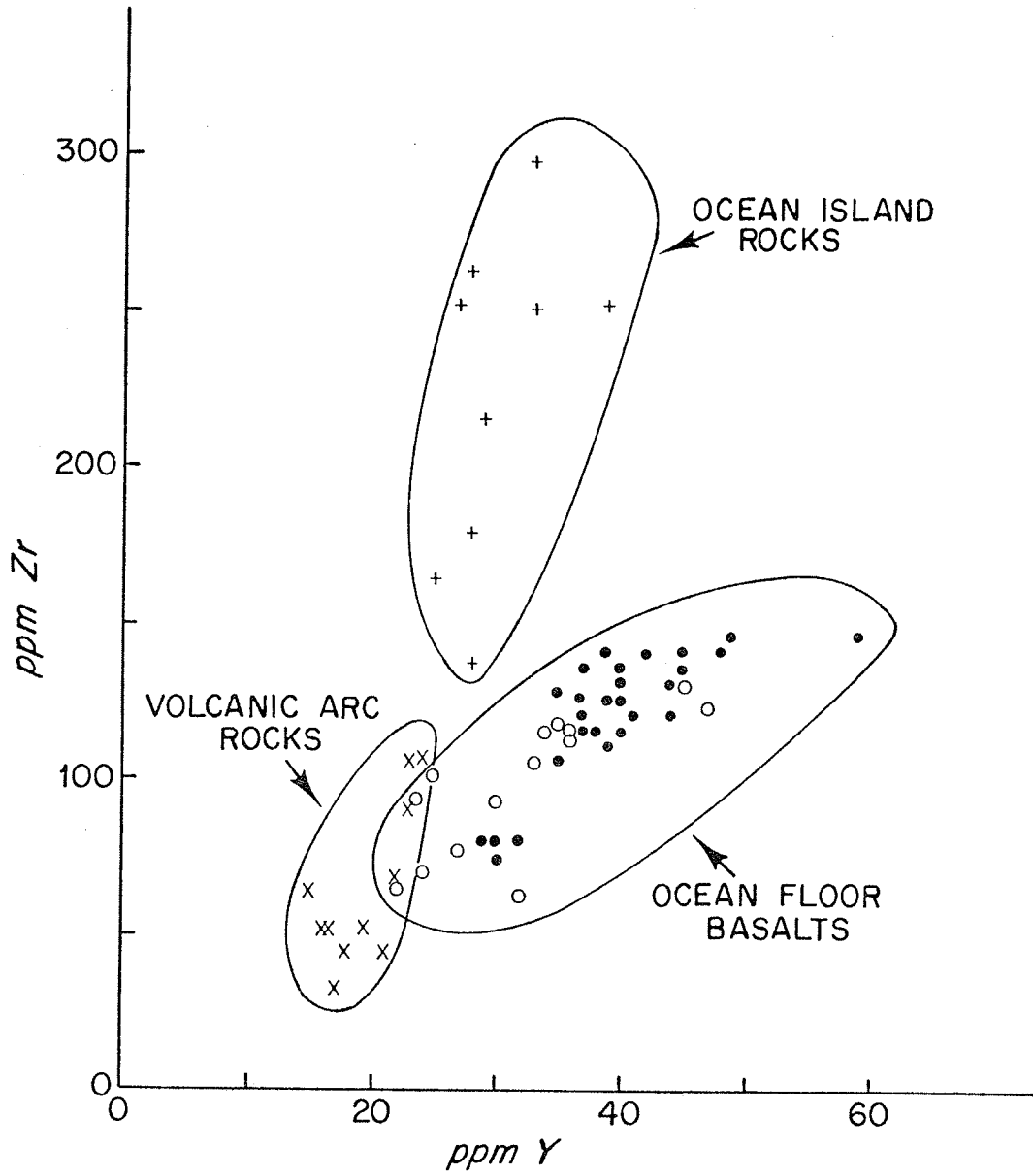


FIGURE 4-20.

Relation between Zr and Y contents of basalts from different  
tectonic settings

(Symbols as for Fig. 4-19)

FIGURE 4-20



4.3.

A. WATER TO REACTED ROCK RATIO.

In the previous section, a definite depletion of Sr was observed during hydrothermal alteration of basalts. Hence, it is of interest to calculate a water-to-reacted-rock ratio from these results, and from the drillhole data from the Reykjanes geothermal system (Mottl et al, 1975), and compare it with the value of 5 - 57: 1 obtained from the Ca and Mg results.

The mass balance of Sr was calculated by normalising the trace element data to constant zirconium, and using the core-to-rim analyses of individual basalts. The differences in Sr concentrations between the cores and rims range from 25 - 111 ppm., with a mean of 55 ppm. The increase in the Sr content of drillhole water from Iceland ranges from 2 - 5 ppm (see Table 4-2). These values give a water-to reacted-rock ratio of between 9 - 37: 1, which is in very close agreement with the estimate made previously.

B. ELEMENTAL FLUXES.

The data presented here have suggested that hydrothermal alteration of basalts results in mobilisation of some of the trace elements. Elements, such as Cu and Sr, show definite depletions in the altered rocks and must be leached out and migrate in the circulating fluid. Other elements, such as Li, B, Mn, Ba, Ni, and Co show sufficient variation in composition compared to the fresh precursor to indicate that some leaching of these elements does take place. However, all of these elements may either subsequently be taken up in the secondary mineral phases, which will give rise to local elemental enrichments, or

TABLE 4-2.

Trace Element Concentration in Reykjanes Geothermal Brines, Iceland.

	Concentrations in ppm.							Concentrations in ppb.				
	B	Li	Ba	Sr	Fe	Mn		Cr	Co	Ni	V	Zn
Reykjanes spring <sup>1</sup>	12	7.4	--	--	0.2	--		<1.0	<1.0	<1.0	0.7	<2.0
Reykjanes drillhole 8 <sup>2</sup>	7	--	10.3	9	0.5	2.0		<0.05	<0.1	<0.1	<0.1	--
Reykjanes spring 1918 <sup>2</sup>	12	--	7.1	12	0.3	4.5		<0.05	<0.1	<0.1	<0.1	--
Seawater	~5	0.1	~0.02	~7	<0.01	<0.01		~0.1	~0.1	~0.5	~0.3	~3

1- Bjornsson et al (1972) and Arnorsson et al (1974)

2- Mottl et al (1975)

may remain in solution to be precipitated on contact with oxygenated seawater. The remaining elements- Y, V, Zr, and Cr- are not affected by hydrothermal alteration.

These exchanges should be reflected in the chemistry of the fluid with which the rocks reacted. It is therefore pertinent to compare these trends with data from the Reykjanes geothermal system and from experimental studies. Table 4-2 summarises the trace element data from the Reykjanes brines, and experimental data for Fe and Mn are listed in Table 1-1. The concentration changes in the circulated fluid are mostly consistent with my observations. B, Li, Ba, Sr, Fe, and Mn concentrations are all higher in the drillhole water than in the entering seawater. Any changes in the concentrations of Cr, Co, Ni, and V could not be determined due to the detection limits of the analytical technique (Mottl, 1976). However, the Li, B, and Ba contents of the fluid are somewhat higher than would be expected from the concentration changes in the altered basalt observed in this study. This may be due to the differences in the secondary mineral assemblages, giving rise to differences in the uptake of these elements.

The calculation of trace elemental fluxes from the analyses of fresh and altered basalts is not meaningful at this time. Uptake of trace elements from the circulating fluid by secondary minerals represent migration within the lithospheric reservoir, and may not result in fluxes from the lithosphere to the oceans; hence, they may not affect the overall geochemical mass balances. The data demonstrate only that some of the trace elements are mobilised during hydrothermal alteration; however, the specific reactions resulting in uptake of some elements into certain secondary mineral phases are not yet certain. Hence, high



concentrations of elements observed in these samples could be due to local enrichments and not representative of the overall elemental fluxes.

#### 4.4. HYDROTHERMAL ALTERATION AND IMPLICATIONS FOR METALLIFEROUS SEDIMENT AND ORE DEPOSIT FORMATION.

My data have indicated that hydrothermal alteration results in leaching of some of the trace metals from the basalt, allowing their subsequent migration in the circulating fluid. This is consistent with the compositions of the fluids reacted with basalt under experimental conditions, and with the composition of the Reykjanes geothermal brines in Iceland. Clearly, some of the leached elements will be reprecipitated or taken up in secondary mineral phases, and will be retained within the basaltic pile. However, hydrothermal alteration provides a mechanism for the production of a metal-enriched solution which can be debouched on to the sea floor, and could be important in the formation of metal-enriched sediments at the active oceanic ridges. The wide variability in the compositions of these sediments may be partly due to different environmental conditions, such as pH, Eh and water-to-rock ratios, encountered during circulation of the fluid, resulting in differences in the leaching and subsequent uptake of the trace metals. However, mixing of hydrothermally precipitated components, and authigenic precipitates from the overlying seawater, as suggested by Dymond and Veeh (1975), and Bischoff and Sayles (1972), may also account for some of the variability.

My observations also clearly indicate that sulphides precipitate in veins within the basaltic pile, most likely when the temperatures are high enough for the reduction of seawater sulphate to occur, and when the

oxygen fugacity is low. However, the source of the sulphur is still equivocal as previously discussed. Scanning photographs of these deposits have shown that they contain Fe, Cu, Zn, and perhaps small quantities of Ni and Co, and so it can be concluded that hydrothermal reactions provide a mechanism of concentration of these trace metals into the sulphide phases. However, the extent of these deposits is not certain. If ophiolites represent uplifted oceanic crust, then the observation that massive sulphide ore bodies occur within the basaltic layer of the ophiolite supports that contention that significant sulphide ore deposits may be formed within the oceanic crust. However, the ophiolitic sulphides may be the end product of a series of processes with hydrothermal alteration being only a first step of concentration of the trace metals, and later stages involving regional metamorphism, meteoric water circulation, or possible further volcanism. Nevertheless, the production of sulphides by reaction between oceanic basalts and hot seawater is feasible, as indicated by my studies, and hydrothermal alteration has the potential for forming sulphide deposits within the oceanic crust.

#### 4.5. CONCLUSIONS.

The effects of hydrothermal alteration on the trace element composition of oceanic basalts can be summarised as follows:

- 1) B and Li are mobilised during hydrothermal alteration; high concentrations are often observed in the chlorite-rich rims of the altered pillows, and pillow interiors are often depleted relative to the fresh precursor.
- 2) Sr is taken up in the epidote-rich assemblage, stays relatively constant in the alteration of pillow interiors to chlorite-rich assemblages, and is lost in the alteration of the rims. The correlation of Sr with Ca is good, indicating that they both are controlled by the same reactions, as would be expected. These observations are consistent with previously published data, which indicated a sympathetic relation with Ca. The flux of Sr was used to calculate a water-to-reacted-rock ratio of 9 - 37: 1, which is in good agreement with those estimated from the Ca and Mg data.
- 3) Ba apparently is not greatly affected by hydrothermal alteration, although some slight mobilisation is indicated with higher Ba concentrations in the altered pillow interiors than in the margins.
- 4) Co, Cr, and Ni concentrations show only slight variations in hydrothermally altered basalts. Enrichment of Co, and particularly Ni, in sulphide-rich samples, and some depletion of Co and Ni in other samples, suggest that there is some mobilisation of these elements.
- 5) In general, copper is leached out of the basalt during hydrothermal alteration. Clearly, as for Ni, some Cu is precipitated as sulphides in the basalt. Qualitative analyses of the sulphides indicate that this is also true for Zn.

6) Y and Zr concentrations show no marked variations in hydrothermally altered basalts, suggesting that their concentrations can be used in order to determine the original tectonic settings of rocks. Consideration of the relations between Ti-Zr and Y-Zr for rocks from different origins indicate that hydrothermally altered oceanic basalts fall into the same field as the fresh oceanic basalts, and hence these parameters can be used to determine the origin of hydrothermally altered basalts.

7) Mn is mobilised during hydrothermal alteration but the metamorphosed samples show a wide variability in the Mn concentrations, as seen in previously published data. The migration of Mn in the circulating fluid is probably dependent on a variety of parameters including the Eh and pH conditions encountered.

8) Hydrothermal alteration is a process by which a metal-enriched solution can be formed. This may play an important role in the formation of the metalliferous sediments at the mid-ocean ridges. The precipitation of sulphides from circulating fluids has been demonstrated, and the potential exists for the formation of sulphide ore deposits; however, the extent to which this reaction takes place is not yet certain.

REFERENCES

- Albee, A. L. and Ray, L. 1970. Correction factors for electron probe microanalysis of silicates, oxides, carbonates, phosphates and sulphates. *Anal. Chim.*, 42: 1408.
- Anderson, R. N. 1972. Petrologic significance of low heat flow on the flanks of slow spreading ridges. *Bull. Geol. Soc. Amer.*, 83: 2947.
- Arnorrson, S. 1970. Underground temperatures in hydrothermal areas in Iceland as deduced from the silica content of the thermal waters. *Geothermics*, spec. issue 2, v. 2, part 1, 536.
- Arnorrson, S., Kononov, V. and Polyak, B. 1974. The geochemical features of Iceland hydrotherms. *Geochem. Int.*, 11(6), 1224.
- Arrhenius, G. and Bonatti, E. 1965. Neptunism and volcanism in the ocean. *Progr. Oceanogr.*, 3: 7.
- Aumento, F. 1968. The mid-Atlantic ridge near 45°N. II. Basalts from the area of Confederation Peak. *Can. J. Earth Sci.*, 5: 1.
- Aumento, F. and Loncarevic, B. 1969. The mid-Atlantic ridge near 45°N. III. Bald Mountain. *Can. J. Earth Sci.*, 6: 11.
- Aumento, F., Loncarevic, B. and Ross, D. I. 1971. Hudson Geotraverse: geology of the mid-Atlantic ridge at 45°N. *Phil. Trans. Roy. Soc. Lond. A.*, 268: 623.
- Aumento, F. and Loubat, H. 1973. The mid-Atlantic ridge near 45°N. XVI. Serpentinised ultramafic intrusions. *Can. J. Earth Sci.*, 8: 631.
- Bender, M., Broecker, W., Gornitz, V., Middel, U., Kay, R., Sun, S. S. and Biscaye, P. 1971. Geochemistry of three cores from the East Pacific Rise. *Earth Plan. Sci. Letts.*, 12: 425.

- Berner, R. A. 1972. Sulphate reduction, pyrite formation, and the oceanic sulphur budget. In: D. Dyrssen and D. Jagner (eds.): The Changing Chemistry of the Oceans. Nobel Symposium 20, p. 347.
- Bischoff, J. L. and Dickson, F. W. 1975. Seawater-basalt interaction at 200°C and 500 bars: implications as to the origin of sea floor heavy metal deposits and regulation of seawater chemistry. Earth Plan. Sci. Letts., 25: 385.
- Bischoff, J. and Sayles, F. 1972. Pore fluid and mineralogical studies of Recent marine sediments: Bauer depression region of the East Pacific Rise. J. Sed. Pet., 42: 711.
- Bjornsson, S., Arnorsson, S. and Tomasson, J. 1972. Economic evaluation of Reykjanes thermal brine area, Iceland. Bull. Am. Ass. Petrol. Geol., 56: 2380.
- Bodvarsson, G. and Lowell, R. P. 1972. Ocean floor heat flow and the circulation of interstitial waters. J. Geophys. Res., 77: 4472.
- Bogdanov, Y. A. and Ploshko, V. 1967. Magmatic and metamorphic rocks of the deep sea Romanche Trench. Dokl. Akad. Nauk. SSSR, 177: 909.
- Bonatti, E. and Joensuu, O. 1966. Deep sea iron deposits from the South Pacific. Science, 154: 643.
- Bonatti, E., Honnorez, J. and Ferrara, G. 1971. Peridotite-gabbro-basalt complex from the equatorial mid-Atlantic ridge. Phil. Trans. Roy. Soc. Lond., A, 268: 385.
- Bonatti, E., Honnorez, J. Kirst, P. and Radicati, F. 1975. Metagabbros from the mid-Atlantic ridge at 06°N: contact-hydrothermal-dynamic metamorphism beneath the axial valley. J. Geol., 83: 61.

- Bonatti, E., Zerbi, M., Kay, R., and Rydell, H. 1976. Metalliferous deposits from the Apennine ophiolites: Mesozoic equivalents of deposits from modern spreading centers. *Bull. Geol. Soc. Amer.*, 87: 83.
- Bostrom, K. and Fisher, D. 1971. Volcanogenic U, V, and Fe in Indian Ocean sediments. *Earth Plan. Sci. Letts.*, 11: 95.
- Bostrom, K. and Peterson, M.N.A. 1966. Precipitates from hydrothermal exhalations on the East Pacific Rise. *Econ. Geol.*, 61: 1258.
- Brewer, P. G. 1975. Minor elements in seawater. In: J. P. Riley and G. Skirrow (eds.): *Chemical Oceanography*, 2nd edition, v. 1, 497. Academic Press, London.
- Cann, J. R. 1969. Spilites from the Carlsberg Ridge, Indian Ocean. *J. Petrol.*, 10: 1.
- Cann, J. R. 1971. Petrology of basement rocks from Palmer Ridge, N. E. Atlantic. *Phil. Trans. Soc. London, A*, 268: 605.
- Cann, J. R. and Funnell, B. 1967. Palmer Ridge: a section through the upper part of the ocean crust. *Nature*, 213: 661.
- Cann, J. R. and Vine, F. J. 1966. An area on the crest of the Carlsberg Ridge: petrology and magnetic survey. *Phil. Trans. Roy. Soc. Lond., A*, 259: 198.
- Chernyseva, V. I. 1971. Greenstone-altered rocks of rift zones in median ridges of the Indian Ocean. *Int. Geol. Rev.*, 13: 903.
- Constantinou, G. and Govett, G.J.S. 1973. Geology, geochemistry and genesis of the Cyprus sulphide deposits. *Econ. Geol.*, 68: 843.
- Cook, H. E. 1971. Iron and manganese-rich sediments overlying oceanic basalt basement, equatorial Pacific, Leg 9, Deep Sea Drilling Project. (Abstract) *Geol. Soc. Amer. Abstracts with Program*, 3: 530.

- Cooper, A. F. 1972. Progressive metamorphism of metabasic rocks from the Haast Schist Group of Southern New Zealand. *J. Petrol.*, 13: 457.
- Corliss, J. 1971. Origin of metal-bearing submarine hydrothermal solutions. *J. Geophys. Res.*, 76: 8128.
- Corliss, J., Graf, J., Skinner, B. and Hutchinson, R. W. 1972. Rare earth data for Fe- and Mn-rich sediments associated with sulphide ore bodies of the Troodos Massif, Cyprus (abstract). *Geol. Soc. Amer. Abstracts with Program*, 4: 476.
- Crerar, D. and Barnes, H. 1974. Deposition of deep-sea manganese nodules. *Geochim. Cosmochim. Acta*, 38: 279.
- Cronan, D. S. 1973. Basal ferruginous sediments cored during Leg 16, Deep Sea Drilling Project. In: Initial Reports of the Deep Sea Drilling Project, v. 16, Washington, D. C., U. S. Govt. Printing Office, 601.
- Cronan, D. S. 1974. Authigenic minerals in deep-sea sediments. In: E. Goldberg (ed.): *The Sea*, v. 5: 491. Wiley, New York.
- Cronan, D. S., Van Andel, T. H., Heath, G. R., Dinkelman, M. K., Bennett, R. H., Bukry, D., Charleston, S., Kaneps, A., Rodolfo, K. S. and Yeats, R. S. 1972. Iron-rich basal sediments from the eastern equatorial Pacific: Leg 16, Deep Sea Drilling Project. *Science*, 175: 61.
- Dasch, E., Dymond, J. and Heath, G. R. 1971. Isotopic analysis of metalliferous sediment from the East Pacific Rise. *Earth Plan. Sci. Letts.*, 13: 175.



- Deffeyes, K. S. 1970. The axial valley: a steady state feature of the terrain. In: H. Johnson and B. L. Smith (eds.): Megatectonics of continents and oceans, p. 194. Rutgers University Press.
- Dmitriev, L., Barsukov, V. L. and Udintsev, G. 1970. Rift zones of the oceans and the problem of ore formation. *Geokhimiya*, 4: 937.
- Drever, J. I. 1974. The magnesium problem. In: E. Goldberg (ed.): *The Sea*, v. 5: 337. Wiley and Sons, New York.
- Dymond, J., Corliss, J., Heath, G. R., Field, C. W., Dasch, E. J. and Veeh, H. H. 1973. Origin of metalliferous sediments from the Pacific Ocean. *Bull. Geol. Soc. Amer.*, 84: 3355.
- Dymond, J. and Veeh, H. H. 1975. Metal accumulation rates in the south-east Pacific and the origin of metalliferous sediments. *Earth Plan. Sci. Letts.*, 28: 13.
- Elder, J. W. 1965. Physical processes in geothermal areas. *Amer. Geophys. Un. Mono.*, 8: 211.
- Elderfield, H., Gass, I. G., Hammond, A., and Bear, L. M. 1972. The origin of ferromanganese sediments associated with the Troodos Massif in Cyprus. *Sedimentology*, 19: 1.
- Engel, A. E., Engel, C. G. and Havens, R. G. 1965. Chemical characteristics of oceanic basalts and the Upper Mantle. *Bull. Geol. Soc. Amer.*, 76: 719.
- Field, C. W., Dymond, J. R., Heath, G. R., Corliss, J. B. and Dasch, E. J. 1976. Sulphur isotope reconnaissance of epigenetic pyrite in ocean floor basalts, Leg 34 and elsewhere. In: R. S. Yeats, S. R. Hart et al. 1976. *Initial Reports of the Deep Sea Drilling Project*, v. 34, Washington (U. S. Govt. Printing Office), 381.

- Finger, L. W. and Hadidiacos, C. G. 1972. Electron microprobe automation. Yb. Carnegie Inst., Washington, 71: 598.
- Flanagan, F. J. 1973. 1972 values for international geochemical reference samples. Geochim. Cosmochim. Acta, 37: 1189.
- Fox, P. J. and Opdyke. 1973a. Geology of the oceanic crust: magnetic properties of oceanic rocks. J. Geophys. Res., 78: 5139.
- Fox, P. J., Schreiber, E. and Peterson, J. 1973b. The geology of the oceanic crust: compressional wave velocities of oceanic igneous rocks. J. Geophys. Res., 78: 5155.
- Frey, F., Dickey, J. S., Thompson, G. and Bryan, W. B. 1976. Eastern Indian Ocean DSDP sites: correlations between petrography, geochemistry and tectonic setting. G.S.A. Memoir (in press).
- Fryer, B. J. and Hutchinson, R. W. 1976. Generation of metal deposits on the sea floor. Can. J. Earth Sci., 13: 126.
- Garrels, R. M. and Christ, C. L. 1965. Solutions, Minerals and Equilibria. Harper and Row, New York. 450 pp.
- Garrels, R. M. and Mackenzie, F. T. 1971. Evolution of Sedimentary Rocks. W. W. Norton and Co., Inc., New York. 397 pp.
- Garrels, R. M. and Perry, E. A. 1974. Cycling of carbon, sulphur and oxygen through geologic time. In: E. Goldberg (ed.): The Sea, v. 5: 303. Wiley and Sons, New York.
- Garrels, R. M. and Thompson, M. E. 1962. A chemical model for seawater at 25°C and one atmosphere total pressure. Am. J. Sci., 260: 57.
- Garrels, R. M., Lerman, A. and Mackenzie, F. T. 1976. Controls of atmospheric O<sub>2</sub> and CO<sub>2</sub>: past, present and future. Am. Scientist, 64: 306.

- Goldich, S. S. 1938. A study in rock weathering. *J. Geol.*, 46: 17.
- Goldschmidt, V. M. 1954. *Geochemistry*. Clarendon Press, Oxford.
- Hajash, A. 1975. Hydrothermal processes along mid-ocean ridges: an experimental investigation. Ph.D. Dissertation, Texas A & M University.
- Hart, R. A. 1970. Chemical exchange between seawater and deep ocean basalts. *Earth Plan. Sci. Letts.*, 9: 269.
- Hart, R. A. 1973. A model for the chemical exchange in the basalt-seawater system of oceanic Layer 2. *Can. J. Earth Sci.*, 10: 799.
- Hart, S. R. and others. 1974. Leg 34, Deep Sea Drilling Project. Oceanic basalt and the Nazca Plate. *Geotimes*, 19: 4.
- Hekinian, R. 1968. Rocks from the mid-oceanic ridge in the Indian Ocean. *Deep Sea Res.*, 15: 195.
- Hekinian, R. and Aumento, F. 1973. Rocks from the Gibbs Fracture Zone and the Minia Seamount near 53°N in the Atlantic Ocean. *Mar. Geol.*, 14: 47.
- Helgeson, H. C. 1969. Thermodynamics of hydrothermal systems at elevated temperatures and pressures. *Am. J. Sci.*, 267: 729.
- Horn, M. and Adams, J. 1966. Computer-derived geochemical balance and element abundances. *Geochim. Cosmochim. Acta*, 30: 279.
- Horowitz, A. and Cronan, D. S. 1976. The geochemistry of basal sediments from the North Atlantic Ocean. *Mar. Geol.*, 20: 205.
- Hyndman, R. D. and Rankin, D. S. 1972. The mid-Atlantic ridge near 45°N. XVIII. Heat flow measurements. *Can. J. Earth Sci.*, 7: 226.
- Ingamells, C. O. 1970. Lithium metaborate flux in silicate analysis. *Anal. Chim. Acta*, 52: 323.

- Jen, L. S. 1973. The determination of iron (II) in silicate rocks and minerals. *Anal. Chim. Acta*, 66: 315.
- Keays, R. R. and Scott, R. B. 1976. Precious metals in ocean ridge basalts: implications for basalts as source rocks for gold mineralization. *Econ. Geol.*, 71: 705.
- Kennedy, G. C. 1950. A portion of the system silica-water. *Econ. Geol.*, 45: 629.
- Lafon, G. and Mackenzie, F. 1974. Early evolution of the ocean - a weathering model. In: W. W. Hay (ed.): *Studies in Paleo-oceanography*. S.E.P.M. Spec. Pub., 20: 205.
- Langseth, M. G. and Von Herzen, R. P. 1971. Heat flow through the floor of the world oceans. In: A. E. Maxwell (ed.): *The Sea*, v. 4, part 1, 299. Wiley-Interscience, New York.
- Le Pichon, X. and Langseth, M. G. 1969. Heat flow from mid-ocean ridges and sea floor spreading. *Tectonophysics*, 8: 319.
- Li, Y. H. 1972. Geochemical mass balances among lithosphere, hydrosphere and atmosphere. *Am. J. Sci.*, 272: 119.
- Lister, C.R.B. 1972. On the thermal balance of a mid-ocean ridge. *Geophys. J. Roy. Astr. Soc.*, 26: 515.
- Lister, C.R.B. 1974. Water percolation in the oceanic crust. *EOS Trans. Amer. Geophys. Un.*, 55: 740.
- Mackenzie, F. T. and Garrels, R. M. 1966. Chemical mass balance between rivers and oceans. *Am. J. Sci.*, 264: 507.
- Matthews, D. H. 1962. Altered lavas from the floor of the eastern North Atlantic. *Nature*, 194: 368.

- Melson, W., Bowen, V. T., Van Andel, T. H. and Siever, R. 1966a. Greenstones from the central valley of the mid-Atlantic ridge. *Nature*, 209: 604.
- Melson, W. and Van Andel, T. H. 1966b. Metamorphism in the mid-Atlantic ridge, 22°N latitude. *Mar. Geol.*, 4: 165.
- Melson, W., Thompson, G. and Van Andel, T. H. 1968. Volcanism and metamorphism in the mid-Atlantic ridge, 22°N latitude. *J. Geophys. Res.*, 73: 5925.
- Melson, W. and Thompson, G. 1971. Petrology of a transform fault zone and adjacent ridge segments. *Phil. Trans. Roy. Soc. Lond., A*, 268: 423.
- Miyashiro, A., Shido, F. and Ewing, M. 1971. Metamorphism on the mid-Atlantic ridge near 24 and 30°N. *Phil. Trans. Roy. Soc. Lond., A*, 268: 589.
- Moore, E. M. and Vine, F. J. 1971. The Troodos Massif, Cyprus and other ophiolites as oceanic crust: evaluation and implications. *Phil. Trans. Roy. Soc. Lond., A*, 268: 443.
- Mottl, M. J. 1976. Chemical exchange between seawater and basalt during hydrothermal alteration of the oceanic crust. Ph.D. dissertation. Harvard University, 187 pp.
- Mottl, M. J., Corr, R. and Holland, H. D. 1974. Chemical exchange between seawater and mid-ocean ridge basalt during hydrothermal alteration: an experimental study (Abstract). *Geol. Soc. Amer. Abstracts with Programs*, 6: 879.
- Mottl, M. J., Corr, R. and Holland, H. D. 1975. Trace element content of the Reykjanes and Svartsengi thermal brines, Iceland (Abstract). *G.S.A. Abstracts with Programs*, 7: 1206.

- Muehlenbachs, K. and Clayton, R. 1972. Oxygen isotope geochemistry of submarine greenstones, mid-Atlantic ridge. *Can. J. Earth Sci.*, 9: 471.
- Nicholls, G. and Islam, M. 1971. Geochemical investigations of basalts and associated rocks from the ocean floor and their implications. *Phil. Trans. Roy. Soc. Lond., A*, 268: 469.
- Ozima, M., Saito, K., Matsuda, J., Zashu, S., Aramaki, S. and Shido, F. 1976. Additional evidence of existence of ancient rocks in the mid-Atlantic ridge and the age of the opening of the Atlantic. *Tectonophysics*, 31: 59.
- Palmason, G. 1967. On heat flow in Iceland in relation to the mid-Atlantic ridge. Symposium Report, Geoscience Soc. Iceland, Reykjavik.
- Pearce, J. A. and Cann, J. R. 1971. Ophiolite origin investigated by discriminant analysis using Ti, Zr and Y. *Earth Plan. Sci. Letts.*, 12: 339.
- Pearce, J. A. and Cann, J. R. 1973. Tectonic setting of basic volcanic rocks determined using trace element analyses. *Earth Plan. Sci. Letts.*, 19: 290.
- Quon, S. H. and Ehlers, E. G. 1963. Rocks of the northern part of the mid-Atlantic ridge. *Bull. Geol. Soc. Amer.*, 74: 1.
- Robertson, A.H.F. and Hudson, J. D. 1973. Cyprus umbers: chemical precipitates on a Tethyan ocean ridge. *Earth Plan. Sic. Letts.*, 18: 93.
- Robie, R. A. and Waldbaum, D. R. 1968. Thermodynamic properties of minerals and related substances. U.S.G.S. Bull. No. 1259.

- Rona, P. A., McGregor, B. A., Betzer, P. R. and Krause, D. C. 1974. Anomalous water temperatures over mid-Atlantic ridge crest at 26°N (Abstract). EOS, Trans. Amer. Geophys. Un., 55: 193.
- Rozanova, T. V. and Baturin, G. N. 1971. Hydrothermal ore shows on the floor of the Indian Ocean. Oceanology, 11: 874.
- Sclater, J. G. and Klitgord, K. G. 1973. A detailed heat flow, topographic and magnetic survey across the Galapagos spreading center at 86°W. J. Geophys. Res., 78: 6951.
- Scott, M. R., Scott, R. B., Morse, J. W., Betzer, P. R., Butler, L. W. and Rona, P. A. 1974a. Transition metals in sediments adjacent to the TAG hydrothermal field. EOS, Trans. Amer. Geophys. Un., 55: 294.
- Scott, M. R., Scott, R. B., Rona, P. A., Butler, L. W. and Nalwalk, A. J. 1974b. Rapidly accumulating manganese deposit from the median valley of the mid-Atlantic ridge. Geophys. Res. Letts., 1: 355.
- Shido, F., Miyashiro, A. and Ewing, M. 1974. Compositional variation in pillow lavas from the mid-Atlantic ridge. Mar. Geol., 16: 177.
- Sillen, L. G. 1961. The physical chemistry of seawater. In: M. Sears (ed.): Oceanography. Am. Assoc. Adv. Sci. Publ., 67: 549.
- Sillitoe, R. H. 1973. Environment of formation of volcanogenic massive sulphide deposits. Econ. Geol., 68: 1321.
- Skornyakova, I. S. 1964. Dispersed iron and manganese in Pacific Ocean sediments. Int. Geol. Rev., 7: 2161.
- Sleep, N. H. 1969. Sensitivity of heat flow and gravity to mechanisms of sea floor spreading. J. Geophys. Res., 72: 542.

- Spooner, E. 1974. Sub-sea floor metamorphism, heat and mass transfer; an additional comment. *Contr. Mineral. Petrol.*, 45: 169.
- Spooner, E. and Fyfe, W. 1973. Sub-sea floor metamorphism, heat and mass transfer. *Contr. Mineral. Petrol.*, 42: 287.
- Spooner, E., Beckinsale, R., Fyfe, W. and Smewing, J. 1974.  $O^{18}$  enriched ophiolitic metabasic rocks from East Liguria (Italy), Pindos (Greece), and Troodos (Cyprus). *Contr. Mineral. Petrol.*, 47: 41.
- Stumm, W. and Brauner, P. A. 1975. Chemical speciation. In: J. P. Riley and G. Skirrow (eds.): *Chemical Oceanography*, 2nd edition, v. 1, 173 pp. Academic Press, London.
- Sverdrup, H. U., Johnson, M. W. and Fleming, R. H. 1942. *The Oceans: Their Physics, Chemistry and General Biology*. Prentice-Hall, Inc., New Jersey, 1087 pp.
- Swanson, S. and Scott, R. B. 1974. Hydrothermal products of Leg 34 basalts: Deep Sea Drilling Project (Abstract). *Geol. Soc. Amer. Abstracts with Program*, 6: 979.
- Talwani, M., Windisch, C. C. and Langseth, M. 1971. Reykjanes ridge crest: a detailed geophysical study. *J. Geophys. Res.*, 76: 473.
- Tardy, Y. and Garrels, R. M. 1974. A method of estimating the Gibbs energies of formation of layer silicates. *Geochim. Cosmochim. Acta*, 38: 110.
- Thompson, G. 1973a. A geochemical study of the low temperature interaction of seawater and oceanic igneous rock. *EOS, Trans. Amer. Geophys. Un.*, 54: 1015.
- Thompson, G. 1973b. Trace element distributions in fractionated oceanic rocks. 2. Gabbros and related rocks. *Chem. Geol.*, 12: 99.



- Thompson, G. and Bankston, D. C. 1969. A technique for trace element analysis of powdered materials using the d.c. arc and photo-electric spectrometer. *Spectrochim. Acta*, 24B: 335.
- Thompson, G. and Melson, W. G. 1970. Boron contents of serpentinites and metabasalts in the oceanic crust: implications for the boron cycle in the oceans. *Earth Plan. Sci. Letts.*, 8: 61.
- Thompson, G. and Melson, W. G. 1972a. The petrology of oceanic crust across fracture zones in the Atlantic Ocean: evidence of a new kind of sea floor spreading. *J. Geol.*, 80: 526.
- Thompson, G., Shido, F. and Miyashiro, A. 1972b. Trace element distributions in fractionated oceanic basalts. *Chem. Geol.*, 9: 89.
- Thompson, G., Woo, C. C. and Sung, W. 1975. Metalliferous deposits on the mid-Atlantic ridge (Abstract). *Geol. Soc. Amer. Abstracts with Programs*, 7: 1297.
- Tomasson, J. and Kristmannsdottir, H. 1972. High temperature alteration minerals and thermal brines. Reykjanes, Iceland. *Contr. Mineral. Petrol.*, 36: 123.
- Turekian, K. K. and Wedepohl, L. H. 1961. Distribution of elements in some major units of the earth's crust. *Bull. Geol. Soc. Amer.*, 72: 175.
- Udintsev, G. and Dmitriev, L. 1970. Ultrabasic rocks. In: A. E. Maxwell (ed.): *The Sea*, v. 4: part 1, 521. Wiley-Interscience, New York.
- Vallance, T. G. 1974. Spilitic degradation of a tholeiitic basalt. *J. Petrol.*, 15: 79.
- Vine, F. 1968. Magnetic anomalies associated with mid-ocean ridges. In: R. A. Phinney (ed.): *The History of the Earth's Crust*. 73 pp. Princeton University Press, Princeton.

- von der Borch, C. C., Nesterhoff, W. and Galehouse, J. 1971. Iron-rich sediments cored during Leg 8 of the Deep Sea Drilling Project. In: Initial Reports of the Deep Sea Drilling Project, VIII, Washington, D. C., 541 pp.
- von der Borch, C. C. and Rex, R. W. 1970. Amorphous iron oxide precipitates in sediments cored during Leg 5, Deep Sea Drilling Project. In: Initial Reports of the Deep Sea Drilling Project, v. 5, Washington, D. C., U. S. Govt. Printing Office, 541.
- Von Herzen, R. P. and Anderson, R. N. 1972. Implications of heat flow and bottom water temperature in the eastern equatorial Pacific. *Geophys. J. Roy. Astr. Soc.*, 26: 427.
- Wenner, D. and Taylor, H., 1971. Temperature of serpentinisation of ultramafic rocks based on  $O^{18}/O^{16}$  fractionation between serpentine and magnetite. *Contr. Mineral. Petrol.*, 32: 165.
- Williams, D. L. 1974. Heat loss and hydrothermal circulation due to sea floor spreading. Ph.D. dissertation, M.I.T./W.H.O.I. Joint Program in Oceanography, 139 pp.
- Williams, D. L. and Von Herzen, R. P. 1974. Heat loss from the earth: new estimate. *Geology*, 2: 327.
- Williams, D. L., Von Herzen, R. P., Sclater, J. G. and Anderson, R. N. 1974. The Galapagos spreading center: lithospheric cooling and hydrothermal circulation. *Geophys. J. Roy. Astr. Soc.*, 38: 587.
- Wolery, T. J. and Sleep, N. H. 1976. Hydrothermal circulation and geochemical flux at mid-ocean ridges. *J. Geol.*, 84: 249.

APPENDIX I

RESULTS OF MINERALOGICAL AND CHEMICAL ANALYSES

TABLE AI-1

Feldspar Analyses - Fresh Basalts and Interiors

Ch-44	2-1 a)	Phenocryst
	2-1 b)	Microlite
Ch-44	2-3 (1)	Phenocryst
	(2)	Microlite
	(3)	Microlite
AII-42	1-96C (1)	Microlite
	(2)	Microlite
AII-42	1-97B	Phenocryst
AII-42	1-98 (1)	Microlite
	(2)	Microlite
AII-42	1-108B (1)	Microlite
	(2)	Microlite
AII-42	1-118B (1)	Phenocryst
	(2)	Phenocryst
	(3)	Microlite
AII-42	1-130	Microlite
AII-42	1-141 (1)	Microlite

TABLE AI-1

Sample No.	Ch-44 2-1 a)	Ch-44 2-1 b)	Ch-44 2-3 (1)	Ch-44 2-3 (2)	Ch-44 2-3 (3)	AII-42 1-96C (1)	AII-42 1-96C (2)	AII-42 1-97B	AII-42 1-98 (1)
SiO <sub>2</sub>	48.12	50.72	50.97	51.77	51.80	51.59	51.51	47.63	52.89
Al <sub>2</sub> O <sub>3</sub>	32.80	30.73	30.76	30.52	30.11	30.73	30.64	33.56	29.80
FeO*	0.30	0.74	0.48	0.61	0.50	0.54	0.52	0.25	0.67
MgO	0	0.09	0.14	0.17	0.37	0	0.03	0.14	0.22
CaO	15.99	13.41	14.52	13.78	13.49	13.26	13.57	17.38	11.95
Na <sub>2</sub> O	2.49	3.64	3.63	4.05	4.15	3.60	3.69	1.52	4.24
K <sub>2</sub> O	0.01	0.01	0.01	0	0.01	0.02	0	0	0.01
MnO	0	0	0	0	0	0	0	0	0
Total	99.71	99.34	100.31	100.70	100.43	99.54	99.96	100.48	99.78
	Cations Per 8 Oxygens								
Si	2.212	2.317	2.319	2.345	2.351	2.346	2.344	2.176	2.400
Al	1.777	1.655	1.650	1.619	1.611	1.653	1.644	1.807	1.594
Fe	0.012	0.028	0.018	0.023	0.019	0.021	0.020	0.010	0.025
Mg	--	0.006	0.009	0.011	0.025	0	0.002	0.010	0.015
Ca	0.788	0.657	0.698	0.669	0.656	0.648	0.662	0.851	0.581
Na	0.222	0.383	0.320	0.356	0.365	0.319	0.326	0.135	0.373
K	0.001	0.001	0.001	0	0.001	0.001	0	0	0.001
Mn	0	0	0	0	0	0	0	0	0
Total	5.012	5.041	5.015	5.023	5.028	4.988	4.998	4.989	4.989
% An	78.0	63.2	68.6	65.3	64.3	67.0	67.0	86.3	60.90

Table AI-1 (Continued)

Sample No.	AII-42 1-98 (2)	AII-42 1-108B (1)	AII-42 1-108B (2)	AII-42 1-118B (1)	AII-42 1-118B (2)	AII-42 1-118B (3)	AII-42 1-141 (1)	
SiO <sub>2</sub>	52.74	52.78	52.75	47.19	46.87	51.25	52.82	
Al <sub>2</sub> O <sub>3</sub>	30.01	28.98	28.14	33.62	33.75	31.07	28.64	
FeO*	0.84	0.93	0.94	0.38	0.33	0.48	0.73	
MgO	0.17	0.31	0.09	0.21	0.18	0.23	0.02	
CaO	12.25	13.08	13.08	17.47	17.37	13.93	13.01	
Na <sub>2</sub> O	3.78	3.80	4.14	1.70	1.78	3.49	4.18	
K <sub>2</sub> O	0.01	0	0	n.a.	n.a.	n.a.	0.02	
MnO	0	0	0	n.a.	n.a.	n.a.	0	
Total	99.80	99.98	99.14	100.57	100.28	100.45	99.42	
			Cations Per 8 Oxygens					
Si	2.393	2.400	2.422	2.159	2.151	2.323	2.416	
Al	1.605	1.554	1.523	1.813	1.826	1.660	1.544	
Fe	0.032	0.036	0.036	0.015	0.013	0.018	0.028	
Mg	0.011	0.021	0.006	0.014	0.012	0.016	0.001	
Ca	0.596	0.637	0.644	0.857	0.854	0.677	0.638	
Na	0.333	0.335	0.369	0.151	0.158	0.307	0.371	
K	0.001	0	0	--	--	--	0.001	
Mn	0	0	0	--	--	--	0	
Total	4.971	4.983	5.000	5.009	5.014	5.001	4.999	
% An	64.2	65.5	63.6	85.0	84.4	68.8	63.2	

TABLE AI-2.

Olivine- Fresh Basalts.

Ch-44	2-3 (1)	Phenocryst
	(2)	Microphenocryst

TABLE AI-2

Sample No.	Ch-44 2-3 (1)	Ch-44 2-3 (2)
SiO <sub>2</sub>	39.96	39.68
Al <sub>2</sub> O <sub>3</sub>	0.04	0.13
FeO*	14.37	15.38
MgO	44.95	44.16
CaO	0.32	0.38
Na <sub>2</sub> O	0.03	0.02
K <sub>2</sub> O	0.01	0
MnO	0.10	0.12
Total	99.78	99.87
Cations Per 4 Oxygens		
Si	1.002	0.999
Al	0.001	0.004
Fe	0.301	0.324
Mg	1.681	1.658
Ca	0.009	0.010
Na	0.001	0.001
K	0	0
Mn	0.002	0.002
Total	2.997	2.998
% Fo	84.8	83.7



TABLE AI-3

Feldspar Analyses - Altered Basalts

AII-60	2-14 (1)	Altered Microlite
	2-14 (2)	Altered Microlite
Ch-44	3-2 (1)	Albitised Phenocryst
	3-2 (2)	Albitised Phenocryst
	3-8 (1)	Albitised Phenocryst
	3-8 (2)	Partially Albitised Phenocryst
	3-8 (3)	Inner Portion of 3-8 (2)
	3-12	Microphenocryst
	3-126	Albitised Phenocryst
AII-42	1-96B (1)	Microlite
	1-96B (2)	Microphenocryst
AII-42	1-106 (1)	Altered Groundmass Plagioclase
	1-106 (2)	Relict Plagioclase
	1-108A	Albite Replacing Altered Groundmass
	1-118A	Albitised Phenocryst
	1-129 (1)	Transformation of Plag → Albite + Epidote
	1-129 (2)	Unaltered Microlite
	1-129 (3)	Altered Microlite

TABLE AI-3

Sample No.	AI-60 2-14 (1)	AI-60 2-14 (2)	Ch-44 3-2 (1)	Ch-44 3-2 (2)	Ch-44 3-8 (1)	Ch-44 3-8 (2)	Ch-44 3-8 (3)	Ch-44 3-12
SiO <sub>2</sub>	60.38	66.04	66.67	66.07	64.76	66.25	48.21	51.88
Al <sub>2</sub> O <sub>3</sub>	24.17	21.49	21.21	20.77	23.51	21.00	32.46	30.05
FeO*	1.59	0.29	0.29	0.20	0	0	0.39	0.54
MgO	1.04	0	0	0	0	0	0.18	0.26
CaO	5.76	2.48	0.98	0.80	1.44	1.73	15.68	13.32
Na <sub>2</sub> O	7.32	9.94	11.10	11.47	10.18	10.33	2.52	4.15
K <sub>2</sub> O	0.06	0.06	0.27	0.02	0.06	0.07	0.01	0.02
MnO	0	0	0	0	0	0	0	0
Total	100.32	100.30	100.52	99.33	99.94	99.38	99.45	100.22
Cations Per 8 Oxygens								
Si	2.688	2.893	2.913	2.920	2.838	2.919	2.221	2.358
Al	1.268	1.109	1.093	1.082	1.214	1.091	1.763	1.610
Fe	0.059	0.011	0.011	0.007	0	0	0.015	0.021
Mg	0.069	0	0	0	0	0	0.012	0.018
Ca	0.275	0.116	0.046	0.038	0.068	0.082	0.774	0.649
Na	0.632	0.844	0.941	0.982	0.865	0.883	0.225	0.366
K	0.003	0.003	0.015	0.001	0.003	0.004	0.001	0.001
Mn	0	0	0	0	0	0	0	0
Total	4.994	4.976	5.019	5.030	4.988	4.979	5.011	5.023
% An	30.3	13.7	4.7	3.7	7.3	8.5	77.5	63.9

Table AI-3 (Continued)

Sample No.	Ch-44 3-126	AII-42 1-96B (1)	AII-42 1-96B (2)	AII-42 1-106 (1)	AII-42 1-106 (2)	AII-42 1-108A	AII-42 1-118A
SiO <sub>2</sub>	66.85	50.25	49.56	68.05	50.39	67.68	65.84
Al <sub>2</sub> O <sub>3</sub>	20.76	30.82	31.09	19.80	30.63	20.46	22.92
FeO*	0.17	0.49	0.47	0.10	0.46	0.04	0.04
MgO	0	0.21	0.21	0	0.19	0	0
CaO	2.45	14.51	15.14	0.30	14.46	1.03	2.70
Na <sub>2</sub> O	10.06	3.27	3.10	12.18	3.05	11.39	8.97
K <sub>2</sub> O	0.04	0.00	0.03	n.a.	n.a.	n.a.	0.12
MnO	0	0	0	n.a.	n.a.	n.a.	0
Total	100.53	99.55	99.60	100.43	99.18	100.60	100.59

Cations Per 8 Oxygens

Si	2.923	2.305	2.278	2.970	2.316	2.947	2.864
Al	1.070	1.666	1.684	1.018	1.659	1.050	1.175
Fe	0.006	0.019	0.018	0.004	0.018	0.001	0.001
Mg	0	0.014	0.014	0	0.013	0	0
Ca	0.115	0.713	0.746	0.014	0.712	0.048	0.126
Na	0.853	0.290	0.276	1.030	0.271	0.962	0.757
K	0.002	0	0.002	--	--	--	0.001
Mn	0	0	0	--	--	--	0
Total	4.969	5.008	5.018	5.036	4.989	5.008	4.924

% An	11.9	71.09	72.99	1.34	72.43	4.75	14.27
------	------	-------	-------	------	-------	------	-------

Table AI-3 (Continued)

Sample No.	AII-42 1-129 (1)	AII-42 1-129 (2)	AII-42 1-129 (3)
SiO <sub>2</sub>	63.50	52.14	66.81
Al <sub>2</sub> O <sub>3</sub>	22.18	29.51	19.75
FeO*	0	0.75	0.18
MgO	0	0.11	0
CaO	2.87	13.07	1.28
Na <sub>2</sub> O	10.64	4.30	11.20
K <sub>2</sub> O	n.a.	0.01	0.03
MnO	n.a.	0	0
Total	99.19	99.89	99.25
Cations Per 8 Oxygens			
Si	2.828	2.378	2.954
Al	1.164	1.586	1.029
Fe	0	0.029	0.007
Mg	0	0.007	0
Ca	0.137	0.639	0.061
Na	0.919	0.380	0.960
K	--	0.001	0.002
Mn	--	0	0
Total	5.048	5.020	5.013
% An	12.97	62.71	5.97

TABLE AI-4.

Epidote Analyses- Altered Basalts

AII-60	2-141A (1)	Crystals in Veins
	(2)	" " "
Ch-44	3-126 (1)	Euhedral Grain in Altered Groundmass
	(2)	Euhedral Grain in Altered Groundmass
Ch-44	3-8 (1)	Vein Mineral
	(2)	Vein Mineral
AII-42	1-129	Pc. Altered to Albite + Epidote
	1-141	Rounded Pc. of Albite + Epidote

TABLE AI-4

Sample No.	AI-60 2-141A (1)	AI-60 2-141A (2)	Ch-44 3-126 (1)	Ch-44 3-126 (2)	Ch-44 3-8 (1)	Ch-44 3-8 (2)	AI-42 1-129	AI-42 1-141
SiO <sub>2</sub>	37.42	37.17	37.20	37.55	37.50	37.24	37.75	37.65
Al <sub>2</sub> O <sub>3</sub>	25.20	24.50	24.98	24.13	24.83	24.85	24.36	24.16
FeO*	11.05	11.97	10.91	11.39	10.45	10.91	11.75	11.26
MgO	0.18	0.03	0.02	0.02	0.03	0	0.27	0.02
CaO	22.91	23.68	22.90	23.34	23.40	23.08	22.83	22.23
Na <sub>2</sub> O	0	0	0	0	0.01	0	0.04	0.13
K <sub>2</sub> O	0	0	0.01	0.01	0.03	0.02	0	0.01
MnO	0.44	0	0.13	0	0.03	0	0.16	0
Total	97.02	97.35	96.15	96.44	96.28	96.10	97.16	95.46
Cations Per 13 O, OH								
Si	3.162	3.156	3.174	3.204	3.190	3.179	3.198	3.233
Al	2.510	2.452	2.512	2.427	2.490	2.500	2.433	2.445
Fe	0.781	0.850	0.778	0.813	0.743	0.779	0.833	0.809
Mg	0.023	0.004	0.003	0.003	0.004	0	0.034	0.003
Ca	2.075	2.155	2.093	2.134	2.133	2.111	2.073	2.045
Na	0	0	0	0	0.002	0	0.007	0.022
K	0	0	0.001	0.001	0.003	0.002	0	0.001
Mn	0.031	0	0.009	0	0.002	0	0.011	0
Total	8.582	8.617	8.570	8.582	8.567	8.571	8.589	8.558

TABLE AI-5

Chlorite Analyses - Altered Basalts

AII-60	2-141B (1)	Chlorite-actinolite intergrowth in groundmass
	2-141B (2)	Chlorite and quartz vein
	2-142B	Chlorite vein
Ch-44	2-5 (1)	Chlorite in vesicle
	2-5 (2)	Alteration of fs. phenocryst
Ch-44	3-8 (1)	Pseudomorph after olivine phenocryst
	3-8 (2)	Pseudomorph after olivine phenocryst
Ch-44	3-12 (1)	Pseudomorph after olivine phenocryst
	3-12 (2)	Chlorite associated with amphibole in groundmass replacement
Ch-44	3-17 (1)	Pseudomorph after olivine phenocryst
	3-17 (2)	Pseudomorph after olivine phenocryst associated with pyrite
AII-42	1-96A (1)	Alteration of groundmass
	1-96B	Pseudomorph after phenocryst
	1-96C (1)	Pseudomorph ol. pc. associated with pyrite
	1-96C (2)	Pseudomorph ol. pc. associated with pyrite
AII-42	1-97B (1)	Pseudomorph ol. phenocryst
	1-97B (2)	Vesicle filling
AII-42	1-108A	Vesicle filling
AII-42	1-118A	Chlorite in altered groundmass
AII-42	1-118B (1)	Vesicle filling
	1-118B (2)	Groundmass alteration
AII-42	1-129	Pseudomorph after ol. pc.
AII-42	1-130	Pseudomorph after ol. pc. associated with opaque
AII-60	2-14	Chlorite-filled vesicle lined with quartz
AII-60	2-143	Chlorite vein

Table AI-5

Sample No.	AI-60 2-141B (1)	AI-60 2-141B (2)	AI-60 2-142B	Ch-44 2-5 (1)	Ch-44 2-5 (2)	Ch-44 3-8 (1)	Ch-44 3-8 (2)	Ch-44 3-12 (1)	Ch-44 3-12 (2)
SiO <sub>2</sub>	28.78	28.81	27.50	28.24	28.34	28.95	28.39	28.42	28.81
Al <sub>2</sub> O <sub>3</sub>	17.61	17.10	18.41	16.83	17.00	18.18	18.42	17.54	18.77
FeO*	20.64	18.98	21.04	21.72	21.30	18.51	18.61	23.33	20.96
MgO	19.92	20.95	19.86	19.57	20.19	20.84	20.71	17.41	18.58
CaO	0.17	0.16	0.02	0.10	0.07	0.11	0.10	0.13	0.19
Na <sub>2</sub> O	0.01	0.09	0.16	0.10	0.07	0.01	0.04	0.01	0
K <sub>2</sub> O	0.02	0.04	0.01	0.02	0.03	0.05	0.03	0.03	0.01
MnO	0.19	0.19	0.13	0.25	0.16	0.20	0.16	0.14	0.14
Total	87.34	86.32	87.13	86.83	87.16	86.68	86.46	87.01	87.46
Cations Per 28 O, OH									
Si	5.925	5.958	5.702	5.901	5.880	5.920	5.841	5.956	5.916
Al	4.273	4.168	4.499	4.145	4.158	4.382	4.467	4.333	4.543
Fe	3.553	3.282	3.648	3.796	3.696	3.166	3.202	4.089	3.599
Mg	6.113	6.458	6.138	6.096	6.245	6.353	6.352	5.439	5.687
Ca	0.037	0.035	0.004	0.022	0.016	0.024	0.022	0.029	0.042
Na	0.004	0.036	0.064	0.041	0.028	0.004	0.016	0.004	0
K	0.005	0.011	0.003	0.005	0.008	0.013	0.008	0.008	0.003
Mn	0.033	0.033	0.023	0.044	0.028	0.035	0.028	0.025	0.024
Total	19.943	19.981	20.081	20.050	20.059	19.897	19.928	19.883	19.814



Table AI-5 (Continued)

Sample No.	Ch-44 3-17 (1)	Ch-44 3-17 (2)	AII-42 1-96A	AII-42 1-96B	AII-42 1-96C (1)	AII-42 1-96C (2)	AII-42 1-97B (1)	AII-42 1-97B (2)	AII-42 1-108A
SiO <sub>2</sub>	29.65	28.13	27.85	28.61	28.60	29.24	29.18	30.03	28.66
Al <sub>2</sub> O <sub>3</sub>	17.40	17.59	17.25	17.52	17.88	17.49	17.86	17.08	18.19
FeO*	20.64	23.62	18.57	20.04	21.51	21.45	21.16	21.19	20.14
MgO	19.55	17.59	20.95	20.73	20.25	20.91	20.80	20.03	20.71
CaO	0.08	0.09	2.85	0.05	0.07	0.09	0.08	0.10	0.03
Na <sub>2</sub> O	0.14	n.a.	n.a.	0.03	n.a.	n.a.	n.a.	n.a.	n.a.
K <sub>2</sub> O	0.01	n.a.	n.a.	0.01	n.a.	n.a.	n.a.	n.a.	n.a.
MnO	0.11	0.21	0.11	0.06	0.10	0.09	0.09	0.05	0.10
Total	87.58	86.29	87.58	87.05	88.41	89.27	89.17	88.50	87.83
Cations Per 28 O, OH									
Si	6.069	5.895	5.729	5.890	5.839	5.903	5.886	6.094	5.844
Al	4.198	4.345	4.183	4.252	4.303	4.162	4.247	4.085	4.372
Fe	3.533	4.140	3.195	3.450	3.673	3.622	3.570	3.596	3.435
Mg	5.965	5.495	6.425	6.362	6.163	6.293	6.255	6.059	6.295
Ca	0.018	0.020	0.628	0.011	0.015	0.019	0.017	0.022	0.007
Na	0.056	--	--	0.012	--	--	--	--	--
K	0.003	--	--	0.003	--	--	--	--	--
Mn	0.019	0.037	0.019	0.010	0.017	0.015	0.015	0.009	0.013
Total	19.861	19.932	20.179	19.990	20.010	20.014	19.990	19.865	19.966

Table AI-5 (Continued)

Sample No.	AII-42 1-118A	AII-42 1-118B (1)	AII-42 1-118B (2)	AII-42 1-129	AII-42 1-130	AII-60 2-14	AII-60 2-143
SiO <sub>2</sub>	30.60	31.28	29.62	27.57	29.13	28.89	27.50
Al <sub>2</sub> O <sub>3</sub>	16.79	16.88	16.69	17.53	17.66	17.50	17.06
FeO*	19.61	19.28	19.25	21.43	19.88	21.21	20.77
MgO	19.57	20.08	19.85	19.46	19.78	19.78	20.61
CaO	0.14	0.07	0.09	0.13	0.04	0.03	0.03
Na <sub>2</sub> O	n.a.	0.27	0.01	n.a.	0.08	0.08	0
K <sub>2</sub> O	n.a.	0.04	0.07	n.a.	0	0.03	0
MnO	0.09	0.01	0.05	0.03	0.07	0.25	0.12
Total	86.94	87.85	85.63	86.15	86.64	87.77	86.09
Cations Per 28 O, OH							
Si	6.268	6.309	6.160	5.794	6.007	5.935	5.773
Al	4.054	4.013	4.091	4.343	4.293	4.238	4.221
Fe	3.360	3.252	3.348	3.767	3.428	3.644	3.646
Mg	5.976	6.037	6.154	6.097	6.081	6.058	6.449
Cu	0.031	0.015	0.020	0.029	0.009	0.007	0.007
Na	--	0.106	0.004	--	0.032	0.032	0
K	--	0.010	0.019	--	0	0.008	0
Mn	0.016	0.002	0.009	0.005	0.012	0.044	0.021
Total	19.705	19.744	19.810	20.035	19.844	19.966	20.117

TABLE AI-6.

Amphibole Analyses- Altered Basalts

AII-60	2-141B	Chlorite-actinolite inter-growth replacing groundmass
Ch-44	3-12	Amphibole replacing phenocryst and associated with chlorite
Ch-44	3-17	Amphibole replacing phenocryst and associated with chlorite
Ch-44	3-126 (1)	Altered cpx (?) microphenocryst
Ch-44	3-126 (2)	" " "
AII-42	1-108B	Actinolite intergrown with chlorite and associated with haematite
AII-42	1-130	Alteration of groundmass

TABLE AI-6

Sample No.	AI-60 2-141B	Ch-44 3-12	Ch-44 3-17	Ch-44 3-126 (1)	Ch-44 3-126 (2)	AI-42 1-108B
SiO <sub>2</sub>	51.01	51.86	49.39	50.55	49.75	49.35
Al <sub>2</sub> O <sub>3</sub>	2.43	3.90	7.26	4.30	6.30	5.19
FeO*	13.32	15.45	16.43	15.84	17.40	15.68
MgO	15.16	13.41	13.34	14.36	12.66	14.70
CaO	12.63	10.26	10.49	11.53	11.78	12.43
Na <sub>2</sub> O	0.33	0.40	0.44	0.65	0.55	n.a.
K <sub>2</sub> O	0.07	0.05	0.04	0.05	0.06	n.a.
MnO	0.14	0.25	0.35	0.10	0.12	0.20
Total	95.09	95.58	97.74	97.38	98.62	97.67
Cations Per 24 O, OH						
Si	7.946	8.022	7.539	7.754	7.588	7.573
Al	0.446	0.711	1.306	0.777	1.133	0.939
Fe	1.735	1.998	2.097	2.032	2.219	2.012
Mg	3.520	3.092	3.035	3.284	2.878	3.363
Ca	2.108	1.701	1.716	1.895	1.925	2.044
Na	0.099	0.120	0.130	0.193	0.163	--
K	0.014	0.010	0.008	0.010	0.012	--
Mn	0.018	0.033	0.045	0.013	0.016	0.026
Total	15.886	15.687	15.876	15.958	15.934	15.957
% Tremolite	66.9	60.7	59.1	61.8	56.5	62.6

TABLE AI-7.

Major Element Analyses of Fresh and Altered Basalts from 4°S (AII-42),  
22°N. (Ch-44), and 22°S. (AII-60).

(Analyses in wt%;  $\rho$  (density) in g/cm<sup>3</sup>).

Concentrations in Wt. %

Sample No.	AII-42 1-96A	AII-42 1-96B	AII-42 1-96C	AII-42 1-97A	AII-42 1-97B	AII-42 1-98	AII-42 1-99	AII-42 1-106	AII-42 1-108A	AII-42 1-108B
SiO <sub>2</sub>	49.64	49.59	48.61	42.59	49.52	49.22	47.08	41.63	41.81	50.96
Al <sub>2</sub> O <sub>3</sub>	14.65	15.16	14.66	15.03	15.23	15.73	15.17	14.75	16.69	15.31
FeO*	9.43	8.68	7.83	12.04	7.87	8.48	10.03	12.77	11.04	8.29
MgO	11.05	9.85	6.96	14.34	7.71	6.91	12.20	13.23	12.39	5.80
CaO	2.63	2.78	11.56	4.55	11.52	10.86	3.22	4.96	4.55	11.28
Na <sub>2</sub> O	2.90	3.74	2.59	2.46	2.87	3.35	2.04	2.14	2.61	3.33
K <sub>2</sub> O	0.28	0.30	0.27	0.32	0.32	0.29	0.24	0.29	0.27	0.30
TiO <sub>2</sub>	1.40	1.33	1.26	1.46	1.37	1.40	1.49	1.46	1.98	1.43
P <sub>2</sub> O <sub>5</sub>	0.23	0.13	0.22	0.18	0.16	0.22	0.18	0.21	0.20	0.27
MnO	0.11	0.11	0.13	0.17	0.11	0.14	0.11	0.18	0.18	0.14
H <sub>2</sub> O <sup>-</sup>	0.68	0.76	1.00	0.72	0.52	0.42	0.69	0.88	0.65	0.54
Ig loss	6.92	6.99	4.50	6.62	2.69	2.63	6.92	6.77	7.02	2.50 <sup>-222</sup>
Total	99.94	99.41	99.59	100.47	99.71	99.66	99.37	99.28	99.40	100.14
H <sub>2</sub> O <sup>+</sup>	6.89	6.88	3.55	6.04	2.29	2.64	6.10	6.51	6.67	1.97
FeO	7.98	6.40	5.34	10.63	5.76	6.06	8.51	11.03	9.65	5.28
Fe <sub>2</sub> O <sub>3</sub>	1.62	2.52	2.77	1.56	2.34	2.69	1.69	1.94	1.55	3.34
ρ (g/cc)	2.57	2.57	2.79	2.63	2.79	2.78	2.58	2.56	2.54	2.79
Fe <sub>2</sub> O <sub>3</sub> /FeO	0.20	0.39	0.52	0.15	0.41	0.44	0.20	0.18	0.16	0.63

Table AI-7 (Continued)

Sample No.	Concentrations in Wt%.								
	AII-42 1-118A	AII-42 1-118B	AII-42 1-129	AII-42 1-57	AII-42 1-130	AII-42 1-141	Ch-44 2-1	Ch-44* 2-2	Ch-44 2-3
SiO <sub>2</sub>	46.78	49.79	49.27	49.54	49.29	49.80	50.21	49.10	50.77
Al <sub>2</sub> O <sub>3</sub>	16.14	15.01	15.54	15.66	15.54	15.93	16.07	15.27	14.99
FeO*	9.02	8.09	8.41	9.30	9.58	8.83	9.05	10.65	9.03
MgO	8.50	7.48	6.52	8.07	8.01	7.04	7.37	8.09	7.12
CaO	6.83	10.86	11.04	12.13	10.95	11.78	11.41	10.61	11.42
Na <sub>2</sub> O	3.49	2.58	2.99	2.92	3.66	3.49	2.95	2.86	3.13
K <sub>2</sub> O	0.31	0.28	0.28	0.15	0.17	0.16	0.29	0.25	0.21
TiO <sub>2</sub>	1.53	1.35	1.44	1.20	1.50	1.55	1.51	1.73	1.65
P <sub>2</sub> O <sub>5</sub>	0.19	0.20	0.17	0.11	0.15	0.18	0.13	0.16	0.23
MnO	0.14	0.10	0.13	0.17	0.13	0.21	0.17	0.20	0.19
H <sub>2</sub> O <sup>-</sup>	0.70	0.84	0.50	0.86	0.38	0.52	0.46	0.25	0.56
lg loss	5.11	3.77	2.35	1.50	1.09	1.79	0.62	-----	0.74
Total	98.74	100.36	98.65	101.59	100.44	101.29	100.24	99.73 <sup>1</sup>	100.04
H <sub>2</sub> O <sup>+</sup>	4.65	2.81	2.14	1.34	0.90	1.31	0.57	0.56	0.67
FeO	7.47	5.65	6.17	6.90	6.94	5.98	7.15	8.36	6.02
Fe <sub>2</sub> O <sub>3</sub>	1.73	2.71	2.49	2.66	2.93	3.17	2.11	2.54	3.35
ρ (g/cc)	2.75	2.77	2.79	2.81	2.83	2.82	2.82	2.79	2.81
Fe <sub>2</sub> O <sub>3</sub>	0.23	0.48	0.40	0.39	0.42	0.53	0.30	0.30	0.56

\*- From Melson et al (1968)

1- Total includes wt.% H<sub>2</sub>O<sup>+</sup>

Table AI-7 (Continued)

Sample No.	Concentrations in Wt. %									
	Ch-44 2-5	Ch-44* 3-2	Ch-44* 3-3	Ch-44* 3-6	Ch-44* 3-7	Ch-44 3-8	Ch-44 3-12	Ch-44 3-13	Ch-44 3-17	Ch-44 3-126
SiO <sub>2</sub>	48.70	50.14	48.18	50.84	51.70	48.46	47.55	49.36	46.71	48.31
Al <sub>2</sub> O <sub>3</sub>	15.08	16.30	15.17	15.25	14.70	16.94	15.84	15.47	14.64	15.21
FeO*	9.24	7.44	9.48	7.15	7.67	7.27	9.32	8.06	9.72	9.56
MgO	8.84	6.35	9.47	9.32	7.13	8.64	6.88	6.31	9.17	8.39
CaO	7.19	12.56	7.61	6.44	10.76	8.98	9.54	11.17	7.81	6.64
Na <sub>2</sub> O	2.89	3.11	3.27	4.48	3.98	3.62	4.02	3.39	3.44	3.58
K <sub>2</sub> O	0.11	0.11	0.06	0.05	0.08	0.12	0.11	0.19	0.35	0.14
TiO <sub>2</sub>	1.48	0.91	1.74	1.38	0.99	1.09	1.50	0.96	1.67	1.62
P <sub>2</sub> O <sub>5</sub>	0.22	0.14	0.15	0.10	0.08	0.19	0.19	0.23	0.24	0.23
MnO	0.17	0.11	0.16	0.16	0.11	0.09	0.21	0.12	0.18	0.17
H <sub>2</sub> O-	1.41	0.54	0.97	0.74	0.55	0.80	0.94	0.72	1.26	1.87
ig loss	5.39	-----	-----	-----	-----	3.44	4.32	3.39	4.35	4.23
Total	100.72	99.57 <sup>1</sup>	99.71 <sup>1</sup>	99.17 <sup>1</sup>	99.68 <sup>1</sup>	99.64	100.42	99.37	99.54	99.95
H <sub>2</sub> O <sup>+</sup>	4.17	1.86	3.45	3.26	1.93	3.22	3.79	2.80	3.88	3.76
FeO	7.20	3.92	7.18	4.55	4.77	5.55	4.78	4.10	7.17	6.90
Fe <sub>2</sub> O <sub>3</sub>	2.26	3.91	2.56	2.89	3.22	1.91	5.05	4.40	2.84	2.95
ρ	2.64	2.68	2.74	2.72	2.73	2.68	2.66	2.68	2.62	2.60
Fe <sub>2</sub> O <sub>3</sub> /FeO	0.32	0.99	0.36	0.64	0.68	0.34	1.06	1.07	0.40	0.43

-224-

\* - From Melson et al (1968)

1 - Total includes wt. % H<sub>2</sub>O<sup>+</sup>



Table AI-7 (Continued)

Sample No.	Concentrations in Wt. %.						
	AI-60 2-14	AI-60 2-141A	AI-60 2-141B	AI-60 2-142A	AI-60 2-142B	AI-60 2-142C	AI-60 2-143
SiO <sub>2</sub>	49.84	50.07	48.57	39.31	47.70	52.30	48.62
Al <sub>2</sub> O <sub>3</sub>	15.85	13.41	14.77	17.59	14.15	14.79	17.95
FeO*	8.60	8.26	9.32	12.71	9.50	8.17	7.96
MgO	7.41	11.34	8.80	12.67	9.70	6.03	7.39
CaO	9.88	4.53	8.24	3.35	8.40	9.83	8.12
Na <sub>2</sub> O	3.51	3.40	3.41	2.98	2.97	3.22	3.85
K <sub>2</sub> O	0.40	0.29	0.11	0.14	0.13	0.15	0.10
TiO <sub>2</sub>	1.87	1.63	1.63	2.25	1.75	1.63	1.57
P <sub>2</sub> O <sub>5</sub>	0.27	0.14	0.14	0.15	0.14	0.16	0.12
MnO	0.04	0.10	0.16	0.11	0.10	0.14	0.15
H <sub>2</sub> O-	0.48	1.94	1.41	1.32	1.92	0.80	0.54
lg loss	2.36	4.70	3.42	6.68	3.36	1.88	2.67
Total	100.51	99.81	99.98	99.26	99.82	99.10	99.04
H <sub>2</sub> O+	2.35	4.51	3.26	6.53	3.26	1.85	2.72
FeO	6.54	6.09	5.97	9.37	6.81	6.82	6.43
Fe <sub>2</sub> O <sub>3</sub>	2.29	2.41	3.72	3.72	2.99	1.49	1.70
ρ	2.81	2.62	2.70	2.65	2.71	2.79	2.78
Fe <sub>2</sub> O <sub>3</sub> /FeO	0.35	0.40	0.62	0.40	0.44	0.22	0.26

TABLE AI-8

Modal Analyses of Fresh and Altered Basalts

(1000 counts/sample)

Altered Samples	AII-42 1-96A	AII-42 1-96B	AII-42 1-96C	AII-42 1-97A	AII-42 1-97B	AII-42 1-98	AII-42 1-99	AII-42 1-106	AII-42 1-108A	AII-42 1-108B	AII-42 1-118A
Albite <sup>1</sup>	15	18		29			22	25	24		25
Actinolite	--	2		10			2	6	10		1
Chlorite	60	54		40			54	50	55		45
Epidote	<1	--		3			2	4	1		--
Quartz	20	10		4			19	5	5		14
Pyrite	2	3		2			1	2	3		--
Pumpellyite	--	--		--			--	--	--		--
Unaltered groundmass	2	13		12			--	8	2		15
Sphene	--	--		--			--	--	--		--

Fresh Samples

Plagioclase - microclites	24	10	25							25	
pc and mpc	2	5	<1							--	
Unaltered glass	60	65	60							65	
Olivine	--	--	--							--	
Augite	--	--	--							--	
Chlorite	12	16	12							8	
Opauques	2	4	2							2	

<sup>1</sup>Includes unalbitised pc and microclites.

Table AI-8 (Continued)

	AII-42 1-118B	AII-42 1-129	Ch-44 2-3	Ch-44† 2-5	Ch-44† 3-2	Ch-44† 3-3	Ch-44† 3-6	Ch-44† 3-7	Ch-44 3-8	Ch-44 3-12	Ch-44 3-13	Ch-44 3-17
<u>Altered Samples</u>												
Albite				25	50	30	25	20	35	40	20	25
Actinolite				40	40	35	45	50	15	25	45	48
Chlorite				25	5	15	20	2	7	2	10	20
Epidote				1	20	10	2	25	2	10	20	3
Quartz				5	--	--	--	--	<1	--	--	--
Pyrite				--	--	--	3	--	--	1	--	1
Pumpellyite				--	--	trace	--	--	--	--	--	--
Unaltered glass				--	--	--	--	--	40	--	--	--
Sphene				4	2	5	3	3	--	2	2	2

-227-

Fresh Samples

Plagioclase - microclites	10	45	38
pc and mpc	2	2	53
Unaltered glass	70	50	3
Olivine	--	--	4
Augite	--	2	--
Chlorite	15	1	2
Opagues	3		

†From Melson et al. (1966).

Table AI-8 (Continued)

Altered Samples	Ch-44 3-126	AII-60 2-14	AII-60 2-143	AII-60 2-141A	AII-60 2-141B	AII-60 2-142A	AII-60 2-142B	AII-60 2-142C
Albite	25	30	25	25	25	20	21	
Actinolite	35	20	30	15	9	9	10	
Chlorite	25	6	12	45	55	55	45	
Epidote	13	<1	1	4	2	2	4	
Quartz	--	1	2	6	10	10	6	
Pyrite	--	3	5	5	4	4	2	
Pumpellyite	--	--	--	--	--	--	--	
Unaltered glass	--	40	25	--	--	--	12	
Sphene	2	--	--	--	--	--	--	

-228-

Fresh Samples

Plagioclase - microclites	25							15
pc and mpc	2							2
Unaltered glass	55							70
Olivine	--							--
Augite	--							--
Chlorite	15							10
Opauques	3							3

TABLE AI-9

Trace Elements

(ppm)

Sample I.D.	B	Li	V	Co	Cr	Ni	Cu	Ba	Sr	Y	Zr
AII-42 1-57	4	5	265	42	530	113	78	4	110	32	64
1-96A	7	9	230	56	290	135	295	5	47	35	105
1-96B	5	9	245	46	310	130	245	5	52	30	80
1-96C	<2	4	260	30	320	130	60	19	160	39	110
1-97A	18	9	245	60	275	155	45	4	65	40	115
1-97B	5	4	260	46	290	130	70	12	120	35	105
1-98	<5	4	260	46	320	140	26	10	125	37	115
1-99	9	8	220	46	275	150	220	4	30	35	105
1-106	13	10	235	60	295	165	58	4	53	44	130
1-108A	15	14	260	55	370	180	23	10	125	45	135
1-108B	10	3	280	49	300	120	80	15	150	40	125
1-118A	11	10	265	53	330	145	55	25	205	39	125
1-118B	4	3	260	48	290	135	90	18	160	38	115
1-129	2	4	275	35	320	140	62	12	140	41	120
1-130	5	5	270	43	345	135	47	4	108	33	105
1-141	5	3	290	38	365	130	155	1	110	36	112
Ch-44 2-1	5	4	270	37	305	105	63	5	110	34	115
2-2*	<10	8	245	75	290	150	115	6	110	--	125
2-3	9	6	285	42	320	78	73	5	120	36	115
2-5	6	10	300	32	210	115	12	14	120	49	145
3-2	6	4	230	47	215	100	10	12	250	32	80
3-3*	<10	20	250	45	210	115	80	6	120	--	110
3-6*	<10	22	230	35	310	105	70	8	130	--	90
Ch-44 3-7*	<10	4	225	70	225	85	290	6	220	--	75
3-8	<2	6	200	45	515	170	23	11	125	30	75
3-12	13	4	295	42	240	115	36	16	215	48	140
3-13	<2	4	235	38	195	98	12	8	230	29	80
3-17	6	8	285	30	260	110	55	12	105	45	140
3-126	9	11	280	33	220	115	17	12	110	44	140
AII-60 2-14	3	4	300	34	280	100	205	4	115	42	140
2-141A	7	14	230	40	310	130	135	2	45	40	130
2-141B	6	5	255	40	300	140	38	2	85	37	120
2-142A	12	19	330	47	405	140	140	5	180	59	145
2-142B	9	7	300	40	230	95	115	2	85	40	135
2-142C	5	3	300	42	230	100	58	4	135	39	130
2-143	2	3	280	37	235	98	21	2	92	37	135

\* Melson et al. (1968).

TABLE AI-10

Mn Analyses

Sample I.D.	Mn (ppm)
AII-42 1-96A	1060
1-96B	1068
1-96C	1392
1-97A	1567
1-97B	1283
1-98	1261
1-99	1269
1-106	1695
1-108A	1623
1-108B	1201
1-118A	1231
1-118B	1288
1-129	1268
1-57	1305
1-130	1277
1-141	1274
Ch-44 2-1	1315
2-3	1264
2-5	1609
3-2	1664
3-8	1808
3-12	1886
3-13	1074
3-17	1685
3-126	1250
AII-60 2-14	1481
2-141A	1552
2-141B	1508
2-142A	2548
2-142B	1837
2-142C	1375
2-143	1471

APPENDIX II

ANALYTICAL PROCEDURES

1) Electron Microprobe Analysis

Major element analyses of minerals and fluxed glasses were carried out using the M.A.C. electron microprobe at the Department of Earth and Planetary Sciences at M.I.T. This microprobe is part of an automated system designed by Finger and Hadidiacos (1972) employing three spectrometers with analyzing crystals of RAP, PET, and LiF. Data reduction was executed on-line with a PDP 11/20 computer using "Geolab" program of Finger and Hadidiacos (1972) which includes the correction scheme of Albee and Ray (1970). The standard operating conditions used were as follows:

filament voltage: 15 kV

beam current: 300 nanoamps

counting time: 30 seconds per element.

Standards used for the mineral analyses were the microprobe standard minerals of the Department of Earth and Planetary Sciences and are listed in Table AII-1. Standards for fluxed glasses were prepared from the reference rocks USGS BCR-1, GSJ JB-1 and USGS W-1, using the same techniques as for the unknown samples.

USGS BCR-1 was used for the initial standardization. Four replicate counts were taken for each element during the standardization. If the ratio of the standard deviation of the counts to that predicted from counting statistics was greater than two, the element was restandardized.

All reported analyses of the fluxed glasses are the average of at least five analyses, using a beam diameter of about 15  $\mu$ . The reported analyses of the fresh minerals are the average of between three and five analyses using a beam diameter of about 5  $\mu$ , depending on the grain size. Many of the altered minerals were so fine-grained that analyses of individual grains were not possible. A dispersed beam was therefore used, giving an average analysis of several grains. The reported analyses are the average of at least two of these dispersed analyses. This applies in particular to chlorite and amphibole analyses.

During the analyses of the unknowns, USGS W-1 was used as an internal standard, and was run every fifth analysis. This allowed any peak drifts due to temperature changes to be monitored, and allowed any major problems to be detected. In either case, the element was restandardized.

The accuracy and precision of the analyses were checked during the runs by replicate analyses of GSJ JB-1 being run as an unknown, and these results are listed in Table AII-2. Accuracy and precision are  $\pm 1\%$  of reported values greater than 10%,  $\pm 5\%$  of values between 1 and 10%, and  $\pm 25\%$  of values less than 1%.



TABLE AII-1

Microprobe Standards Used in this Study for  
Mineral Analyses

Si, Al, Ca	Plagioclase	AN- 60
Mg, Fe	Olivine	P-140
	Orthoclase	
Ti	Pyroxene	DI2TI
Cr	Pyroxene	CRCATS
Mn	Mn-ilmenite	MNILM
Na	Pyroxene	DI65 JD35

TABLE AII-2

(a)

Analyses of JB-1 During Electron Microprobe Analysis of AII-42 Samples in Wt. %.

	1	2	3	4	5	6	Mean	S	Recommended (Flanagan, 1973)
SiO <sub>2</sub>	53.57	53.16	53.35	53.62	54.03	52.95	53.45	0.38	53.35
Al <sub>2</sub> O <sub>3</sub>	14.78	15.06	14.74	14.51	14.75	14.77	14.77	0.17	14.88
FeO	7.95	8.00	8.18	8.52	8.32	8.15	8.19	0.21	8.33
MgO	7.64	7.83	7.82	8.14	7.96	7.88	7.88	0.17	7.89
CaO	9.29	9.44	9.35	9.09	9.57	9.35	9.35	0.16	9.43
Na <sub>2</sub> O	2.65	2.68	2.80	2.80	2.59	2.66	2.70	0.09	2.86
K <sub>2</sub> O	1.41	1.39	11.39	1.31	1.32	1.37	1.37	0.04	1.45
TiO <sub>2</sub>	1.36	1.33	1.45	1.38	1.42	1.39	1.39	0.04	1.37
P <sub>2</sub> O <sub>5</sub>	0.28	0.23	0.30	0.25	0.24	0.30	0.27	0.03	0.27
MnO	0.19	0.11	0.15	0.18	0.12	0.21	0.16	0.04	0.16
Total	99.12	99.23	99.53	99.80	100.32	99.03	99.53		99.99

-234-

TABLE AII-2

(b)

Analyses of JB-1 During Electron Microprobe Analysis of Ch-44 and AII-60 Samples in Wt. %.

	1	2	3	4	5	6	7	8	9	10	Mean	S	Recommended (Flanagan, 1973)
SiO <sub>2</sub>	53.36	53.33	53.29	53.22	53.46	53.35	52.86	53.03	53.21	52.96	53.21	0.20	53.35
Al <sub>2</sub> O <sub>3</sub>	14.99	14.87	14.76	14.68	14.73	14.91	14.64	14.79	14.74	14.91	14.80	0.11	14.88
FeO*	8.34	8.30	8.34	8.34	8.41	8.33	8.51	8.29	8.30	8.25	8.34	0.07	8.33
MgO	7.72	7.82	7.84	7.80	7.80	8.09	7.83	7.79	7.93	7.80	7.84	0.10	7.89
CaO	9.59	9.39	9.33	9.33	9.11	9.52	9.36	9.27	9.53	9.38	9.38	0.14	9.43
Na <sub>2</sub> O	2.90	2.86	2.87	2.66	2.68	2.90	2.72	2.68	2.71	2.66	2.76	0.10	2.86
K <sub>2</sub> O	1.44	1.39	1.46	1.47	1.32	1.53	1.38	1.36	1.43	1.40	1.42	0.06	1.45
TiO <sub>2</sub>	1.39	1.41	1.35	1.45	1.37	1.37	1.32	1.35	1.42	1.32	1.35	0.04	1.37
P <sub>2</sub> O <sub>5</sub>	0.21	0.28	0.30	0.26	0.24	0.26	0.28	0.31	0.26	0.26	0.27	0.03	0.27
MnO	0.14	0.13	0.18	0.17	0.20	0.12	0.19	0.18	0.15	0.21	0.17	0.03	0.16
Total	100.08	99.78	99.72	99.38	99.32	100.38	99.09	99.05	99.68	99.15	99.57		99.99

2) Preparation of Fluxed Glasses for Major Element Analyses

a) Preparation of Flux

About 4 g of lithium tetraborate and about 3 g of lithium carbonate were dried in porcelain crucibles at 550°C overnight. Approximately 2 g of lanthanum oxide were ignited in a platinum crucible at 900°C for two hours. The compounds were then weighed accurately into a vial in the following proportions:

3.80 g lithium tetraborate

2.96 g lithium carbonate

1.32 g lanthanum oxide.

The contents of the vial were then well-mixed by shaking for 30 minutes, and the mixture was then ignited in a platinum crucible at 1000°C for 20 minutes. The melt was poured on to a sheet of aluminum, about ½ inch thick, and quenched to form a clear bead. The cooled bead was then placed between two pieces of glass paper, crushed and broken by tapping with a hammer. It was then ground to a coarse powder in a boron carbide mortar, and stored in a dessicator.

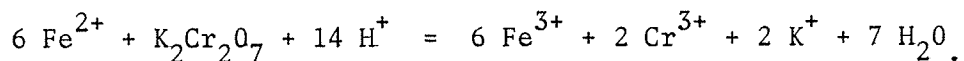
b) Preparation of Glasses

Each rock powder (ground to less than 200 mesh) and the reference rocks were ignited at 1000°C for two hours in ceramic crucibles. Precisely 0.100 (± 0.5%) g of each sample was weighed into a small vial, and 0.200 (± 0.5%) g of flux was added. The vial was then shaken for 15 minutes to obtain a homogeneous mixture.

The flux-sample mixture was then transferred to a graphite crucible which had been pre-ignited at 1000°C for 15 minutes, so that some loose graphite powder would form and prevent the melt from sticking. The mixture was then ignited at 1000°C for 20 minutes. The melt was quenched by pouring on to the aluminum sheet to form a clear bead. The cooled glass bead was shattered by placing it between glass paper and tapping with a hammer, and then the chips were mounted in one inch diameter plastic discs using epoxy. They were then ground and polished to 0.1 μ grit. The discs were stored in a vacuum dessicator to prevent uptake of water until analysis - a period always less than 24 hours - and were carbon coated immediately before analysis.

### 3) Determination of Ferrous and Ferric Iron

Ferrous iron was determined by a modification of the method of Jen (1973). This method depends on the quantitative oxidation of ferrous salts in cold acid solution to a ferric state by potassium dichromate according to the reaction:



The procedure followed was that described by Jen, except that the amount of sulphuric acid added was doubled as this was found to give more accurate results.

The accuracy and precision of the method was determined by replicate analyses of two reference rocks (Table AII-3) of similar type

to those to be analyzed. Precision and accuracy are approximately 1% of the reported values.

Ferric iron was then determined by subtraction of FeO from the total iron analyses obtained by electron microprobe, assuming that:

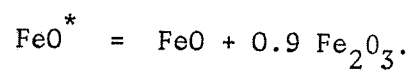


TABLE AII-3

Determination of FeO (Wt. %) in BCR-1 and CRPG-BR

	1	This Study					Mean	S <sup>1</sup>	V <sup>2</sup>	Recommended Value (Flanagan, 1973)
		2	3	4	5					
BCR-1	8.75	8.69	8.76	8.79	8.89	8.78	0.073	0.83%	8.80	
CRPG-BR	6.54	6.52	6.44	6.69	6.51	6.54	0.092	1.41%	6.57	

<sup>1</sup> Standard Deviation.

<sup>2</sup> Coefficient of Variation:  $\frac{100 S}{\bar{x}}$ .

#### 4) Emission Spectroscopy

Trace element analyses were carried out by G. Thompson of Woods Hole Oceanographic Institution by direct-reading optical emission spectrometry (Thompson and Bankston, 1969). Table AII-4 shows the analyses of the standard rocks determined concurrently with the samples. The precision and accuracy of the method is approximately  $\pm 10\%$  of the reported values, and is discussed more fully in Chapter 4 for individual elements.

TABLE AII-4

Analyses of Standard Rocks Determined During Trace Element

Analyses by Direct-Reading Emission Spectroscopy

in ppm

	W-1		BCR-1		BR	
	Found	Flanagan (1973)	Found	Flanagan (1973)	Found	Flanagan (1973)
B	10	15 <sup>1</sup>	6	5 <sup>1</sup>	8	--
Li	8	14 <sup>2</sup>	13	13 <sup>3</sup>	11	9 <sup>1</sup>
V	240	264 <sup>2</sup>	430	400 <sup>2</sup>	280	240 <sup>3</sup>
Cr	113	114 <sup>2</sup>	16	18 <sup>1</sup>	415	420 <sup>3</sup>
Ni	77	76 <sup>2</sup>	18	16 <sup>2</sup>	270	270 <sup>3</sup>
Cu	112	110 <sup>3</sup>	16	18 <sup>2</sup>	67	70 <sup>3</sup>
Ba	145	160 <sup>3</sup>	690	675 <sup>3</sup>	1080	1050 <sup>3</sup>
Sr	170	190 <sup>3</sup>	400	330 <sup>3</sup>	1320	1350 <sup>3</sup>
Y	23	25 <sup>3</sup>	42	37 <sup>2</sup>	48	27 <sup>1</sup>
Zr	102	105 <sup>3</sup>	180	190 <sup>1</sup>	315	240 <sup>3</sup>

<sup>1</sup>Magnitude Estimate.

<sup>2</sup>Average Value.

<sup>3</sup>Recommended Value.



5) Water and Ignition Loss Determinations

$H_2O^-$  and ignition loss were determined during preparation of the fluxed glasses. Powdered samples (ground to less than 200 mesh) were weighed into small polypropylene vials that had previously been heated to  $110^{\circ}C$  overnight, and then cooled in a dessicator. The samples were then dried overnight at  $110^{\circ}C$ , cooled in a dessicator and reweighed. This weight was reported as  $H_2O^-$ .

The samples were then reweighed into porcelain crucibles that had been ignited overnight at  $1000^{\circ}C$  and stored in a dessicator. The samples were ignited at  $1000^{\circ}C$  overnight, cooled in a dessicator and reweighed. This weight loss was reported as ignition loss.

$H_2O^-$  results vary from laboratory to laboratory, so comparison of reference rock results with their recommended values are not very meaningful. However, analyses of reference rocks for ignition loss are shown in Table AII-5. Accuracy and precision are approximately 20%.

$H_2O^+$  was determined on an F and M Model 185 C-H-N analyzer. The powdered rock samples, which had previously been dried overnight at  $110^{\circ}C$  and then stored in a dessicator, were introduced into the oxidizing furnace in small aluminum foil boats that had also been previously dried at  $110^{\circ}C$ . The samples were analyzed in duplicate. The relation between peak height/weight sample and the published water content was determined by a least squares fit, using standard reference rocks. GSJ JB-1 and CRPG-BR were treated as samples and replicate analyses were run; these are shown in Table AII-6. The precision is approximately 10%.

TABLE AII-5  
Ignition Loss of Reference Rocks

	1	2	3	4	5	$\bar{x}$	s	Flanagan (1973)
USGS-AGV-1	1.43	0.98	1.23	1.02	1.19	1.17	0.18	0.86 <sup>1</sup>
CRPG-BR	2.90	2.77	3.04	3.05	2.71	2.90	0.15	3.16 <sup>1</sup>

<sup>1</sup>Calculated as  $(H_2O^+ + CO_2)$ .

TABLE AII-6  
Determination of  $H_2O^+$  on Standard Reference Rocks

	1	2	3	$\bar{x}$	s	Flanagan (1973)
GSJ-JB-1	0.87	0.96	1.09	0.97	0.11	1.00
CRPG-BR	2.25	2.64	2.20	2.36	0.24	2.30

6) Analysis of Manganese

Manganese analyses were carried out using a Spectrametrics Spectra-span 2, owned by the U. S. Geological Survey. This instrument is equipped with a D.C. argon plasma jet and an echelle diffraction grating. The operating conditions used were:

wavelength: 2576.104 Å

arc amperege: 7.3 amps.

integration time: 10 secs.

blank: distilled water.

A series of standards containing varying amounts of Mn were made up in a synthetic basalt matrix (Table AII-7), which had been fluxed in a similar manner to the samples.

The samples and reference rocks were fluxed with lithium metaborate and dissolved in dilute nitric acid, according to the method of Ingamells (1970). Analyses of these solutions were then carried out on the Spectra-span in small groups, with the standards being rechecked between groups. Triplicate readings were taken for each sample, and reference rocks were run as unknowns every third analysis.

Results of the replicate analyses of four U.S.G.S. reference rocks are given in Table AII-8, and are compared with the average values reported by Flanagan (1973). The accuracy of the results is better than 10%, and the precision is 5-6%; this method compares well with atomic absorption spectrophotometry.

TABLE AII-7

Synthetic Basalt Matrix

1.5666 g	SiO <sub>2</sub>
0.4320 g	Al <sub>2</sub> O <sub>3</sub>
0.2508 g	Fe <sub>2</sub> O <sub>3</sub>
0.1185 g	MgO
0.2249 g	CaCO <sub>3</sub>
0.1352 g	NaCl
0.1154 g	KCl
21.1566 g	LiBO <sub>2</sub>

TABLE AII-8  
Reference Rock Analyses During Mn Determinations

	A9V-1	BCR-1	W-1	JB-1
Conc. of Mn (ppm)				
	755	1517	1460	1206
	747	1483	1454	1184
	743	1483	1449	1184
	736	1480	1444	1178
	734	1467	1443	1167
	728	1455	1424	1165
	728	1435	1410	1147
	728	1435	1406	1142
	724	1433	1403	1138
	723	1430	1401	1133
	715	1429	1382	1127
	705	1421	1376	1122
	703	1402	1364	1119
	697	1391	1364	1119
	668	1379	1352	1112
			1328	1091
Mean	728	1442	1404	1146
Standard Deviation	22	38	40	32
99% Conf. Interval	740 705	1473 1412	1434 1373	1170 1122
Average Values (Flanagan, 1973)	763	1406	1278	1239 <sup>1</sup>
Accuracy	4.5%	2.0%	9.8%	7.9%
Precision	7.5%	5.5%	5.4%	5.7%

<sup>1</sup> Calculated from reported average value of Wt. % MnO.

## 7) Density Determinations

Density was determined with a method using Archimedes principle in a 1 ml pycnometer. About 0.1 g of sample was used, and the weight of fluid of known density that was displaced, was measured.

The standard used was Specpure aluminum powder, and values obtained are given in Table AII-9. The precision is only about 5% because of the small volume changes involved.

TABLE AII-9

Density of Aluminum Powder During Determinations of the  
Density of Samples

1	2	3	4	5	Mean	s	Recommended <sup>1</sup> Value
2.68	2.75	2.69	2.70	2.68	2.70	0.03	2.702

<sup>1</sup>CRC Handbook of Chemistry and Physics (53rd Edition), 1972-1973.

VITA

SUSAN E. HUMPHRIS

Woods Hole Oceanographic Institution  
Woods Hole, Massachusetts 02543

Born: August 12, 1951

Nationality: British

Education:

University of Lancaster, U. K.

B. A. (Hons.), Environmental Sciences, 1972.

Joint MIT/WHOI Student of Chemical Oceanography, 1972-1976.

Ph.D. under Dr. G. Thompson.